JAHRESBERICHT
2004

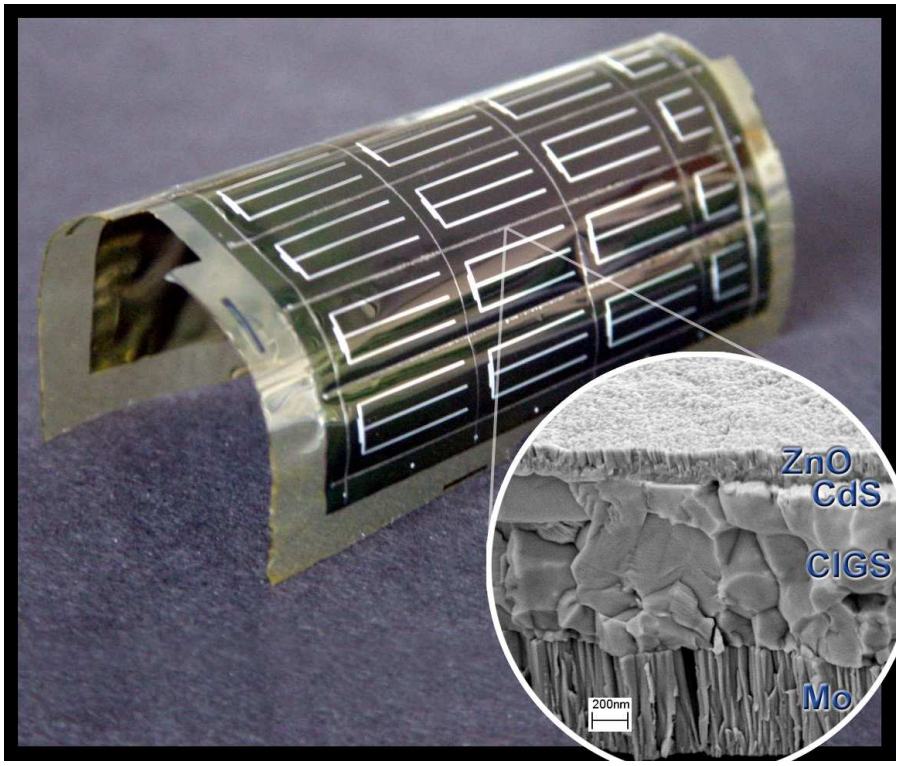

Laboratorium für Festkörperphysik
der
Eidgenössischen Technischen Hochschule
Zürich

Cover page:

Flexible CIGS solar cells on a 25cm^2 polyimide substrate. The demonstrated conversion efficiency of 14.1 % sets a new world record for flexible solar cells on polymers. The solar cells consist of several different layers (inset: SEM cross-sectional view) and are less than 4 mum thick. (J. Appl. Phys. 97, 084903 (2005))

This annual report was edited by: C. Ellenberger.

PREFACE

The year 2004 has been a successful one for the laboratory for solid state physics. Prof. Bertram Batlogg received the ”Wissenschaftspreis des Landes Vorarlberg” for his contributions to superconductivity. Dr. Andreas Fuhrer was awarded the IBM prize of the Swiss Physical Society for his PhD thesis on ”Transport through quantum rings”. Congratulations to both of them!

The staff of the laboratory for solid state physics has been active at all levels of undergraduate and graduate teaching in physics at ETH Zurich. In many meetings and committees the members of the institute prepared activities to take place in 2005, the world year of physics and simultaneously the 150th anniversary of ETH Zurich.

The search for new professors in the laboratory for solid state physics has been ongoing in 2004. It is expected that soon we will add a new direction in solid state physics to the scientific profile of our institute.

We are grateful for the technical support of the machine shop and all other technical help provided by the physics department. The financial support from the ETH board as well as from external sources such as the Schweizerischer Nationalfonds and KTI are gratefully acknowledged.

Zürich, April 2005

Der Vorsteher

Prof. Dr. K. Ensslin

Contents

Chapter 1

Physics of new materials

(http://www.solidphys.ethz.ch/pnm)

Head
Prof. Dr. Bertram Batlogg

Academic Staff

Markus Brühwiler	Claudia Goldmann	Dr. David J. Gundlach
Simon Haas	Cornelius Krellner	Daniel Oberhoff
Kurt Pernstich	Benjamin Rössner	

Semester/Diploma Students

Sven Burkardt	Matthias Grüter	Arne Kloke
Cornelius Krellner	Daniel Oberhoff	Georg Wilckens

Technical Staff

Kurt Mattenberger	Hans Peter Staub

Administrative Staff
Gabriela Strahm

High pressure materials synthesis group

Head
Dr. Janusz Karpinski

Academic Staff

Peter Geiser	Jan Jun	Dr. Sergei Kazakov
Dr. Krzysztof Rogacki	Dr. Götz Schuck	Dr. Nikolai Zhigadlo

Academic Guests
Dr. Nikolay Nikolaev, Russian Academy of Sciences, Troitsk (Russia)
Dr. Roman Puzniak, Polish Academy of Sciences, Warsaw (Poland)
Dr. Andrzej Wisniewski, Polish Academy of Sciences, Warsaw (Poland)

1.1 Organic molecular crystals

1.1.1 Development of a trap spectroscopy for organic molecular semiconductores

C. Krellner, S. Haas, C. Goldmann, D. J. Gundlach and B. Batlogg

A key issue in the field of organic semiconductors is the determination of the spectral density and the role of the trap states. Whereas in inorganic semiconductors the trap density is typically measured by optical methods, strong intermolecular excitations render the application of the same measurement techniques to organic molecular crystals difficult. Here, space-charge limited current measurements offer the unique advantage of allowing the determination of the density of trap states by a solely electrical measurement. We have established the method of temperature-dependent space-charge limited current measurements in terms of both experimental implementation and data analysis. Systematic studies of structurally and chemically pure rubrene single crystals have been carried out. These studies reveal deep states with a density as low as 10^{15} cm^{-3} (cf. Fig. 1.1), several orders of magnitude lower than the values reported so far for high quality pentacene single crystals. In our best rubrene crystals, charge injection at highest voltages moves the quasi-Fermi level close to the mobility edge (within ∼0.05 eV), where an exponentially increasing density of shallow states is found (Fig. 1.1, red symbols).

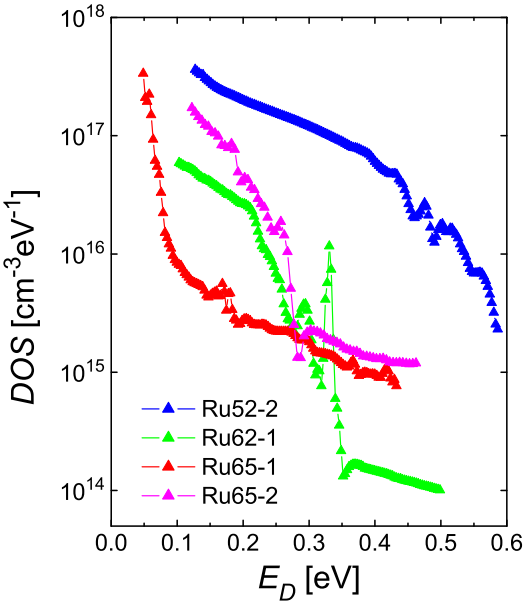

Figure 1.1: Density of states above the valence band edge E_D=0 for different rubrene single crystals. The best crystals (Ru 65-1) reveal a remarkably low density of deep trap states, and pronounced exponentially towards the valence band.

1.1.2 Oxygen induced trap level in rubrene crystals

C. Krellner, S. Haas, C. Goldmann, D. J. Gundlach and B. Batlogg

In addition to measuring the in-gap density of states as described above, we have studied the influence of external conditions on the density of bulk traps. We were able to intentionally induce additional traps in rubrene single crystals by oxygen exposure or X-ray irradiation and determine their density and energetic position within the band gap. The energetic position of oxygen-induced trap states in rubrene single crystals was thus identified at ∼0.27 eV above the valence band edge, as can be seen in Fig. 1.2.

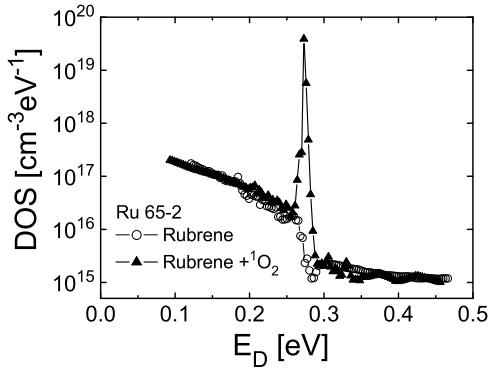

Figure 1.2: Study of intentionally generated traps in rubrene single crystals: Density of states above the valence band edge before and after exposure of the crystal to oxygen. An oxygen-induced defect state in rubrene at 0.27 eV above the valence band edge has been identified.

1.1.3 Trap spectroscopy of various organic molecular crystals

C. Krellner, S. Haas, C. Goldmann, D. J. Gundlach and B. Batlogg

Pentacene single crystals were also studied in detail using temperature-dependent SCLC spectroscopy technique. The measured DOS is found to be more than one order of magnitude lower than the best reported DOS for pentacene in the literature (D. Lang, 2004.) Compared to best rubrene crystals, the DOS in the band gap is by 1-2 orders of magnitude higher. Exposure to oxygen doesn't reveal any significant peak in the DOS. While the higher DOS in general might mask small changes in the DOS, we consider the electrically inactive nature of the 2-fold oxygenated form of pentacene (pentacene-quinone) the main reason for the absence of a peak similar to the case of rubrene.

Other single crystals investigated by temperature-dependent space-charge limited current measurements include alpha-sexithiophene and hexabenzocoronene. Their in-gap DOS is comparable to that in pentacene and rubrene crystals, both in regard to the absolute value and the broad spectral dependence.

1.1.4 Surface transport in organic molecular crystals: Influence of an electric field on the density of trapped charges

C. Goldmann, D. J. Gundlach and B. Batlogg

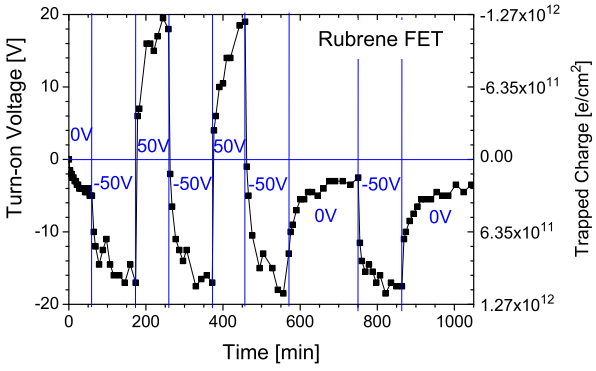

Figure 1.3: Shift of the turn-on voltage $V_{\rm on}$ in a Rubrene single crystal FET, demonstrating the reversible filling and emptying of interface traps on the order of 10^{12}/cm^{-2} upon the application of gate bias stress. The time intervals for a gate bias stress of -50V, +50V and 0V (stress-free relaxation) are indicated. At the times given by the data points the stress was shortly interrupted and a full IV-characteristic was measured, from which $V_{\rm on}$ and other parameters were extracted.

Charge transport at the surface of organic single crystals has been studied using a gated four-terminal "flip-crystal" field-effect transistor technique with thermal SiO_2 as the gate insulator. In contrast to the very low trap density in the bulk discussed in the previous sections, we typically observe surface charge trapping of order 10^{11} to 10^{12} cm^{-2} even in high quality Rubrene single crystals. We have studied charge transport and the density of surface trap states in Rubrene single crystals under the influence of different ambient conditions as well as under the influence of an electric field perpendicular to the crystal surface ("gate bias stress"). In these studies the trap density is monitored via the evolution of the turn-on voltage $V_{\rm on}$ and the threshold voltage V_t, which are proportional to the amount of trapped charge. Our measurements show that both $V_{\rm on}$ and V_t shift in a reversible and reproducible way upon the application of a gate bias voltage (cf. Fig. 1.3). The details of this shift indicate that the microscopic origin of this behavior is solely the filling and emptying of deep traps (10^{12} cm^{-2}) at the interface and most likely not a chemical modification of the material which would lead to trap generation. Interestingly, the mobility of holes in the FET channel is only little affected by the trapped charge.

This "chemical stability" of Rubrene is in contrast to the behavior of Pentacene single crystals, for which it has been reported that bias stress leads to "chemical instability", namely to H-diffusion between the molecules and thus to the generation of traps (D. Lang et al., PRL 93, 076601).

The relaxation times for the process we observe in Rubrene are on the order of tens of minutes at room temperature (cf. Fig. 1.3). Future studies will focus on the microscopic origin of different kinds of surface and bulk traps and their influence on the transport properties.

1.1.5 Rocking curves of iodine-intercalated pentacene crystals

S. Haas and B. Batlogg

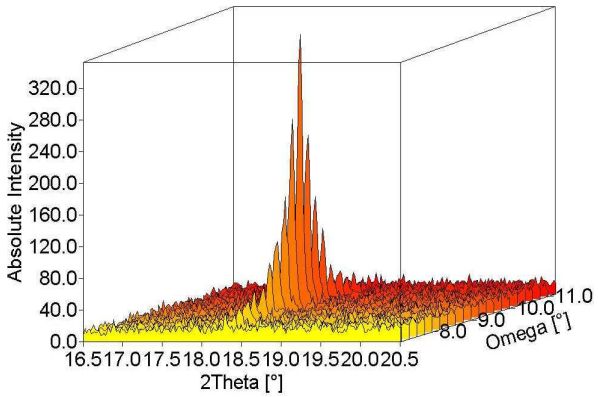

Figure 1.4: The 003 reflection originating from the intercalated phase was recorded by a PSD (2θ-axis) for various ω-positions of the sample (stepsize: 0.2°). Intensity integrated over 2θ versus ω corresponds to a conventional rocking curve.

One approach to induce charge in organic molecular semiconductors is bulk chemical doping with intercalated charge donors. In contrast to conventional semiconductors, here we have about as many iodine ions as pentacene molecules, which modifies the structural properties drastically. The interlayer spacing (d_{001}) is enhanced by 30 % from 14.1 Å to 19.2 Å. Therefore the samples suffer from structural degradation: While the virgin pentacene crystals have rocking curve widths as low as a few 1/100 degrees, this value increases to ∼1 degree. The enhanced d-spacing is well defined, reflected in a narrow peak width in 2θ. Due to more grain boundaries and thus more structural flexibility, the quality of thin films, as seen in the rocking curves, is lower to start with ($\Delta\omega$ ∼0.2°), but is relatively less affected by the intercalation process ($\Delta\omega$ ∼0.4°.)

The heavy doping leads to a metallic T-dependence of the resistance at low temperature, but the resistivity is rather high due to the structural defects. After partial desorption of iodine, the room temperature resistance increases by a factor of ∼100, and the T-dependence becomes non-metallic.

1.1.6 Anisotropic and negative thermal expansion of acene molecular crystals

S. Haas, T. Siegrist (Bell Labs, Murray Hill NJ) and B. Batlogg

Organic molecular crystals usually exhibit a lower symmetry than conventional inorganic materials, and the thermal expansion is anisotropic. We have performed structure studies at various temperatures on high-quality pentacene and rubrene crystals.

In order to compare crystals of different symmetry, it's necessary to transform the expansion along the (usually non-orthogonal) crystal axes to an orthogonal system. The resulting values of the three main axes of the expansion ellipsoid for molecular crystals of acenes are shown in figure 1.5. The plot is based on our measurements, and on data from the literature. Significant negative expansion (contraction) in a particular crystal direction is seen for tetracene and pentacene.

The anisotropic (and negative) expansion requires slow cooling and heating rates to minimize mechanical strain of the crystals, including particularly the first cooling after crystal growth and the numerous thermal cycles necessary for the SCLC trap spectroscopy described above (1.1.1).

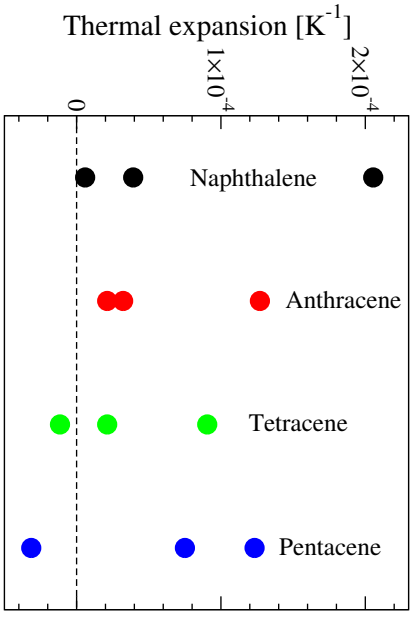

Figure 1.5: Crystals of linear acenes have strongly anisotropic thermal expansion. Tetracene and pentacene contract along one axis upon warming.

1.2 Organic thin film transistors

1.2.1 A new Bi-Thiophene oligomer as organic semiconductor

K. P. Pernstich and B. Batlogg

D. Iosip - Institute of Macromolecular Chemistry, Romania

S. Destri, M. Pasini, W. Porzio - Istituto per lo Studio delle Macromolecole, Italy

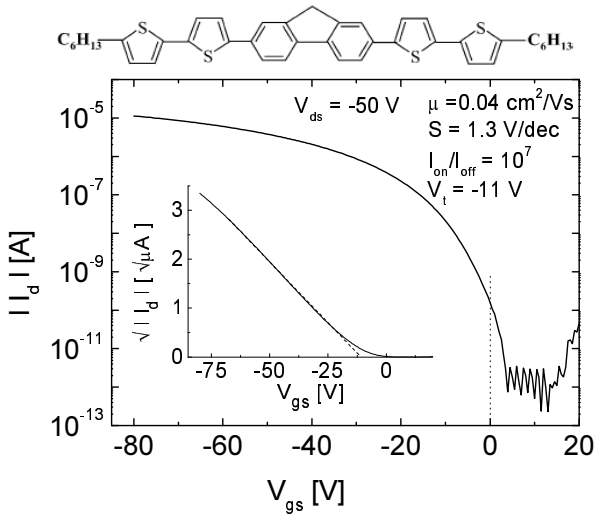

Figure 1.6: Molecular structure of the new oligomer (top) and transfer characteristic of a TFT (bottom).

rated to form source and drain contacts.

Measuring the transistors in an inert atmosphere gave a mobility of 0.04 cm^2/Vs, a promising value. The transfer characteristic is shown in Fig. 1.6 together with other electrical parameters. Operating the device in room air resulted in a pronounced offset of the transfer characteristic by a (gate) voltage of approx. 50 V, indicating that the chemical stability of the molecule unit was not optimal. The offset was accompanied with an increase of the trap density as indicated by an increase of the subthreshold swing and could be reversed when operating in an inert atmosphere again. The mobility was found to be temperature dependent (see Fig. 1.7) with an activation energy of approx. 150 meV. Further studies are aimed to optimize the chemical protection of the organic semiconductor during exposure to ambient air.

One big advantage of organic materials is the seemingly endless number of different molecules that can be synthesized. With a proper understanding of the governing mechanisms it is possible to design molecules with tailored properties. In this work we have investigated the semiconducting properties of a new Bi-Thiophene oligomer (see Fig. 1.6 (top)) which consists of different building blocks. We are studying the effect of these building blocks on the environmental stability of the material when used as the active layer in organic transistors.

To this end, we have fabricated thin-film field-effect transistors (TFTs) on heavily doped and oxidized Si wafers which acts as gate electrode and gate insulator. On top of the gate insulator, a monolayer of octadecyltrichlorosilane was formed, which is known to improve the electrical characteristics of many organic TFTs. The new oligomer was thermally evaporated through shadow masks at a base pressure near 10^{-6} mbar. In the last step gold was evapo-

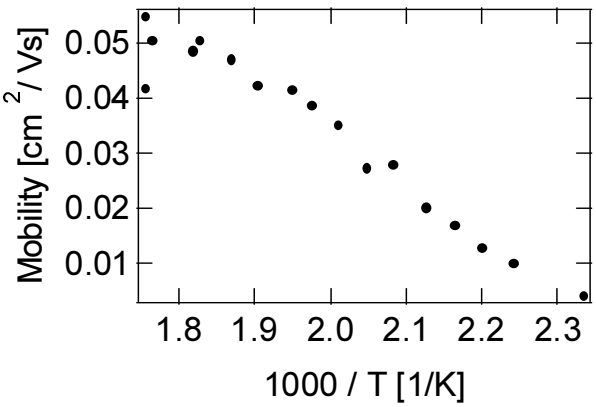

Figure 1.7: Temperature dependance of the mobility.

1.2.2 High mobility n-channel organic TFTs and OTFT complementary inverters

David J. Gundlach, Kurt P. Pernstich, Matthias Grüter, Georg Wilckens, and Bertram Batlogg

Organic thin film transistors (OTFTs) fabricated from organic semiconductors such as pentacene are routinely reported to have performance that is comparable to that of hydrogentated amorphous silicon (a-Si:H) TFTs, thus making

OTFTs of interest as a disruptive technology for current and future large area electronics applications. To date most OTFTs reported on operate as accumulation or weakly depletion mode p-channel devices. OTFTs which operate as accumulation mode n-channel devices with performance matched to that of the best p-channel OTFTs are of technological interest for realizing complementary all-organic circuitry, but realizing similar performance has proven to be difficult. In this study we fabricated n-channel OTFTs on oxidized silicon wafers using N,N'- ditridecylperylene-3,4,9,10-tetracarboxylic diimide (PTCDI-$C_{13}H_{27}$) as the semiconductor and having a field-effect mobility comparable to that typically obtained for pentacene TFTs. Au, Cr, Al, and LiF/Al source and drain contacts were studied. Accumulation mode n-channel transistor operation was demonstrated for all contact metals despite the large differences in their work functions indicating charge injection may occur via a tunneling process. The high field effect mobility near 0.6 cm^2/Vs and large I_{on}/I_{off} of 10^7 achieved compares favorably with the best reported performance for OTFTs fabricated using this material class. Despite the impressive device performance device instability was observed. The charge trapping dynamics are the subject of current study. However, the device instability did not prevent the building of pentacene/PTCDI-$C_{13}H_{27}$ TFT complementary inverters with relatively short propagation delays and high gain.

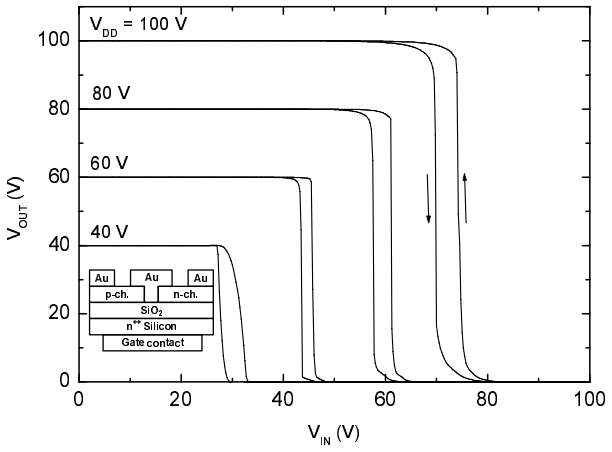

Figure 1.8: Voltage transfer characteristics for a pentacene/PTCDI-$C_{13}H_{27}$ TFT complementary inverter. The inset shows the OTFT complementary inverter cross-section.

The voltage transfer characteristics for a pentacene/PTCDI-$C_{13}H_{27}$ TFT complementary inverter are plotted in the Figure, and the inset to the Figure shows the OTFT complementary inverter cross-section. The voltage sweep direction is given by the arrows and the hysteresis in the transfer characteristics is mainly due to bias stress induced threshold voltage changes for the PTCDI-$C_{13}H_{27}$ (n-channel) TFT. Propagation delays as short as 250 ms were extracted from pulsed measurements and from the voltage transfer characteristics we extract gain as large as 140 for large V_{DD}. The propagation delay is mainly limited by the mobility of the n-channel device and channel length (50 μm). Significant improvements are expected for optimized circuit designs.

1.3 Superconducting oxides: $RbOs_2O_6$ with pyrochlore structure

M. Brühwiler, S.M. Kazakov, J. Karpinski and B. Batlogg

The pyrochlores constitute ideal systems to study to what degree itinerant electrons are affected by geometrically frustrated interactions, and what ground states are realized in such systems. This is because the network of the relevant metal atoms consists of corner-sharing tetrahedra. The pyrochlore structure in general is of type $A_2B_2O_6O'$ with space-group $Fd\bar{3}m$. The recently discovered β-pyrochlore $RbOs_2O_6$ is derived from the parent compound by replacing the O′ atoms by Rb atoms, leaving the 16d site empty, and occupying the B site by the transition metal cation Os.

We have developed a detailed analysis for the extraction of thermodynamic parameters for samples containing a superconductor of interest and a second metallic non-superconducting component. We have applied the analysis, which we call condensation energy analysis (CEA), to $RbOs_2O_6$ to extract its *intrinsic thermodynamic parameters*. Some of the main results from our analysis are as follows: $RbOs_2O_6$ is a strong type-II superconductor ($\kappa(T_c) = 23$) and the superconducting electronic specific heat indicates conventional s-wave pairing. From the upper critical field $\mu_0 H_{c2} \approx 6\,\mathrm{T}$ at $0\,\mathrm{K}$, we estimate a Ginzburg-Landau coherence length $\xi \approx 74\,\text{Å}$.

In particular, we have been able to extract the electronic specific heat in the superconducting state $C_{\rm es}(T)$ showing the specific heat jump at the critical temperature to be $1.9 \cdot \gamma T_{\rm c}$. This value corresponds to an electron-phonon coupling constant $\lambda_{\rm ep} = 1 \pm 0.1$. Together with the Sommerfeld coefficient of $44\,{\rm mJ/mol_{f.u.}/K^2}$, which is rather high for a pyrochlore, our results indicate a remarkably large enhancement of the Sommerfeld coefficient by a factor of 4 compared to the calculated band value. Additional to the electron-phonon enhancement $\lambda_{\rm ep}$, there is thus a strong enhancement of unknown origin $\lambda_{\rm add} \approx 2$. We expect that the additional enhancement is due to electron-electron correlation effects.

It remains to be elucidated, if the origin of this mass enhancement lies in the 3-dimensional triangular nature of the pyrochlore lattice. In any case, the characterization of this osmate promises to provide new insight into the physics of correlated electron systems.

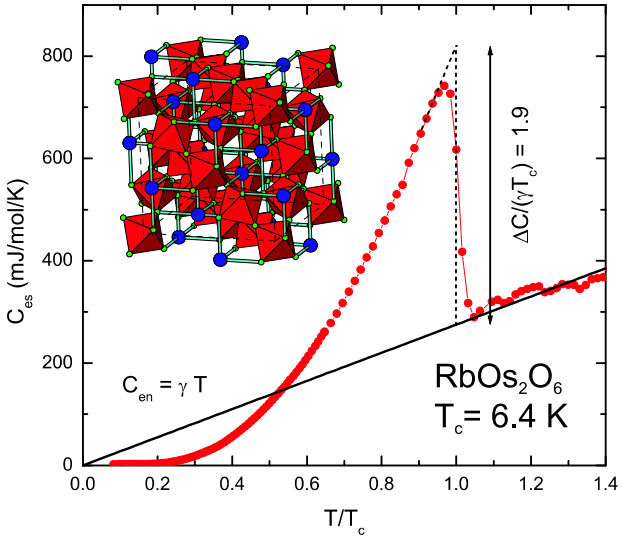

Figure 1.9: Superconducting electronic specific heat of $\rm RbOs_2O_6$ $C_{\rm es}(T)$ showing the specific heat jump at the critical temperature of $1.9 \cdot \gamma T_{\rm c}$. This jump corresponds to an electron-phonon coupling constant of $\lambda_{\rm ep} \approx 1$, leaving an additional enhancement of $\lambda_{\rm add} \approx 2$ due to other mechanisms. The inset shows the β-pyrochlore structure of $\rm RbOs_2O_6$.

1.4 SiGe modulation doped heterostructures

B. Rössner, H. von Känel and B. Batlogg in collaboration with D. Chrastina, G. Isella (Politecnico di Milano)

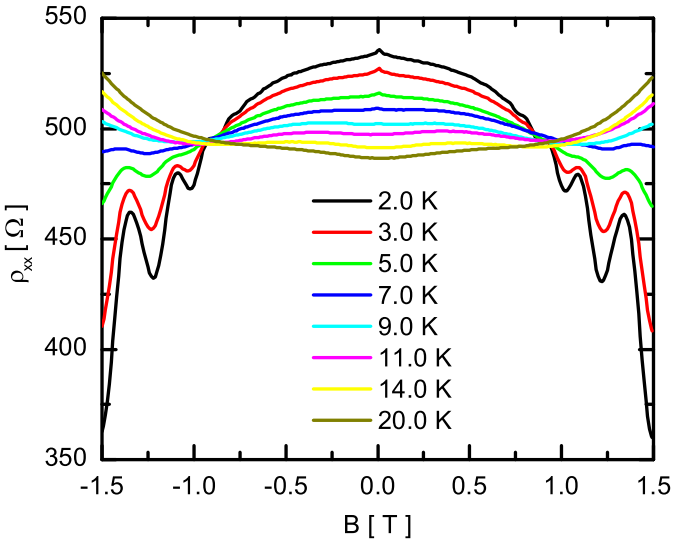

Figure 1.10: Magnetoresistance of sample 7158-22 between 2 K and 20 K. Note the common intersection of all traces at about $B = 0.9$ T. This kind of behaviour is expected for interaction contribution to conductivity. The carrier density in this example is 2.87×10^{11} cm^{-2}, mobility $\mu = 44000\,{\rm cm^2/Vs}$.

Silicon-Germanium heterostructures are of high importance for future high-speed electronics, replacing pure silicon. They offer superior performance while being compatible with current processing technology. To make use of pure Germanium as channel material, thick graded buffers are commonly used. The Low Energy Plasma Enhanced Chemical Vapour Deposition (LEPECVD) process is ideally suited for this task, offering growth rates up to 10 nm/s. By changing the growth conditions, precise layer thickness control can be achieved which was used to grow a range of p-modulation doped heterostructures with a 15-17 nm channel of pure Ge embedded in $\rm Si_{0.3}Ge_{0.7}$ cladding.

To further broaden our understanding of the charge transport mechanism in such structures, we investigate the magnetotransport at liquid helium temperatures. When a magnetic field is applied perpendicular to the layer plane, the 2-dimensional hole gas shows magnetoresistance whose sign depends on temperature and carrier density. As the temperature is decreased below a critical temperature, interaction effects increase the zero-field resistance. Furhtermore there exists a magnetic field at which the resistance is temperature independent. The figure shows an example.

At low carrier densities an almost parabolic B-dependence of ρ_{xx} is observed and attributed to electron-electron interaction in the diffusive transport regime. Owing to the large spin-split coefficient $\kappa = 3.41$ of the $|3/2 \pm 3/2\rangle$ states of the heavy hole band in Germanium (Silicon: $\kappa = -0.42$) the field induced energy shift between spin

directions can not be neglegted. It leads to a significant modification of the Hartree interaction between opposite spin directions. The Fermi liquid parameter F acts as a measure of the relative importance of common spin and opposite spin Hartree correction to conductivity. As the carrier density is increased, the Zeeman term becomes more important, indicating increasing F.

1.5 Materials synthesis and high pressure crystal growth

1.5.1 Crystal growth of pure and substituted MgB_2 and $YBa_2Cu_4O_8$ superconductors

N. D. Zhigadlo, S. M. Kazakov, J.Jun, J.Karpinski

For the investigation of intrinsic properties of strongly anisotropic compounds such as HTS or MgB_2 single crystals are necessary. Due to non-congruent melting of majority of these compounds single crystal growth is a difficult task. In most cases single crystals can be grown only from a non-stoichiometric melt. The melt used for the growth of cuprates or borides contains gaseous or volatile components such as O_2, Hg or Mg. Partial pressure of these components at meting temperature can reach values of tens or hundreds of bars. Therefore two kinds of pressure effects have been used in our laboratory for the crystal growth: high gas pressure of volatile component or/and high hydrostatic pressure for the stabilization of the structure of grown single crystals. In year 2004 growth of pure and substituted MgB_2 crystals has been investigated. Mg has been substituted with Al, Fe, Mn and Co, while B has been substituted with C. Various levels of substitutions have been done with a goal to obtain homogeneous crystals for physical studies. This is a difficult task due to complicated chemistry leading to precipitation of different phases in the crystals. In the case of Mn and C substitution it was possible to grow single phase crystals in a substitution range up to $x = 0.07$ and $x = 0.3$ in $Mg_{1-x}Mn_xB_2$ and $MgB_{2-x}C_x$ respectively, while Al substitution turn out to be more difficult and single phase crystals were grown up to $x = 0.1$. Fe substitution was possible up to $x = 0.03$, but $Mg_{1-x}Fe_xB_2$ crystals contain intergrowth of non-superconducting phase with larger content of Fe. Preliminary experiments with Co and Cr substitutions have been performed and samples are investigated. Crystal growth process of pure MgB_2 has been further developed and crystals for various physical experiments have been grown. Crystal growth experiments of $YBa_2Cu_4O_8$ have been continued with an aim to grow crystals for spectroscopic studies.

1.5.2 New high pressure anvil apparatus

In 2004 a new high pressure anvil device has been put into operation. It is a uni-axial, opposite anvil device, in which pressures up to 70 kbar at temperatures up to 1800 °C can be reached. This equipment will be used for the synthesis of compounds at pressure higher than 40 kbar available up to now in our lab. Test runs have been performed and diamonds crystals were grown.

1.5.3 Influence of magnetic and non-magnetic substitutions on superconducting and structural properties of MgB_2.

N.D.Zhigadlo, K.Rogacki, S.M.Kazakov, G.Schuck, J.Jun, B.Batlogg, J.Karpinski

We have studied the influence of substitutions on superconducting and structural properties of MgB_2. Single crystals have been grown at high pressure of 30 kbar at temperature 1800-2000°C. The very high crystals quality expresses itself in a low residual resistivity ρ_o(40 K) = 0.5 $\mu\Omega$cm. The presence of two bands with distinct superconducting gaps Δ_σ and Δ_π in the MgB_2 superconductor leads to several unusual properties. An interesting feature is the temperature and field dependent anisotropy, which dominates the magnetic and transport properties. This anisotropy depends on the intraband electron diffusivities as well as on the interband scattering. Both the intraband and the interband scattering can be modified in a controlled way by partial substitution of nonmagnetic ions for Mg (e.g. Al) or B

(e.g. C). The critical temperature T_c as a function of substitution is shown in Fig.1.11. An additional tuning of the diffusivities, and thus the control of the superconducting and normal state properties, can be performed by appropriate substitutions with magnetic ions (Mn, Fe, Co, Ni). Pair-breaking by the exchange interaction between the band electrons and the 3d electrons has been studied.

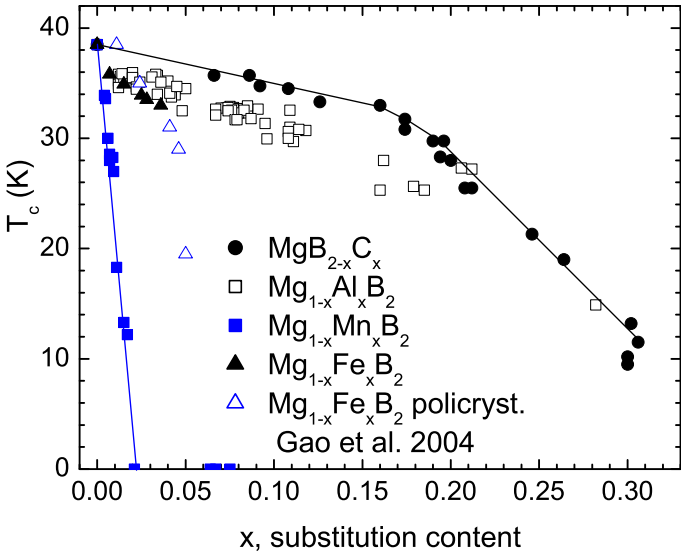

Figure 1.11: Influence of C, Al, Mn and Fe substitution on the critical temperature T_c of MgB_2.

The magnetic properties of substituted crystals were investigated with SQUID and torque magnetometers, and electrical transport properties with the Quantum Design PPMS. Al and C substitutions influence the electronic structure, increase scattering and decrease the mean free path which in the case of carbon substituted crystals leads to the strong increase of the upper critical field for both directions of field $H||ab$ and $H||c$. $H_{c2}^{||c}$ increases from 3.5 T (0 K) to about 8 T (0 K). Al substitution has a minor influence on the upper critical fields, and from the H_{c2} slopes near T_c one concludes that the diffusivity in the σ - band slightly decreases within the layers, but increases perpendicular to the layers. The upper critical field anisotropy decreases significantly for both Al and C substitutions. Mn as a magnetic impurity causes T_c to drop rapidly due to strong interaction of the band electrons with the 3d local moments.

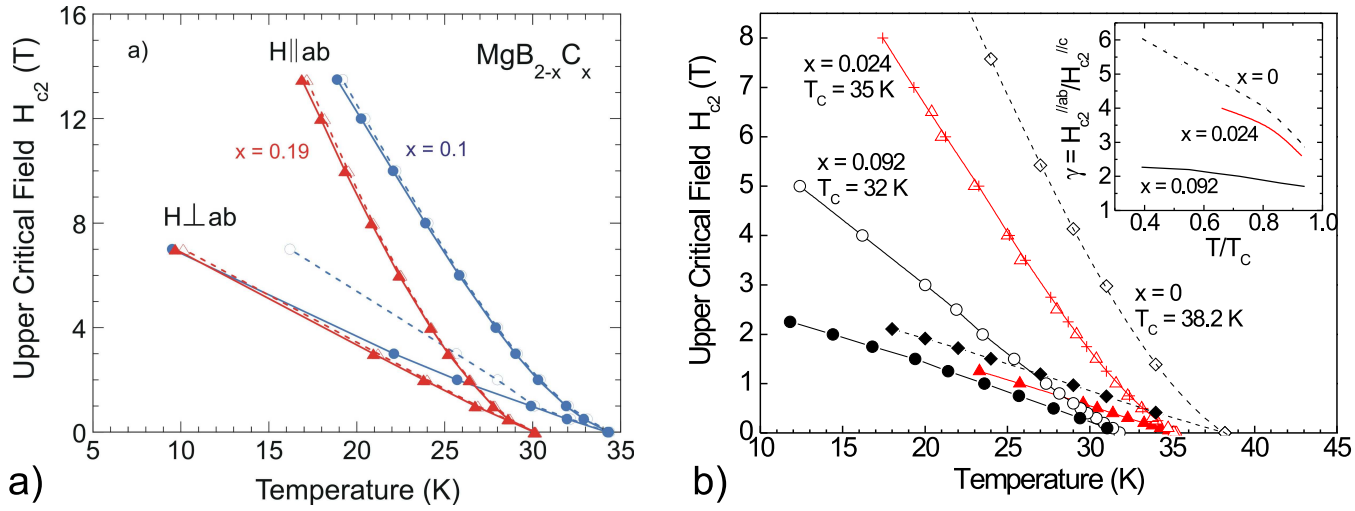

Figure 1.12: Influence of C (a) and Al (b) substitutions on the upper critical field and the H_{c2} anisotropy ($Mg_{1-x}Al_xB_2$) investigated by resistivity (a) and by both magnetization and resistivity (crosses) measurements (b).

1.5.4 Structure analysis of $Mg_{1-x}Al_xB_2$ and $MgB_{2-x}C_x$ single crystals.

G. Schuck, S. M. Kazakov, J. Karpinski (in collaboration with E. Müller and Ch. Soltmann)

Many as grown crystals show a variety of structural defects such as intergrowth, twinning, inclusions of other phases, precipitation of the same phase with different composition etc. In order to make physical studies more reliable careful structural analyses have to be made on the same crystal used later for other investigations.

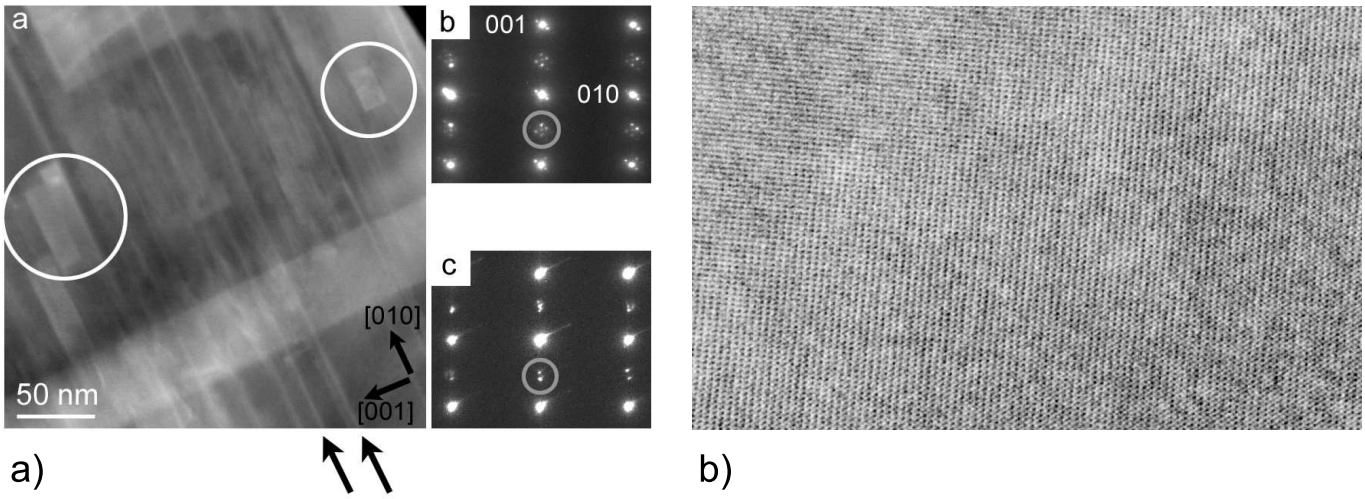

Figure 1.13: a) $Mg_{1-x}Al_xB_2$ crystal: HRTEM atomic mass-contrast image of an area containing rectangular shaped areas with brighter contrast (white circles), which are Al - rich domains. b) HRTEM image of $MgB_{2-x}C_x$ crystal showing nearly perfect structure without any precipitations.

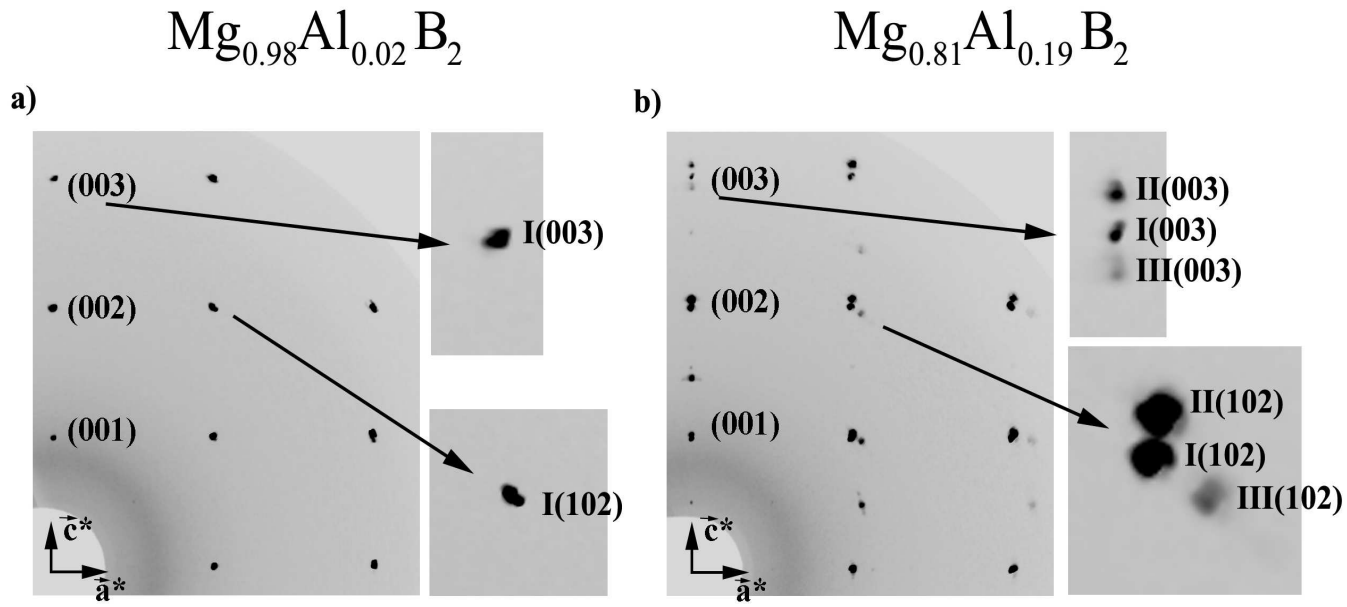

Figure 1.14: Reconstructed layers (0kl) of $Mg_{1-x}Al_xB_2$ single crystals. One can notice splitting of the reflections due to phase separation for 19% Al substitution.

For the carbon substituted crystals, the two-dimensional profiles of x-ray reflections show the elongation of the reflections along the c* direction in reciprocal space. This indicates crystal disorder, but HRTEM investigations indicate a perfect structure (Fig.1.13b)). Refinement of the structure shows a possible lower occupation of the Mg position. Most probably these structural defects are responsible for the increase of H_{c2} and the broadening of X-ray reflections. In aluminium substituted crystals, for Al content higher than 10%, phase precipitation of the $MgAlB_4$ phase has been frequently observed. The separation of additional phase leads to a splitting of the reflection peaks. Structural investigations performed with the Image Plate Diffractometer show such splitting due to phase precipitation in the crystals with large Al content (Fig. 1.14). This has been confirmed by HRTEM investigations. Figure 1.13a) shows an example of such a crystal with domains of the $MgAlB_4$ phase.

1.5.5 Synthesis of superconducting pyrochlore $RbOs_2O_6$

S.M.Kazakov, N. D. Zhigadlo, J.Karpinski

Recently materials in which the magnetic interactions are geometrically frustrated have attracted considerable interest [1]. In compounds crystallizing in the pyrochlore structure, with general composition $A_2B_2O_7$, the corner-sharing BO_6 octahedra form a three-dimensional (3D) network of tetrahedrally arranged B atoms, leading to geometric frustration of antiferromagnetic coupling among them. Transition metal oxides with a pyrochlore type structure exhibit a wide range of interesting physical properties, varying from highly insulating to metallic. Recently a new class of transition metal oxide superconductors AOs_2O_6 (A=K, Rb, Cs) have been found [2]. We have synthesized $RbOs_2O_6$ by encapsulation in vacuum and by high pressure techniques. Suitable chemical treatment of the as-prepared sample allowed us to eliminate the impurity phases. The superconducting transition temperature ($T_c = 6.4$ K) of $RbOs_2O_6$ was found to be the same for both preparation methods. Structural investigations showed that Rb atoms occupy the 8b site in the pyrochlore lattice with a lattice parameter of 10.1137(1) Å. A comparison with the other superconducting pyrochlore superconductors suggests that T_c is enhanced by a smaller lattice constant a. Magnetic measurements under hydrostatic pressure reveal very high positive pressure shift $\delta T_c/\delta p = 0.09$ K/kbar, in contrast to the negative pressure shift in conventional superconductors.

[1] J.E. Greedan, J. Mater. Chem. 11 (2001) 37.
[2] S. Yonezawa, Y. Muraoka, Y. Matsushita, and Z. Hiroi, J. Phys.: Condens. Matter. 16 (2004) L9.

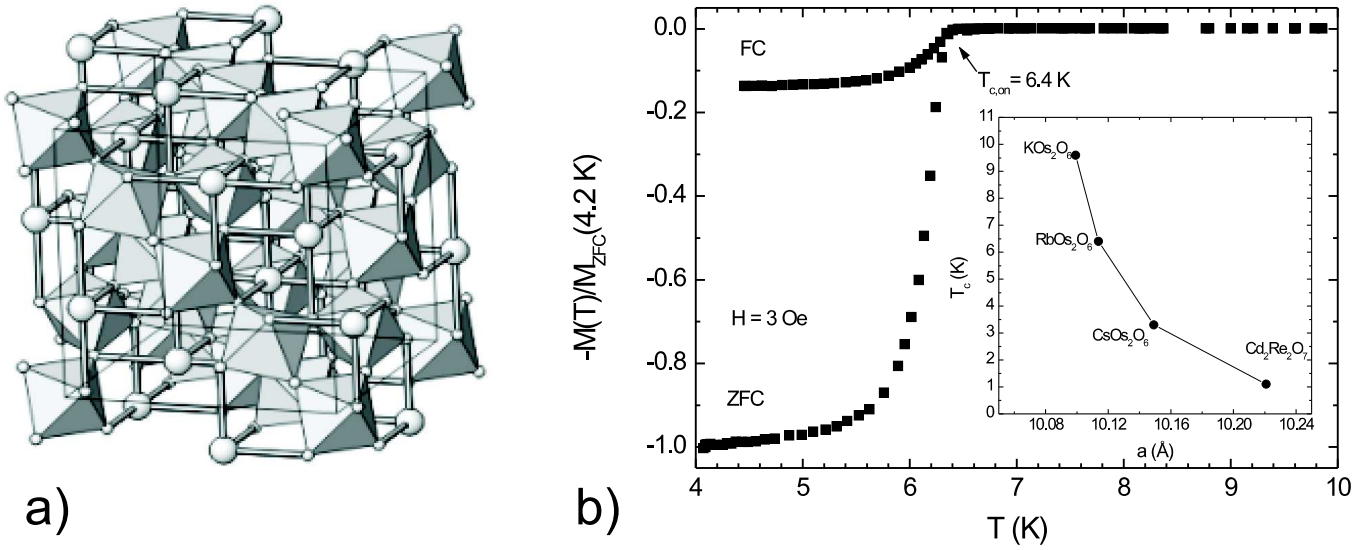

Figure 1.15: a) The structure model for $RbOs_2O_6$. Os atoms are located in the middle of OsO_6 octahedra, the Rb atoms (shown as big spheres) are in 8b site of $Fd\bar{3}m$ space group. (b) The normalized magnetization of the ceramic sample of $RbOs_2O_6$ synthesized under a high-pressure/high-temperature condition. The inset shows the critical temperature T_c as a function of lattice parameter a for superconducting pyrochlores.

1.5.6 Investigations of pure and substituted MgB_2, $Na_{1-x}CoO_2$, $RbOs_2O_6$ and $NaVGe_2O_6$ in collaboration with other laboratories.

1. Effects of neutron irradiation on superconducting properties of MgB_2, $Mg(B_{1-x}C_x)_2$ and $HgBa_2CuO_{4+x}$ single crystals. In collaboration with H.Weber of the Atom Institute in Vienna.

2. Anisotropic properties of MgB_2 by torque magnetometry. In collaboration with R.Puzniak and A.Wisniewski of the Institute of Physics Polish Academy of Sciences in Warsaw.

3. Point-contact spectroscopy of MgB_2, $Mg(B_{1-x}C_x)_2$ and $Mg_{1-x}Al_xB_2$ single crystals. In collaboration with R.Gonnelli of the Politecnico Torino.

4. Isotope effect in the magnetic penetration depth of MgB_2. In collaboration with D. Di Castro and H.Keller of Physik Institut Uni Zürich.

5. Magneto-thermopower of single-crystal MgB_2. In collaboration with T.Plackowski of the Institute of Low Temperature and Structural Research in Wroclaw.

6. De Haas - van Alphen oscillations in the superconducting state of MgB_2. In collaboration with A.Carrington of the University of Bristol.

7. Picosecond dynamics of the superconducting state in MgB_2. In collaboration with R.Sobolewski of the Rochester University.

8. Magnetic field penetration depth measurements in $YBa_2Cu_4O_8$. In collaboration with R.Khasanov and H.Keller of Physik Institut Uni Zürich.

9. NMR investigations of the charge ordering in $Na_{0.7}CoO_2$. In collaboration with J.L.Gavilano and H.R.Ott in our laboratory.

10. Thermal conductivity of pure and substituted MgB_2. In collaboration with A.Sologubenko and H.R.Ott in our laboratory.

11. Pressure effects on the transition temperature and the magnetic field penetration depth in the pyrochlore superconductor $RbOs_2O_6$. R.Khasanov, H.Keller of Physik Institut Uni Zürich.

12. NMR and dc susceptibility studies of $NaVGe_2O_6$. In collaboration with J.L.Gavilano and H.R.Ott in our laboratory.

1.5.7 Temperature dependent Al solubility in $Al_xGa_{1-x}N$ single crystals

P. Geiser, J.Jun, L. Klemm (Isotope Geochemistry and Mineral Resources, ETHZ), P. Wägli, S.M. Kazakov, J. Karpinski, B. Batlogg

After having succeeded in growing $Al_xGa_{1-x}N$ bulk single crystals, as reported in the last annual report, a central question concerns the maximum Al content that can be reached by this technique. Thus we explore the temperature dependence of the Al solubility by studying samples (up to 1 mm length) by XRD, photoluminescence and energy dispersive X-ray analysis. These methods indicate an Aluminum content of up to 30%. A more refined study includes measurements with Laser Ablation Mass Spectrometry (LA-ICPMS). Al concentrations can be measured from the percent down to the ppm range. The method has a spatial resolution of 20 μm (lateral) and less than 0.5μm (depth profile) respectively. Depth profiling of $Al_xGa_{1-x}N$ bulk single crystals provides interesting information: As shown in Figure 1.16, the Al count rate is low near the crystal surface and reaches its bulk concentration only after some time. Calibrating the ablation depth using an optical microscope, the Al free zone near the crystal surface has a thickness of 1 μm on some samples up to 2 μm. The thickness typically increases along a line from the nucleation zone (A in Fig. 1.16) to B. We compared these results with data measured on crystals grown with the high nitrogen

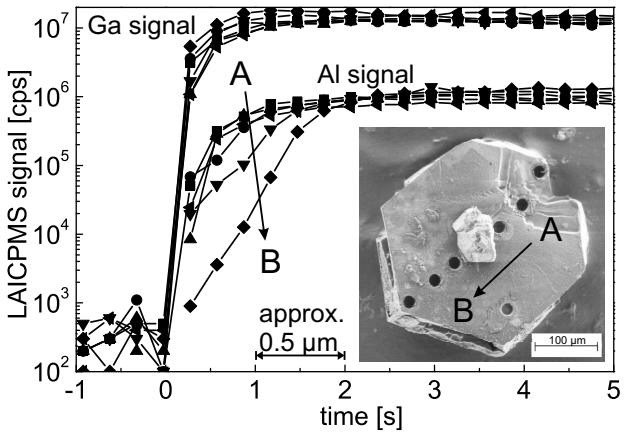

Figure 1.16: $Al_xGa_{1-x}N$ bulk single crystal with holes from laser ablation. The Al count rate reaches its bulk concentration value with some delay in comparison to the Ga signal, indicating a GaN capping layer with increasing thickness along the line from A to B.

pressure solution growth (HNPSG) method. Such crystals also contain (intentionally added) Al, but the method is limited to x < 0.02. We find that a low Al content zone exists on both types of crystals, independent on the availability of Al during crystal growth. From measurements on HNPSG crystals we know further, that the Al solubility shows a clear onset in the temperature range from 1400°C to 1500°C. The formation of an Al free zone on $Al_xGa_{1-x}N$ bulk single crystals can be explained with the experimental procedure. Ramping down the temperature at the end of the process leads to a quick reduction of the Al solubility. At the same time, there is still excess nitrogen dissolved in the alloy surrounding the crystals. With the increased supersaturation at lower temperature, crystallization of Al free GaN occurs. The picture of a thin GaN layer on top of a bulk $Al_xGa_{1-x}N$ single crystal fits well into the picture of the other methods as the data exhibit corresponding features. Based on these results, experimental procedures and sample preparation are optimized.

1.5.8 Scaling up the size of GaN bulk single crystals

P. Geiser, J. Jun, J. Karpinski

GaN bulk single crystals are the best substrates available for group III nitride epitaxy, due to their low dislocation density (4 orders of magnitude lower than every other substrate). Using crystals grown in our 30 mm high pressure autoclave (maximum size $4 \times 5\,mm^2$) we developed the necessary steps (polishing, Plasma etching, MBE growth) over the past years. The work was done in collaboration with the Institute for Geology and FIRST Laboratory at ETHZ. As the crystal size only allows for layer growth but not device processing, we built up a new high pressure autoclave with a bore diameter of 40 mm. Leaving space for heater and thermal isolation, the crucible inner diameter could be increased from 8 mm (30 mm bore hole) to more than 14 mm in the new vessel. The maximum pressure the construction can withstand is 12 kbars. This allows to grow GaN crystals at a temperature up to 1500°C. The new vessel is an extension to our existing 30 mm autoclave. The latter serves as a hydraulic pressure intensifier feeding the 40 mm setup.

During the 3^{rd} and the 4^{th} quarter of 2004 we optimized the growth procedure to make use of the additional space inside the crucible. As shown in Fig. 1.17 good results were achieved running the first set of experiments. The largest crystals found ($5 \times 10\,mm^2$) even exceed the expected size of about 7 mm length. Currently the process is tuned to further suppress growth in c-axis direction. Such features must be removed by time consuming polishing and should be avoided. As shown in Fig 1.17 (red background) crystals can be grown without c-axis features, some areas of the $(000\bar{1})$ face being atomically flat. The sample size and quality available with the new high pressure autoclave allows for homoepitaxy substrate fabrication. The substrates will be suitable for laboratory scale device processing.

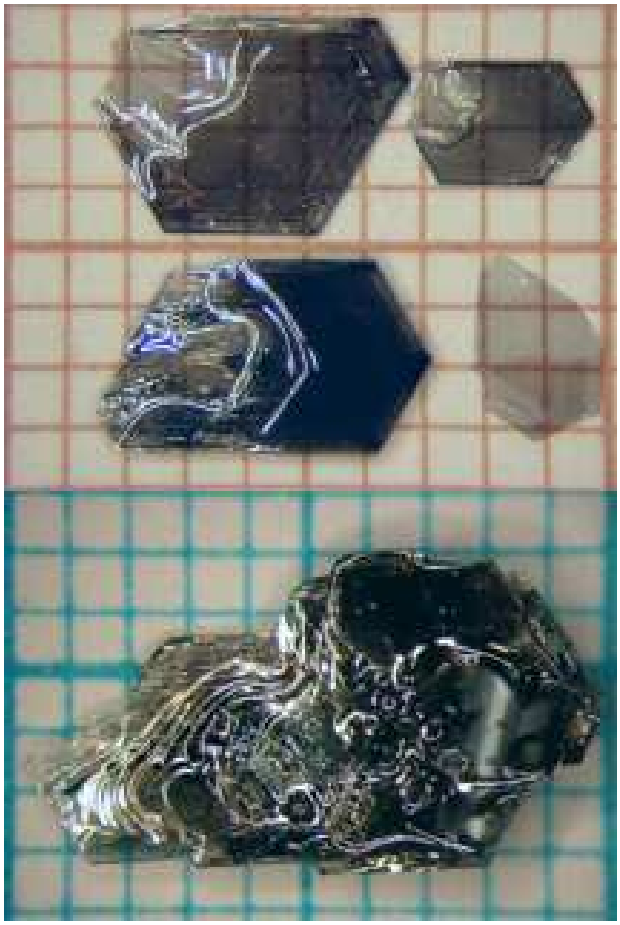

Figure 1.17: GaN single crystals. Red background: (0001) crystal faces, as grown. Suitable conditions allow to suppress fast growth in c-axis direction. Blue background: maximum crystal size possible for an autoclave with 40mm bore hole.

Chapter 2

Physics of mesoscopic structures, semiconductor nanostructures

(http://www.nanophys.ethz.ch)

Head
Prof. Dr. K. Ensslin

Academic Staff

A. Baumgartner	S. Gustavsson	Dr. E. Müller
C. Ellenberger	Dr. T. Ihn	A. Pioda
Dr. M. Ferrier	Dr. S. Kicin	E. Ruh
A. Gildemeister	Dr. K. Kobayashi	Dr. R. Schleser
D. Graf	Dr. R. Leturcq	M. Sigrist
B. Grbic	L. Meier	Dr. B. Simovic

Technical Staff

C. Barengo	P. Studerus

Academic Guests
Prof. Caio Lewenkopf, Univ. of Rio de Janeiro (4.10.2004-8.10.2004)

Administrative Staff
B. Abt

2.1 Spatially resolved manipulation of single electrons in quantum dots using a scanned probe

A. Pioda, S. Kicin, T. Ihn, M. Sigrist, A. Fuhrer, K. Ensslin, in collaboration with A. Weichselbaum and Sergio E. Ulloa, Ohio University, and M.Reinwald W. Wegscheider, Univ. Regensburg

Quantum dots have been defined by room temperature local anodic oxidation with a scanning force microscope which allows to write oxide lines on a semiconductor surface that locally deplete the 2DEG underneath. The number of electrons in the quantum dot can be controlled by the lateral plunger gates. Experiments are performed with a scanning force microscope in a 3He cryostat with a base temperature of 300 mK. The scanning sensor consists of a PtIr wire with an electrochemically sharpened tip (typical radius a few tens of nanometers) mounted on a piezoelectric tuning fork. A local potential is induced below the tip in the 2DEG. Its strength and sign depends on the tip bias voltage, its geometric shape and extent reflects the tip shape and the tip-sample separation.

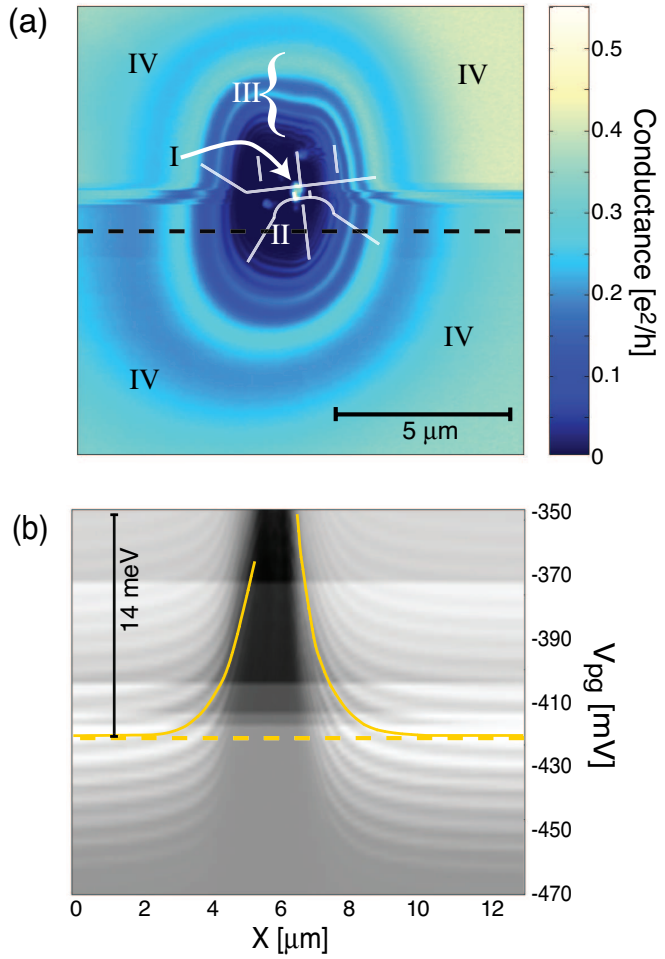

Figure 2.1: Imaging the tip-dot interaction. (a) Scanning gate image measured with the tip ($V_{tip=0}$) scanned in feedback at a distance of a few nanometers from the surface. The oxide lines defining the structure have been drawn as white lines. Regions (I) to (IV) describe the regime of weak coupling (IV) to very strong coupling (I) between tip and to. (b) Dot current obtained while scanning the tip along the horizontal dashed line indicated in (a), for different values of the plunger gate voltage. The lines following specific conductance peaks represent the tip-induced potential. The horizontal dashed line corresponds to the plunger gate voltage V_{pg} used for the scan shown in (a).

Moving the tip in the vicinity of the quantum dot affects its conductance via the induced potential by changing the coupling strength to source and drain and by shifting the energy levels. Scanning gate images are maps of the dot's conductance as a function of tip position.

Figure 2.1(a) shows a scanning-gate image taken at a gate voltage that tunes the dot, in the absence of the tip, into the Coulomb blockade regime. Four different regions labeled I to IV with the dot in the center may be distinguished: (I) The central bright peak of increased conductance when the tip is directly above the quantum dot, (II) the dark blockaded region where no measurable current ows through the dot, (III) the region of concentric conductance peaks around the dark blockaded region and (IV) a region of weakly varying conductance at larger distance from the dot. The setup allows measuring conductance variations in the range of 100 fA on length scales below 30 nm at reasonable scan speeds. The topographic resolution achieved at base temperature is also about 30 nm. The constant conductance region (IV) arises when the tip is too far away from the dot to have signi cant in uence on its conductance. When the tip comes closer [region (III)], the potential energy of electrons in the dot is increased and they spill over into source or drain one by one. Each of the conductance peaks forming the ring-like pattern indicates that a single electron leaves the quantum dot. These conductance oscillations correspond to the oscillations usually induced by the plunger gate rather than by the moving tip-induced potential. The closed curve around the dot defined by the position of a particular conductance peak corresponds to a constant potential in the quantum dot. This means, that conductance peaks map out contour lines of constant interaction potential between the tip and individual electrons in the quantum dot. The non-circular shape of these contour lines (independent

of the scan direction) suggests that the tip is not symmetric with respect to rotation around the z-axis normal to the sample surface. This peculiarity in the tip shape is due to the electrochemical etching process used to sharpen the tip before use. When the tip is scanned even closer to the dot in region (II), the current through the dot becomes smaller than our current resolution because the tip-induced potential pinches off the quantum point contacts coupling the dot to source and drain.

Our scanning gate measurements on a semiconductor quantum dot demonstrate that single electrons can be manipulated one by one with a macroscopic scanning tip. Advanced experiments and setups promise that it may eventually be feasible to get a handle on the local quantum mechanical probability distributions of electronic states in quantum dot structures and coupled mesoscopic systems.

2.2 Interplay between the periodic potential modulation and random background scatterers in an antidot lattice

A. Dorn, E. Bieri, T. Ihn, K. Ensslin, in collaboration with D. D. Driscoll and A. C. Gossard, University of California, Santa Barbara, USA

A two-dimensional electron system imprinted with a regular array of insulating islands is commonly termed an antidot lattice. Magnetoresistance peaks corresponding to commensurate cyclotron orbits enclosing 1, 4, 9, ... antidots have been observed in square antidot arrays and explained in the context of classical billiard models.

At low temperatures, a fine oscillation with a periodicity of approximately one flux quantum through a cyclotron orbit is sometimes observed. The magnetoresistance effects mentioned above arise from the properties of the regular antidot potential modified by the presence of random background scatterers. However in previous investigations the electron density and the overall mobility were not changed independently, so that contributions from the lattice and from the background scatterers were difficult to disentangle. Here we have investigated this interplay by using antidot lattices with a top and back gate that allow us to tune the amount of background scatterers at constant electron sheet density.

The sample was defined by local anodic oxidation of a GaAs heterostructure with a two-dimensional electron system (2DES) 40 nm below the surface and a conducting back gate layer at a depth of $1.3\,\mu$m.

By applying voltages to the gates, the two-dimensional electron density can be tuned capacitively. The availability of a top and a back gate in our samples enables us to sweep one gate and hold the electron density constant by applying suitable voltages to the second gate. This opens up a window on effects connected to changes in wave function symmetry and background mobility without having to take influences from a changing Fermi energy into account. Constant density sweeps were done by setting the top gate voltage to a fixed set of values and then adjusting the back gate voltage until the specified electron density was reached.

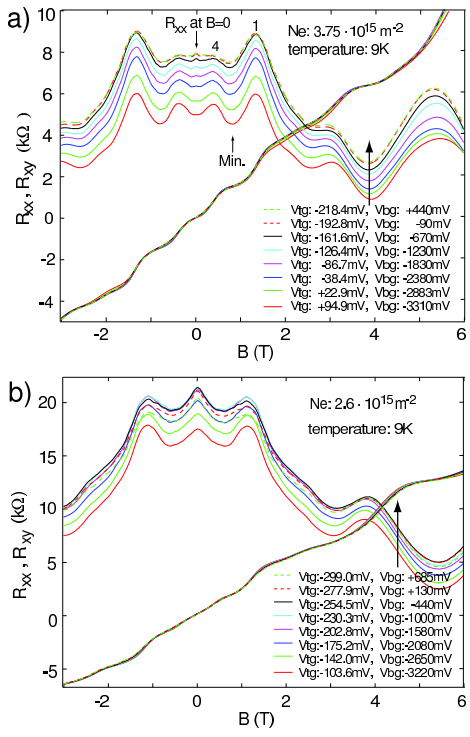

Figure 2.2: Magnetoresistance of a finite antidot lattice at a series of top and back gate voltages at constant electron densities of (a) $3.75 \cdot 10^{15}\mathrm{m}^{-2}$ and (b) $2.6 \cdot 10^{15}\mathrm{m}^{-2}$.

Figure 2.2(a) and (b) show magnetoresistance traces at a series of top and back gate settings for two different constant electron densities at 9 K. The overall resistance decreases and the commensurability features are better resolved at the higher electron density of $3.75 \cdot 10^{15}\mathrm{m}^{-2}$. Within the constant density series at $3.75 \cdot 10^{15}\mathrm{m}^{-2}$ the electron mobility increases towards higher top gate voltages. Only at the lower density of $2.62 \times 10^{15}\,\mathrm{m}^{-2}$ does the mobility increase again at the lowest top gate settings. A possible explanation for the increase in mobility at high top gate voltages is a population of the donor layer (ionized Si atoms) with electrons, leading to improved screening. On the other hand, at very low top gate voltages, all the electrons have left the donor layer and the mobility increases again, because the 2DES is pushed away from the GaAs/GaAlAs interface. This reduces scattering off the ionized donor atoms and from defects close to the GaAs/AlGaAs interface.

Aharonov–Bohm-type oscillations were detected at low electron densities. The periodicity of $0.23\,\mathrm{T}$ precisely matches a flux quantum through a circular orbit with a diameter of a $= 150\,\mathrm{nm}$ ($0.235\,\mathrm{T}$), which can clearly be distinguished from a flux quantum through the square unit cell ($0.183\,\mathrm{T}$). It is surprising that the oscillations persist up to 4 T, more than *twice* the magnetic field of the main commensurability peak, without changing frequency. Instead of a smooth transition to the Shubnikov–de Haas effect, the two oscillations coexist, which is in marked contrast to earlier reports.

2.3 Multiple layer local oxidation for fabricating semiconductor nanostructures

M. Sigrist, A. Fuhrer, T. Ihn, K. Ensslin, in collaboration with D. D. Driscoll and A. C. Gossard, University of California, Santa Barbara, USA

Optical lithography and electron beam lithography are the standard techniques to pattern tunable semiconductor nanostructures. A number of patterning techniques based on scanning force microscopes (SFMs) have been developed. An especially useful technique is to oxidize substrates locally by applying a negative voltage between the SFM tip and the substrate. Sophisticated nanostructures can be fabricated, for example, on shallow Ga[Al]As heterostructures. The two-dimensional electron gas is depleted below oxide lines leading to mutually isolated regions of electron gas. The main experimental parameters influencing the oxidation process are the relative humidity of the environment, leading to a thin water film on the substrate surface, and the magnitude of voltage applied to the tip.

A similar oxidation technique has been used to divide thin Titanium films into areas mutually isolated by oxide lines. Metallic single-electron transistors fabricated with this technique have been reported to show the Coulomb-blockade effect. Local titanium oxidation has also been used on Ga[Al]As heterostructures with a thin Ti top gate film for defining self-aligned split-gates. On the application of appropriate gate voltages, a quantum point contact (QPC) was formed showing clear conductance quantization. Fur further optimized nanostructures a patterning technique is desirable that makes the third spatial dimension accessible.

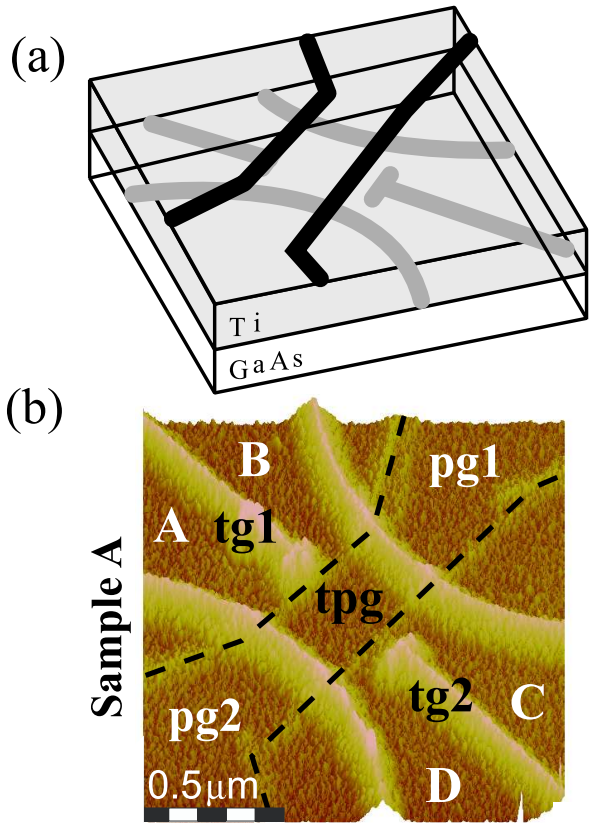

Figure 2.3: (a) Schematic drawing of a four-terminal quantum dot. The 2DEG is depleted below the oxide lines on the GaAs surface (grey). The Ti film is structured into three isolating parts by Ti-oxide lines (black). (b) SFM-micrograph of the dot. In addition to the two in-plane gates pg1 and pg2 in the 2DEG, there are three top gate segments tg1, tg2 and tpg in the Titanium film.

We have demonstrated an approach where the alignment of the top gate structures with the previous oxide structure in GaAs is achieved using a SFM. Our method combines

the direct oxidation of a Ga[Al]As heterostructure (first step) with the subsequent evaporation of a thin titanium gate (second step) which is then patterned using the local oxidation technique with the SFM (third step). We have demonstrated the fabrication technique with the realization of a four-terminal quantum dot (see Fig. 2.3) and a double-quantum dot with integrated charge read-out. The occurrence of Coulomb blockade demonstrates the high quality and stability of the structures. The tuning possibilities of the nanostructures are significantly increased by the metallic Ti gates on top and their alignment with the nanostructure is straightforward.

2.4 Density dependence of microwave induced magneto-resistance oscillations in a two-dimensional electron gas

B. Simovic, C. Ellenberger, and K. Ensslin, in collaboration with H.-P. Tranitz and W. Wegscheider, Univ. Regensburg

The recent discovery of the vanishing of electrical resistance in a ultra-high mobility 2DEG under microwave irradiation has sparked a large interest in the photoresponse of quantum Hall systems. The so-called microwave-induced "zero-resistance" states have been observed in the magnetic field regime where the cyclotron and microwave frequencies, ω_c and ω respectively, are such that $\omega_c \leq \omega$. Independently of this discovery, a different type of microwave related effects, also leading to a strong modulation of the magneto-resistance, has been recently reported to occur in samples with a moderately high mobility of $\mu = 1.3 \times 10^6 \mathrm{cm}^2/\mathrm{Vs}$. In contrast to the 1/B-periodic oscillations mentioned before, these are B-periodic and develop in the field range where $\omega \leq \omega_c$. The same experiment performed on samples of different sizes and electron densities has shown that the period of these B-periodic oscillations increases with density and is inversely proportional to the length of the Hall bar. It is unclear whether the two effects, namely the B-periodic and the 1/B-periodic oscillations, can coexist in one sample.

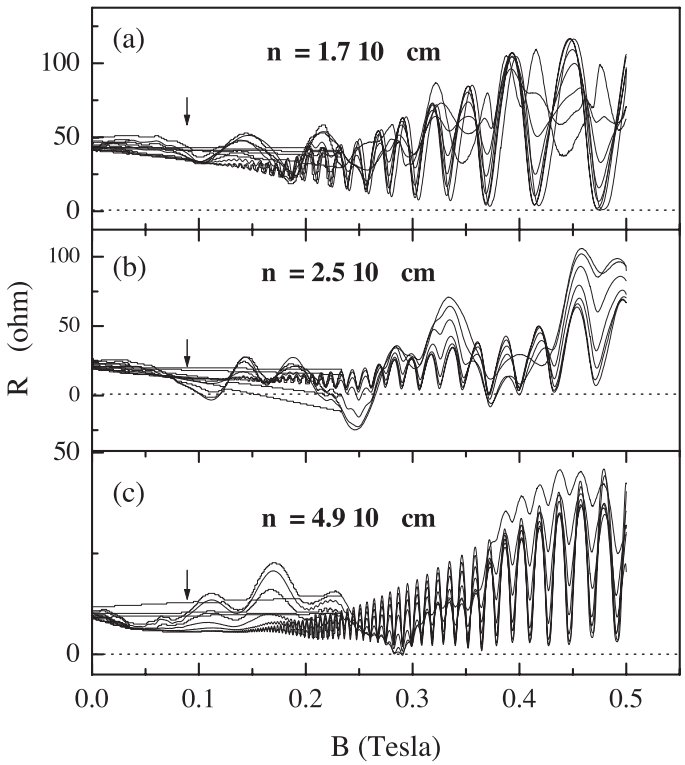

Figure 2.4: Magneto-resistance measured under continuous microwave irradiation for different powers is compared for three different illumination conditions. The microwave power P lies in the range (1μW-1 mW). The electron density n_s=5×10^{11}cm^{-2} and $\mu = 7.50\times10^6\mathrm{cm}^2/\mathrm{V\,s}$ for panel (a) and (b) while n_s=$4 \times 10^{11}\mathrm{cm}^{-2}$ and $\mu = 5.3 \times 10^6\mathrm{cm}^2/\mathrm{V\,s}$ for panel (c).

To this end, we have studied in detail microwave-induced oscillations versus electron density and mobility in a Hall bar patterned on a high-mobility GaAs heterostructure. In contrast to previous experiments where the values of n_s and μ were obtained from a brief exposure to light at low temperature, n_s and μ here are tuned continuously by adjusting a top-gate voltage. This permits a systematic study of microwave-induced effects in a large range of densities and mobilities. By increasing the electron density from 0.5 to $5 \times 10^{11}\mathrm{cm}^{-2}$, we could tune the mobility in the range of $(1-7) \times 10^6\mathrm{cm}^2/\mathrm{Vs}$. In the entire range of densities and mobilities investigated (see Fig. 2.4) we have observed oscillations of large amplitude that are B-periodic accompanied with a dependence to light exposure. Our detailed study as a function of density reveals that the period of the oscillations does not increase linearly with n_s but shows unexpectedly a plateau in the range of (2.4-3)$\times10^{11}\mathrm{cm}^{-2}$ which occurs concomitantly with a continuous phase shifting of the oscillations by two periods.

2.5 Cotunneling-mediated transport through excited states in the Coulomb blockade regime

R. Schleser, T. Ihn, E. Ruh, and K. Ensslin, in collaboration with M. Tews and D. Pfannkuche, University Hamburg, and D. D. Driscoll and A. C. Gossard, University of California, Santa Barbara, USA

In a quantum dot in the Coulomb blockade regime, the energy gap related to the charging energy becomes larger than $k_{\mathrm{B}}T$ and sequential tunneling transport involving only dot ground states is exponentially suppressed. Up to now, the same suppression was assumed for tunneling involving excited dot states which are spectroscopically accessible at elevated bias where the Coulomb blockade is lifted. In the Coulomb blockade, transport is dominated by cotunneling. Elastic cotunneling, prevalent at low bias voltages, involves virtual tunneling of one electron through the dot via a higher-energy state and leaves the dot in the ground state. Inelastic processes imply correlated tunneling of two electrons, leaving the dot in an excited state with energy Δ above the ground state. Inelastic cotunneling sets in once the bias energy $eV_{bias} \geq \Delta$.

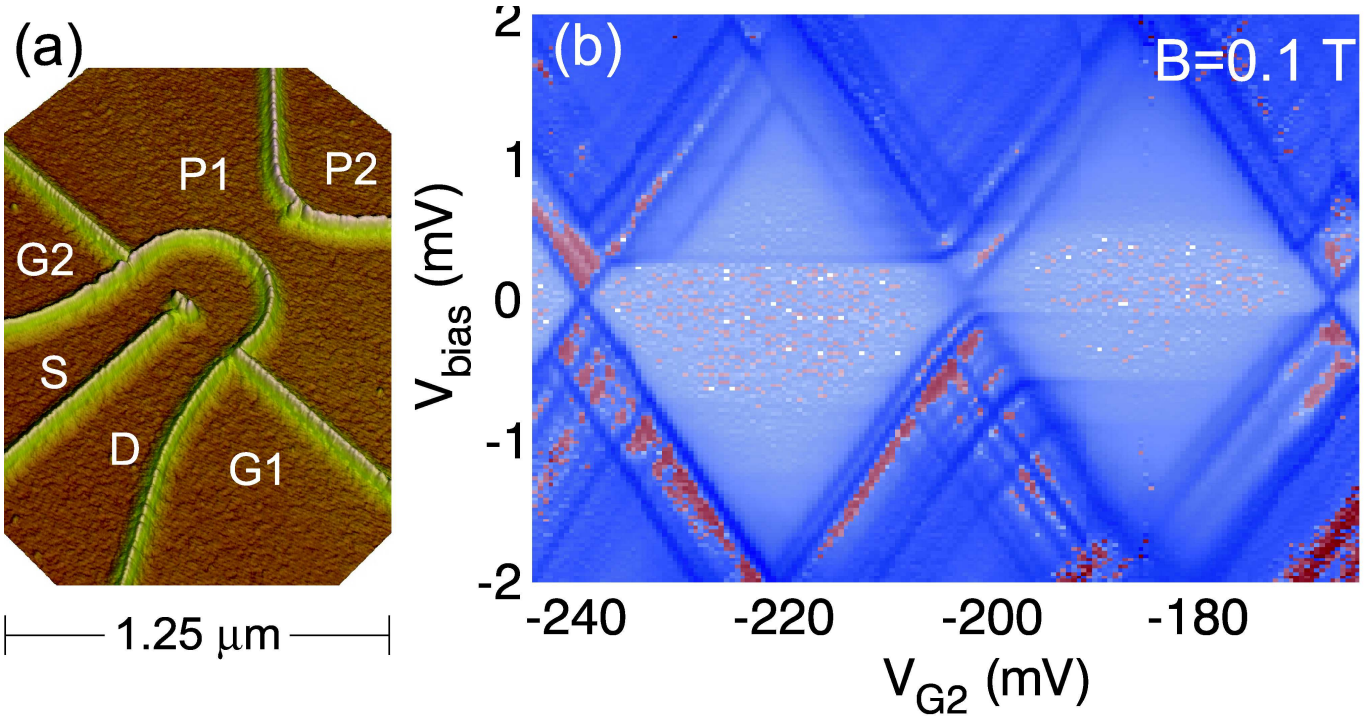

Figure 2.5: (a) AFM micrograph of structure with designations of gates: source (S) and drain (D) of the quantum dot; lateral gates G1 and G2 to control the coupling of the dots to the reservoirs; Plunger gates P1 and P2 to tune the number of electrons on the dot. (b) Finite bias measurement of the dot's differential conductance dI/dV at $B = 0.1T$

Figure 2.5 shows measurements of finite bias differential conductance dI/dV on a strongly nonlinear scale. Inside the diamond-shaped regions, i.e. in the Coulomb blockaded regime, we observe horizontal (constant bias) structures. At the diamond boundary, the horizontal lines seamlessly join some of the most prominent diagonal lines in the non-blockaded region. For positive bias, e.g. in Fig. 2.5(b), additional structure inside the diamond is observed: for bias voltages above the well-resolved horizontal threshold line, diagonal lines parallel to the diamond edges appear. The vertical distance between the diagonal lines and the diamond edge is identical for positively (left of diamond) and negatively sloped lines. When extended towards higher or towards negative voltages, most of the diagonal lines apparently join prominent lines in the non-blockaded regime.

We interpret our findings as follows: the horizontal lines in the blockaded regime mark the onset of inelastic cotunneling connected to specific excited states. The distance from the zero-bias line corresponds to the single-particle

level spacing of these states with respect to the ground state. At the intersection points at the border of the Coulomb diamonds, a direct mapping can be made of the excited states that contribute measurably to inelastic cotunneling and those that open additional transport channels in the non-blockaded, finite-bias regime.

The most unconventional features observed are the diagonal lines inside the Coulomb blockaded regions. The fact that they have the same slope as the diamond edges suggests that they are connected to the alignment of an energy level with source (negative slope) or drain (positive slope).

Signatures of inelastic cotunneling can be observed in the finite bias differential conductance of the quantum dot. These are attributed to specific excited states. An additional peak in dI/dV is visible inside the Coulomb blockaded region. These contributions stem from sequential tunneling after the dot has been left in an excited state by an inelastic cotunneling process.

Elastic cotunneling has earlier been identified as a possible source of uncertainty in the operation of single-electron devices. Our results show that the inelastic contributions can become more prominent, especially if the induced sequential tunneling is taken into account. It follows that in an application relying on Coulomb blockade in quantum dots, e.g. in quantum information processing, the bias must be kept small in comparison to the lowest excitation energy.

2.6 Quantum dots with internal structure

D. Graf, T. Ihn, and K. Ensslin, in collaboration with D. D. Driscoll and A. C. Gossard, University of California, Santa Barbara, USA, and W. Wegscheider, Univ. Regensburg

The sample presented in Fig. 2.6 (a) has 4 terminals whose coupling to the quantum dot (containing 16 antidots) can be tuned by in-plane gate voltages. In the Coulomb blockade regime a bias can be applied to each of the four terminals and the ingoing as well as the three outgoing currents can be measured. This gives rise to 16 elements of the conductance matrix. Such data has been taken as a function of perpendicular magnetic field.

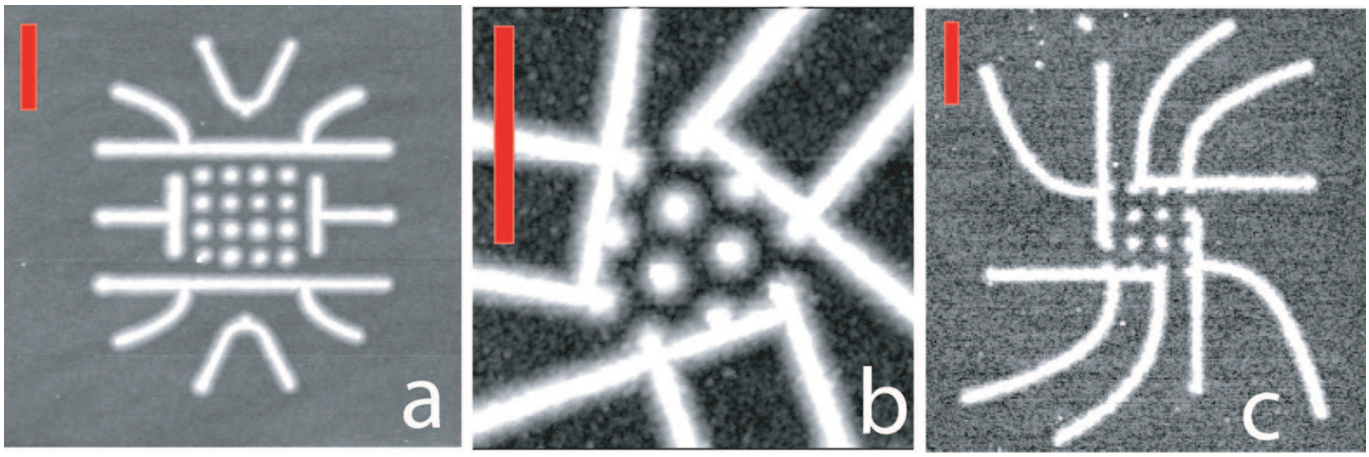

Figure 2.6: Scanning force microscopy images of three sample structures containing a finite array of antidots in a cavity connected to 3 or 4 leads. The red line marks a length of 0.5 μm in all three cases.

Among the many features observed in this matrix it is worth mentioning that all sum rules (current conservation etc.) are fulfilled within experimental accuracy. Several measurements clearly show a B-periodic behavior at high magnetic fields. The period agrees with an Aharonov-Bohm-type argument applied to the area of a ring around an antidot. This is a clear indication that the energy spectrum in this quantum dot shows features which are related to its internal structure. As the back-gate voltage in this system is changed the Fermi energy in the dot as well as in the leads is tuned. This has a distinct influence on the strength and period of the B-periodic oscillations, which are observed in the open as well as in the Coulomb blockade regime.

2.7 Nanostructures on p-type C-doped AlGaAs heterostructures

B. Grbic, C. Ellenberger, T. Ihn, and K. Ensslin, in collaboration with D. Reuter and A. D. Wieck, University of Bochum, Germany

Electronic nanostructures in semiconductors are usually realized in n-type GaAs-AlGaAs heterostructures. In this project we set out to explore two-dimensional hole gases (2DHG) realized on p-type, C-doped GaAs-AlGaAs heterostructures.The main properties which distinguish 2D hole from electron systems are more pronounced effects of spin-orbit and electron-electron interactions. The high quality of such two-dimensional hole gases is demonstrated by pronounced integer quantum Hall plateaus as well as features of the fractional quantum Hall effect in magneto-transport measurements.The mean free path in these heterostructures is determined to be larger than 1μm, which is promising for the fabrication of ballistic nanostructures. In order to realize p-type quantum point contacts (QPC) and dots we employ local oxidation of the surface of the shallow 2DHG with a scanning force microscope.

A QPC was fabricated by oxide lines defining a constriction in the plane of the hole gas. Figure 2.7 shows the conductance of such a structure as a function of top gate voltage. At zero magnetic field we observe a plateau-like feature which is related to the quantization of the conductance in one dimension. However, in contrast to n-type sample of comparable mobility, the conductance trace displays a lot of fine structure most of which is reproducible. At certain gate voltages also time dependent conductance fluctuations occur.In the quantum Hall regime backscattering of edge states from the QPC potential is detected. The next step will be the realization of a quantum dot in p-type material. This will allow us to investigate electronic transport through a quantum dot with very high interaction parameter, a regime not accessible in typical n-type nanostructures.

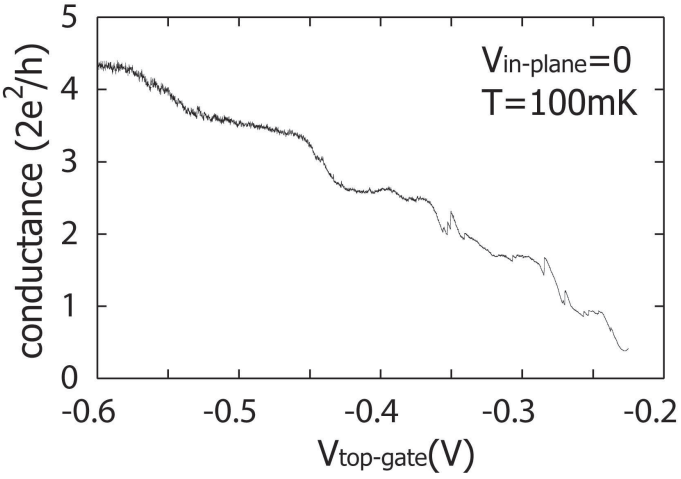

Figure 2.7: Conductance of a quantum point contact as a function of gate voltage at a temperature of 100 mK

2.8 Shot noise in quantum point contacts

K. Kobayashi, R. Leturcq, C. Ellenberger, C. Barengo, P. Studerus, T. Ihn, and K. Ensslin, in collaboration with D. D. Driscoll and A. C. Gossard, University of California, Santa Barbara, USA

The understanding of electron flow in solids has been one of the long-standing central issues in solid-state physics. Recent progress in nanotechnology enables us to precisely explore this subject by using tunable nano-scale devices. So far, conventional resistance measurements have been mainly applied to these systems, while noise measurements are expected to convey us other rich information on the behavior of electrons in solids. Indeed, by investigating noise — fluctuations of electric current through systems, several fundamental aspects of electrons have been revealed, such as the existence of the fractional charge in quantum Hall systems and the anti-bunching of electrons due to their fermionic nature. Noise measurements in mesoscopic devices now start to be applied to many unexplored subjects. Our project of noise measurement aims at the investigation of the high frequency property of quantum dots, current-current correlation out of three-terminal quantum systems, and the interaction between coupled mesoscopic systems.

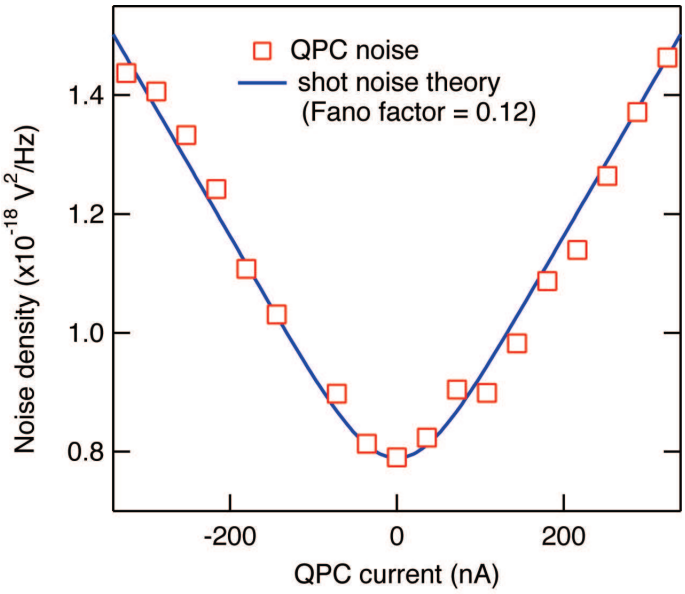

Figure 2.8: Noise power of the quantum point contact (QPC) as a function of current through it. The red mark is the measured noise and the blue curve is the prediction of the shot noise theory. The Fano factor 0.12 indicates the suppression of the shot noise due to quantum effects.

We started noise measurements of coupled quantum point contacts (QPC). This system will enable us to address the above subjects in several ways. Special care should be necessary to measure the noise in nano-scale systems because the typical noise level is very small down to $1nV/Hz^{1/2}$ below 2 K. To this end, we constructed a specially-designed experimental setup and adopted an unconventional technique to measure the noise spectrum (so-called correlation technique). We succeeded in measuring the shot noise of the QPC and observing its quantum reduction from the classical value. Our project, however, needs to overcome several technical challenges. The biggest obstacle arises from the fabricated QPC's made of the two-dimensional electron gas (2DEG) in semiconductor heterostructure, because they often suffer from bistable states, which result in random-telegraph signals and prevent us from extracting intrinsic noise. It was found that this unwanted effect greatly depends on the structure of the 2DEG and it can be reduced. The project will go on by using samples where this effect is not the dominant noise source.

2.9 Kondo density of states in a three-terminal quantum ring

R. Leturcq, L. Schmid, and K. Ensslin, in collaboration with Y. Meir, Ben Gurion University, Israel, and D. D. Driscoll and A. C. Gossard, University of California, Santa Barbara, USA

Quantum dots realized in semiconductor heterostructures allow to confine a controlled number of electrons in a small area, and to probe the electronic properties of these confined electrons by connecting them to external leads. In a quantum dot with an odd number of electrons, the last electron is unpaired and acts as a localized spin. Interactions between this last unpaired electron and the free electrons in the leads contribute to the formation of a singlet state, same as between localized magnetic impurities and conduction electrons in metals, known as the Kondo effect.

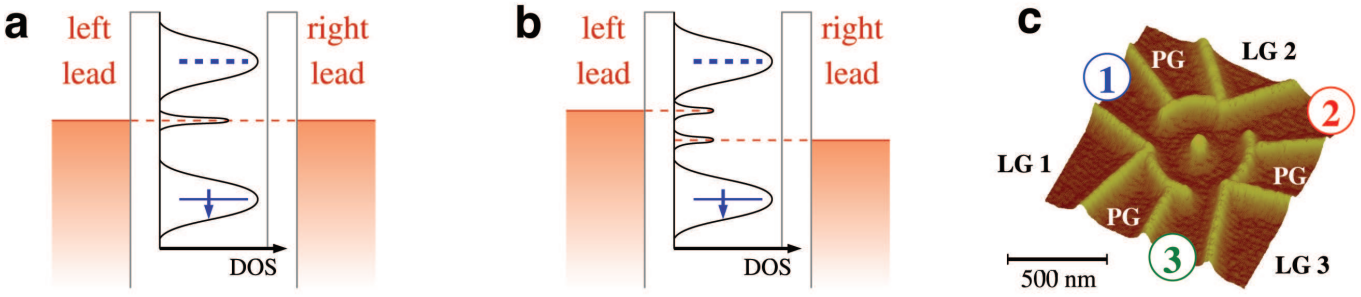

Figure 2.9: Kondo density of states, sample characteristics and measurement set-up. a-b, Scheme of the density of states in a quantum dot in the Kondo regime connected to two Fermi leads (a) in equilibrium and (b) out-of-equilibrium. c, Atomic force microscope (AFM) image of the oxide lines defining the three-terminal quantum ring, fabricated by AFM lithography on an AlGaAs-GaAs heterostructure containing a two-dimensional electron gas (2DEG) 34 nm below the sample surface. The electron gas is depleted below the oxide lines. The three leads labelled 1 to 3 are coupled to the ring through three quantum point contacts controlled by the lateral gates LG1 to LG3. The number of electrons in the ring is controlled by the three plunger gates PG set at the same potential VPG.

In a two-terminal experiment, the current practically probes the total DOS between the two chemical potentials. Thus the differential conductance will be maximal at zero voltage (see 2.9 (a))) and be suppressed at finite bias (see 2.9

(b)), giving rise to a peak of the conductance around zero bias, the so called zero bias anomaly (ZBA). It is thus not possible to observe the splitting of the DOS in a two-terminal experiment. It has been theoretically proposed that, by adding a third weakly coupled lead, and measuring the conductance through this additional lead, one should be able to measure directly the splitting of the DOS.

We have realized a novel geometry a three terminal quantum ring (see 2.9 (c)) that allows us to probe two regimes the single strongly coupled lead regime (and two weakly coupled ones, and the single weakly coupled lead regime . The latter regime allows a direct probe of the Kondo DOS out-of-equilibrium.

For fine tuning of the individual coupling of the dot to each leads, we change the applied perpendicular magnetic field rather than the gate voltage. Our experiments demonstrate that a three-terminal set-up allows to determine the contribution of each lead to the Kondo DOS in a quantum dot. This allows us to measure the Kondo DOS in and out-of-equilibrium. Compared to the generally used two-terminal tunneling measurements, the multi-terminal configuration gives additional insight into the energy spectrum, wave function coupling and many-particle DOS of a quantum system.

Chapter 3

Condensed matter at low temperatures

(http://www.solid.phys.ethz.ch/ott)

Head
Prof. Dr. H. R. Ott

Academic Staff
Dr. C. Beeli
E. Felder
Dr. J.L. Gavilano
Dr. J. Hinderer
Dr. I. Landau
Prof. Dr. R. Monnier
Dr. B. Pedrini
Dr. D. Rau
Dr. Ch. Soltmann
Dr. A. Sologubenko
M. Weller
Dr. G. Wigger

Technical Staff
H.R. Aeschbach
P. Wägli
M. Leopold
R. Wessicken
H. Thomas

Administrative Staff
I. Heer-Mettler
D. Amstad

Academic Guests
Dr. Oscar Bernal, California State University, Los Angeles, USA
Dr. Ko-Ichi Magishi, University of Tokushima, Japan

Melting and freezing

Head
Prof. Dr. J. Bilgram

Academic Staff
H. Singer
M. Fell
O. Wittwer

Technical Staff
H.R. Aeschbach

Solid state optics

Head
PD Dr. L. Degiorgi

Academic Staff
G. Caimi
A.Perucchi

Technical Staff
J. Müller

Thin film physics group

Head
PD Dr. H. Zogg

Academic Staff
D. Abou-Ras
K. Alchalabi
M. Arnold
D. Brmaud
F. Felder
M. Kaelin
A. Romeo
D. Rudmann
Dr. A.N. Tiwari
D. Zimin

Technical Staff
Th. Kmpfer
M. Leopold

Academic Guests
M. Ganchev, Central Laboratory of Solar Energy & New Energy Sources , Sofia, Bulgaria

3.1 Physical properties of rare earth compunds and Kondo systems

3.1.1 Low-Temperature Phase Transitions in the Induced- Moment System PrB_4

G.A. Wigger, E. Felder, R. Monnier, H. R. Ott

We measured the electrical resistivity, the magnetization and the specific heat of PrB_4 below room temperature. The crystal electric field (CEF) splits the $4f^2$-multiplet of the Pr ions into nine singlets. In its ground state, PrB_4 is an induced-moment ferromagnet with a saturation magnetization as high as 2.1 μ_B per praseodymium ion. Contrary to previous experiments, we observed a first-order ferromagnetic to antiferromagnetic transition at $T_C \approx 15.9 \pm 0.1$ K, with a latent heat ΔQ = 8.6 J/mole. The antiferromagnetic long-range order is quenched above T_N = 19.5 K. Susceptibility and specific heat data, as well as the enormous magnetic anisotropy, can be reproduced by a mean field calculation which takes into account the CEF (the parameters of which are derived from a point-charge model, using effective charges obtained from a selfconsistent band structure calculation), a Zeeman term, an anisotropic dipolar magnetic exchange term and an effective quadrupole-quadrupole interaction between the Pr ions.

3.1.2 Kondo behaviour of U in CaB_6

G. Wigger and H.R. Ott

Replacing Ca by U in semiconducting CaB_6 at the few at % level induces metallic behaviour and provides the first experimental evidence for a Kondo effect triggered by dilute U ions I a metallic host. For $Ca_{0.992}U_{0.008}B_6$ the notorious resistance minimum occurs at $T = 17$ K. The subsequent logarithmic increase of the resistivity $\rho(T)$ upon decreasing temperature merges into the expected Fermi-liquid type T^2 dependence below 0.8 K.

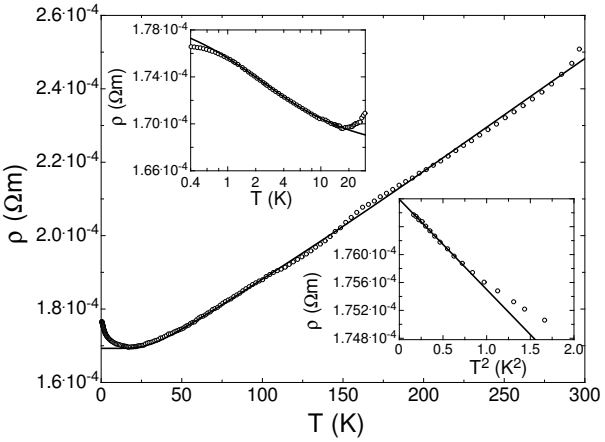

Figure 3.1: $\rho(T)$ of $Ca_{0.992}U_{0.008}B_6$ revealing the Kondo minimum at $T = 17$ K. The insets emphasize the logarithmic and the T^2 temperature dependences at intermediate and low temperatures, respectively.

By comparison with model calculations available in the literature we deduce a Kondo temperature $T_K = 1.9$ K. This value is corroborated by the results of measurements of the magnetization and the specific heat in varying external magnetic fields. Equal amounts of U ions embedded in metallic LaB_6 provoke no evidence for a Kondo effect above 0.4 K. Our observation is of general importance in various respects. In particular, since in CaB_6 the concentration of itinerant charge carriers is of the order of 10^{-4} per unit cell, the number of magnetic moments and conduction electrons, delivered by each U impurity, is practically the same. This signifies that Kondo screening is also achieved if the number of moments to be quenched equals that of the conduction electrons.

3.1.3 NQR-measurements of $CePd_2In$ under hydrostatic pressure

M. Weller, J. Hinderer, B. Pedrini, D. Rau, M. Chiao, J. L. Gavilano, H. R. Ott

$CePd_2In$ is a intermetallic compound, whose low-temperature physical properties suggest the existence of correlated itinerant electrons in a magnetically ordered phase [1,2].

The small values of the involved temperature scales, the Néel temperature T_N = 1.23 K, and the Kondo temperature T_K = 2.5 K, make the compound an interesting candidate for investigation under pressure.

Figure 3.2 displays the results of ^{115}In-NQR measurements at ambient pressure and at 11 kbar. The data show the splitting of the resonance line around 31 MHz, which is associated to the order parameter of the antiferromagnetic transition, as a function of temperature. Application of pressure, shifts the transition to slightly higher temperatures.

The insets display two spectra, below and above T_N respectively. For T = 1.16 K the (nonzero) splitting Δf of the resonance line is clearly identified.

[1] J. L. Gavilano et al., Europhys. Lett. **32**, 361-366 (1995)
[2] P. Vonlanthen et al., Z. Phys. **102**, 347-375 (1997)

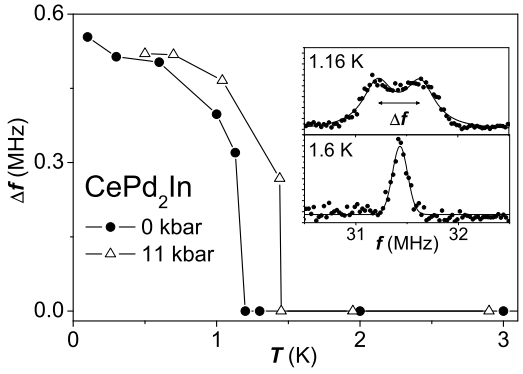

Figure 3.2: The splitting of the ^{115}In-NQR-Resonance at approximately 31.5 MHz ($m_z = \frac{3}{2} \leftrightarrow \frac{5}{2}$) is shown as a function of temperature at two different pressures. The Néel temperature increases with increasing pressure.

3.1.4 NMR studies in CeTe

J. Hinderer, M. Weller, S. M. Weyeneth, J. L. Gavilano, H. R. Ott

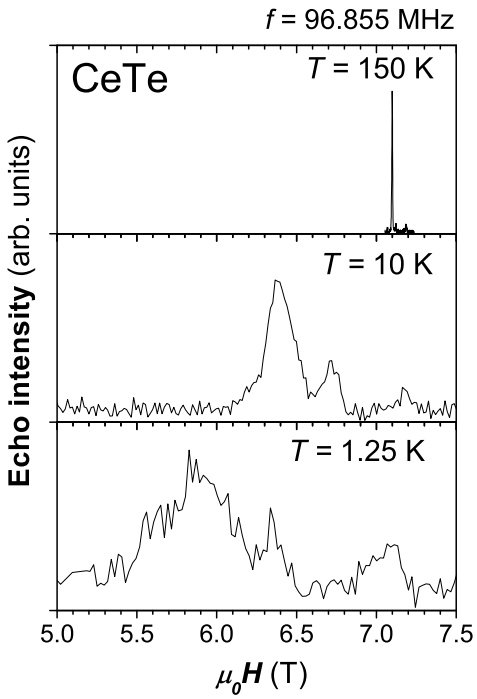

Figure 3.3: NMR spectra of CeTe at three different temperatures.

CeTe is a rocksalt type intermetallic compound. It orders antiferromagnetically at $T_N \approx 2.2$ K with a much reduced ordered moment [1]. We have performed ^{125}Te NMR measurements on CeTe powder at temperatures between 1 and 300 K and in magnetic fields between 3 and 8 T. Due to the very small spin-spin relaxation times T_2, the very broad spectrum (see figure 3.3) and the small NMR sensitivity of the Te nuclei, NMR experiments on this compound are very demanding. From our low-temperature NMR spectra we infer the presence of at least three inequivalent Te sites with a spectral weight ratio of approximately 10:3:2 at 10 K (see figure 3.3). Considering the crystal structure this result is completely unexpected. The linewidth and the Knight shift of the individual lines increase substantially with decreasing temperatures, and follow the temperature dependence of the magnetic susceptibility above 20 K. Hyperfine fields of 1.56, 0.82 and 0.00 T at the Te site per Bohr magneton of Ce moment are deduced from Knight shift vs. magnetic susceptibility measurements for the three Te sites. These values are typical for transferred hyperfine fields via the conduction electrons. A dramatic increase of the spin-spin relaxation rate with decreasing temperature below 10 K is observed.

[1] H. R. Ott, J. K. Kjems, F. Hulliger, Phys. Rev. Lett. **42**, 1378-82 (1979); M. Nakayama et al., Phys. Rev. B **70**, 054421 (2004).

3.1.5 NMR studies in $PrCu_2$

J. Hinderer, M. Weller, B. Pedrini, K. Magishi, J. L. Gavilano, H. R. Ott

$PrCu_2$ is an intermetallic compound, which exhibits different low-temperature phase transitions. Below 50 mK cooperative nuclear-electronic antiferromagnetic order occurs. Around 7K a Jahn-Teller transition was observed, and more recent results of μSR experiments [1] gave evidence for antiferromagnetic order with T_N = 65 K.

For a powder sample we observe that between 20 and 300 K, the temperature evolution of the Knight shift of the ^{63}Cu and ^{65}Cu NMR lines follows a Curie-Weiss type behavior, as expected for an NMR response dominated by the 4f-electron magnetic moments of Pr^{3+} ions (see Figure 3.4). At temperatures above 100 K, the ^{63,65}Cu-NMR spectra exhibit the characteristic powder pattern for a nuclear spin I = 3/2, as expected for Cu nuclei in a noncubic environment. Significant changes in the NMR spectra are observed below 100 K. In particular, changes in the wings between 20 and 100 K may be interpreted as evidence for either (i) a complicated antiferromagnetic order, or (ii) substantial changes in the electric-charge distribution. We have also performed NMR measurements in a single crystalline sample with the b-axis parallel to H_0. The temperature dependence of the NMR spectrum for this particular orientation does not support the scenario of an antiferromagnetically ordered state below 65 K. At 7 K, the Jahn-Teller-transition does not seem to substantially effect the electronic environment of the Cu sites. However, it does change the temperature dependence of the Knight shift at the transition around 7 K. The narrow copper and aluminum lines are due to the sample holder.

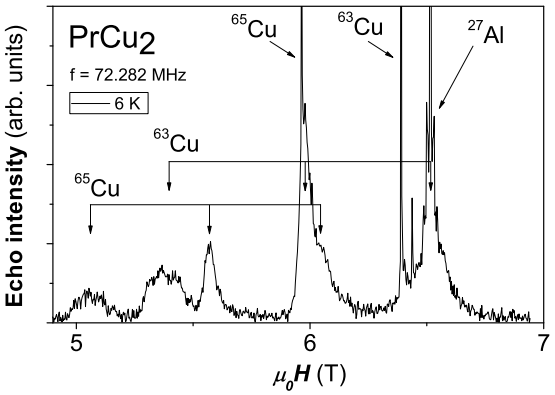

Figure 3.4: $PrCu_2$ single crystalline sample at 6 K. The b-axis is parallel to the applied field.

[1] A. Schenck, F. N. Gygax, and Y. Onuki, Phys. Rev. B **68**, 104422 (2003)

3.1.6 Theory of the thermoelectricity of intermetallic compounds with Ce or Yb ions

R. Monnier, in collaboration with V. Zlatic (Institute of Physics, Zagreb, Croatia)

The thermoelectric properties of intermetallic compounds with Ce or Yb ions are explained by the single-ion Anderson model which takes into account the crystal field splitting of the 4f ground-state multiplet, and assumes a strong Coulomb repulsion which restricts the number of f electrons or f holes to $n_f \leq 1$ for Ce and $n_f^{hole} \leq 1$ for Yb ions. Using the non-crossing approximation, and imposing the charge neutrality constraint on the local scattering problem at each temperature and pressure, the excitation spectrum and the transport coefficients of the model are obtained. The thermopower calculated in such a way exhibits all the characteristic features observed in Ce and Yb intermetallics. Calculating the effect of pressure on various characteristic energy scales of the model, we obtain the (T, p) phase diagram which agrees with the experimental data on $CeRu_2Si_2$, $CeCu_2Si_2$, $CePd_2Si_2$, and similar compounds. The evolution of the thermopower and the electrical resistance as a function of temperature, pressure or doping is explained in terms of the crossovers between various fixed points of the model and the redistribution of the single-particle spectral weight within the Fermi window.

3.2 Superconductivity

3.2.1 Influence of carbon substitution on the heat transport in MgB_2

A.V. Sologubenko, N.D. Zhigadlo, S. M. Kazakov, J. Karpinski, H.R. Ott

The superconducting state of MgB_2 is characterized by at least two widely different gaps in the electronic excitation spectrum. Amazingly, lattice disorder, which is thought to lead to interband scattering and consequently to an equalization of gap amplitudes has very little effect on the two-gap nature of superconductivity in MgB_2. Current studies of MgB_2 aim at a controlled variation of the influence of interband and intraband scattering processes on physical properties of MgB_2, e.g. by selected small variations of the chemical composition, leading to selective variations in the quoted scattering processes.

We measured the thermal conductivity κ of $Mg(B_{1-x}C_x)_2$ (x=0, 0.03 and 0.06) in the basal plane of the hexagonal crystal structure as a function of temperature between 0.5 and 50 K and in external magnetic fields H up to 50 kOe, oriented both parallel and perpendicular to the c-axis. Representative $\kappa(H)$ curves, measured at a $T = 1.0$ K, are shown in In Fig. 3.5.

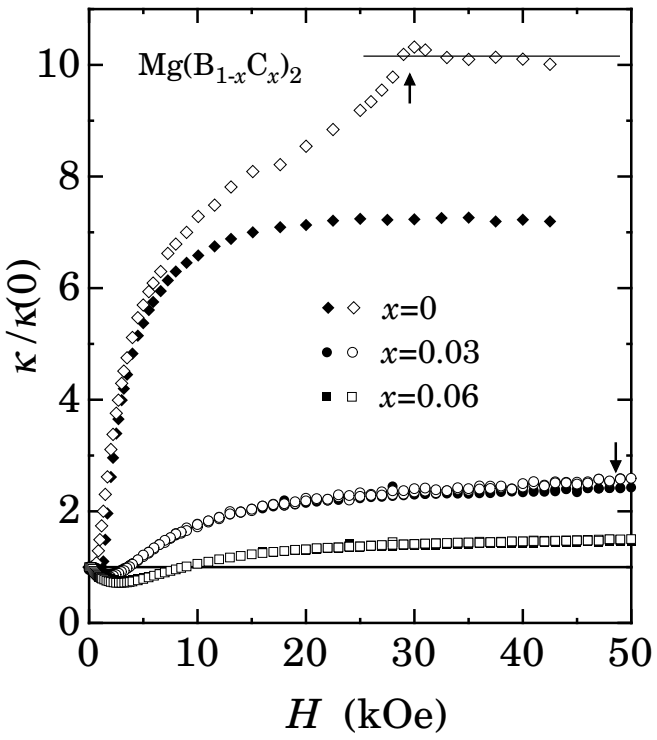

Figure 3.5: Thermal conductivity in the basal plane of $Mg(B_{1-x}C_x)_2$ (x=0, 0.03 and 0.06) vs H at $T = 1.0$ K. The arrows indicate the upper critical field H_{c2}. The closed and open symbols correspond to the field directions perpendicular and parallel to the $c-$axis, respectively.

In MgB_2, the transport is provided by both phonons and itinerant electronic excitations from the σ- and the π-band, such that $\kappa = \kappa_{\rm ph} + \kappa_{e,\sigma} + \kappa_{e,\pi}$. In the mixed state, the quasiparticles associated with the vortices provide additional scattering of phonons and also enhance κ_e. For both pure and carbon-doped MgB_2, an extremely rapid increase of κ_e at fields $H \ll H_{c2}$, which does not scale with H/H_{c2} and is almost independent of field orientation despite the strong anisotropy of H_{c2}, is observed. This unique behavior is explained in terms of a two-band scenario, where the smaller energy gap Δ_π is closed at a relatively low and weakly-anisotropic field $H^*_\pi < H_{c2}$, of the order of 10 kOe for pure MgB_2. Our results suggest that the contribution $\kappa_{e,\pi}$ survives upon carbon doping. The σ-band contribution $\kappa_{e,\sigma}$ only grows when H approaches H_{c2}, the enhancement being strongly anisotropic, reflecting the anisotropy of H_{c2}. The striking difference between carbon-free and carbon-doped samples is that, for the latter, no significant increase in $\kappa(H)$ is observed in the vicinity of H_{c2}. It implies that $\kappa_{e,\sigma}$ is strongly reduced by carbon substitution from about 50% of the total normal-state κ_e for $x = 0$ to a level close to our experimental resolution already for $x = 0.03$. This result agrees with an expectation that carbon substitution for boron should enhance the intraband scattering rate mostly in the σ-band which is formed by the boron sp_xp_y orbitals.

3.2.2 Equilibrium magnetization in the vicinity of the first order phase transition in the mixed state of high-T_c superconductors.

I. L. Landau, H.R. Ott

We present the results of a scaling analysis of the equilibrium isothermal magnetization $M(H)$ measured in the mixed state of high-T_c superconductors (HTSC) in the vicinity of the established first order phase transition. The scaling procedure used for the analysis is based on the single assumption that the Ginzburg-Landau parameter κ is temperature-independent. As was shown in Ref. [3], this assumption is sufficient to derive a relation between the magnetizations at two different temperatures, which may be written as

$$M(H/h_{c2}, T_0) = M(H, T)/h_{c2} + c_0(T)H, \tag{3.1}$$

where $h_{c2}(T) = H_{c2}(T)/H_{c2}(T_0)$ is the ratio of the upper critical fields at T and T_0. The term $c_0(T)H$ was introduced in order to account for the temperature-dependent paramagnetic susceptibility of HTSC's in the normal state. The scaling parameters $h_{c2}(T)$ and $c_0(T)$ are determined by the condition that the $M(H, T_0)$ curves, calculated from the magnetization data measured at different temperatures, collapse onto the same master curve. In this way the temperature dependence of the normalized upper critical field $h_{c2}(T)$ and the equilibrium magnetization curve $M(H, T_0)$ are obtained.

Fig. 3.6 demonstrates that the phase transition is easily identifiable on the scaled magnetization curves. Indeed, the reversible parts of the $M(H)$ curves collapse both above and below the phase transition clearly indicating the corresponding $M_{eq}^{(hp)}(H)$ and $M_{eq}^{(lp)}(H)$ dependencies. The most unexpected result of our analysis is that the magnetization difference $\Delta M = \left|M_{eq}^{(lp)}\right| - \left|M_{eq}^{(hp)}\right|$ across the transition may adopt either sign. This result is difficult to reconcile with the vortex-lattice-melting hypothesis. In the case of vortex lattice melting, the external magnetic field acts as pressure does in traditional solid-liquid melting transitions. Thermodynamic require that the phase corresponding to the higher pressure must have a higher density. In relation with the mixed state of type-II superconductors, the vortex liquid necessarily has to adopt a higher vortex density, i.e., the difference ΔM must always be positive. The negative sign of ΔM, demonstrated in Fig. 1(b), is in serious conflict with the interpretation that the first order phase transition in the mixed state of HTSC's always reflects the melting of the vortex lattice.

[1] T. Sasagawa et al., J. of Low Temp. Phys. **117**, 1399 (1999). [2] T. Sasagawa et al., Phys. Rev. Lett. **80**, 4297 (1998). [3] I. L. Landau and H. R. Ott, Phys Rev. B **66**, 144506 (2002).

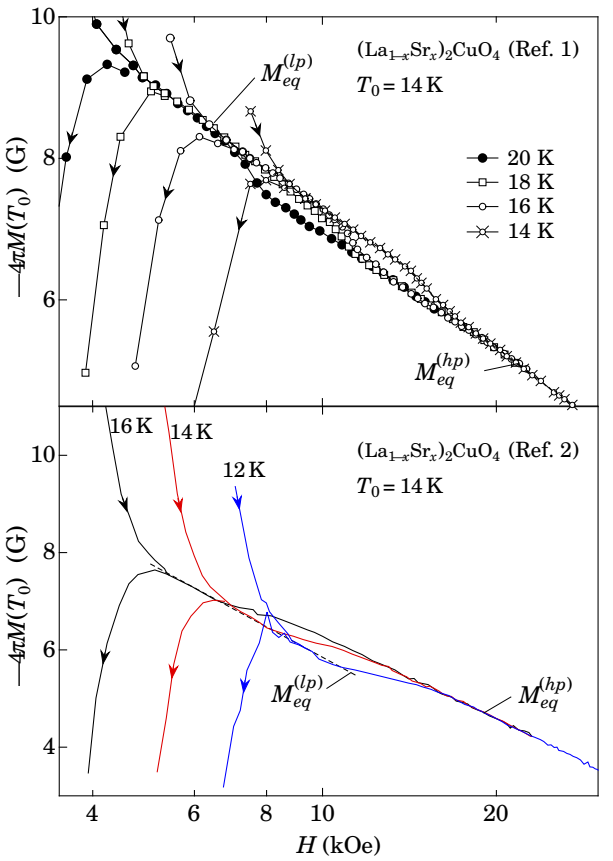

Figure 3.6: The scaled magnetization data for two different $La_{0.954}Sr_{0.046}CuO_4$ single crystals experimentally investigated in Refs. [1] and [2]. $M_{eq}^{(hp)}$ and $M_{eq}^{(lp)}$ denote the equilibrium magnetizations above and below the transition, respectively.

3.2.3 NMR studies of the β-pyrochlore oxide $RbOs_2O_6$

J.L. Gavilano, K. Magishi, B. Pedrini, J. Hinderer, M. Weller, H.R. Ott, S.M. Kazakov, and J. Karpinski

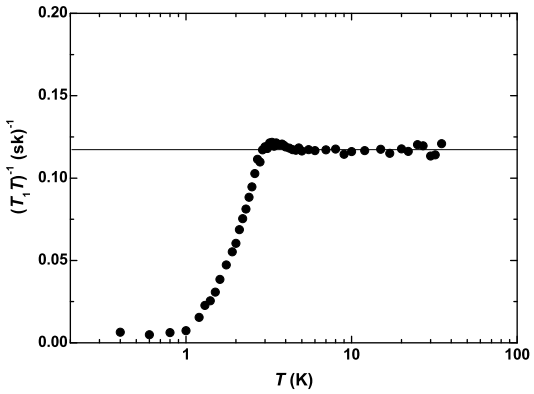

Figure 3.7: $(T_1T)^{-1}(T)$ for $RbOs_2O_6$. The solid line represents the Korringa-type behaviour in the normal state.

In recent years pyrochlore oxides have attracted a great deal of attention because the geometrical frustration inherent to their structures may lead to unusual physical properties. The recently synthesized $RbOs_2O_6$ is one of four pyrochlore oxides exhibiting superconductivity at very low temperatures with T_c = 6.4 K [1,2].

We made measurements of the magnetic susceptibility χ and of the ^{87}Rb-NMR response on polycrystalline samples of $RbOs_2O_6$ in both the normal and the superconducting state. At temperatures exceeding 100 K, the magnetic susceptibility is, to a good approximation, temperature-independent, consistent with the behavior of a simple metal. The superconducting transition is reflected in the onset of a large diamagnetic signal due to the Meissner effect. For $\mu_0 H$ = 50 G, $\chi(T)$ reflects the onset of diamagnetism at T_c = 6.4 K.

The ^{87}Rb-NMR spectrum in the normal state consists of a single narrow line, with a temperature independent Knight shift K. Below T_c, K rapidly decreases with decreasing temperature and the line broadens appreciably due to a distribution of local fields produced by the vortex lattice.

In the normal state the nuclear spin-lattice relaxation rate $T_1^{-1}(T)$ obeys the Korringa relation $(T_1T)_n^{-1}$ = 0.117 $(\mathrm{sK})^{-1}$, as expected for simple metals. In the superconducting state, $T_1^{-1}(T)$ reveals no clear coherence peak just below T_c (= 3.8 K for $\mu_0 H$ = 2.94 T) but drops sharply only below 3 K, i.e., at a temperature significantly lower than T_c. The $T_1^{-1}(T)$ and $K(T)$ data below T_c can qualitatively be explained by the BCS model considering some anisotropy of the gap function.

Our NMR results [3] imply that the superconducting state of $RbOs_2O_6$ is characterized by singlet-pairing of the electrons and that the gap function exhibits a conventional s-wave-type symmetry with a substantial anisotropy of its amplitude.

[1] S. Yonezawa, Y. Muraoka, Y. Matsushita, and Z. Hiroi, J. Phys. Soc. Jpn. **73**, 819 (2004).

[2] M. Brühwiler, S.M. Kazakov, N.D. Zhigadlo, J. Karpinski, and B. Batlogg, Phys. Rev. B **70**, 020503 (2004).

[3] K. Magishi, J.L. Gavilano, B. Pedrini, J. Hinderer, M. Weller, H.R. Ott, S.M. Kazakov, and J. Karpinski, Phys. Rev. B **71**, 24524 (2005).

3.3 Physics of low-dimensional systems

3.3.1 NMR in the low-dimensional system $BaVS_3$

J. Hinderer, M. Weller, J. L. Gavilano, H. R. Ott

In collaboration with O. Bernal

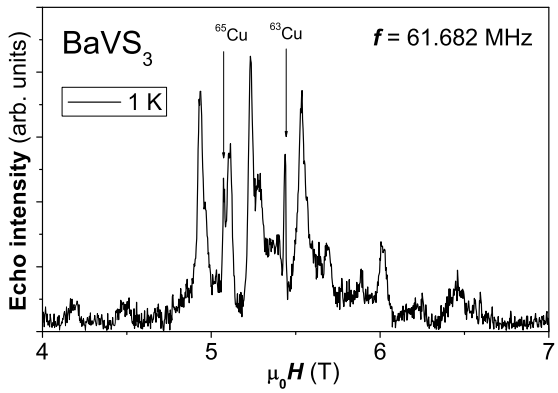

Figure 3.8: NMR spectrum of $BaVS_3$ at 1 K with a variaty of lines. The arrows indicate Cu-lines originating from the RF coil.

$BaVS_3$ is a compound with complex electronic features, which displays a variety of phenomena such as a Mott instability, Jahn Teller effect, orbital and magnetic interactions [1]. Below room temperature, three phase transitions at 240, 70, and 30 K, respectively, are observed whose nature is not fully understood. The metal-insulator transition temperature of 70 K is lowered by the application of hydrostatic pressure and the transition is completely suppressed at 20 kbars.

We have successfully performed measurements of the ^{51}V-NMR spectra on a $BaVS_3$ single crystal. At 45 K, the NMR spectrum displays a single line with a Knight shift of 0.5 percent and a linewidth of slightly more than 1 MHz. The low temperature spectrum at T = 1 K was taken at 61.682 MHz with external magnetic fields covering the range between 3.7 and 7.3 T. The spectrum displays three lines with relatively high intensity and several weaker lines, which may be quadrupolar wings (see figure 3.8). This provides evidence for three different Vanadium sites in the structure. Further investigations with a new batch of higher quality samples are in progress.

[1] L. Forró et al., Phys. Rev. Lett. **85**, 1938 (2000)

3.3.2 Haldane State versus Magnetic Order in $LiVSi_2O_6$

B. Pedrini, J. L. Gavilano, and H. R. Ott

In collaboration with S. M. Kazakov and J. Karpinski

The interest in the recently synthesized insulator $LiVSi_2O_6$ is raised by its structure, consisting of chains of VO_6-octahedra kept apart by SiO_4-tetrahedra. The V^{3+} magnetic moments are expected to form a good physical realization of a one-dimensional antiferromagnetic S = 1 spin system, for which the nonmagnetic ground state (the Haldane phase) is separated by an energy gap from the spin excitations.

This work is part of a project aimed at searching and characterizing Haldane systems. Previous investigations performed by our group on structurally related compounds, namely $LiVGe_2O_6$ [1] and $NaVGe_2O_6$ [2], have shown that the expected Haldane phases do not develop at low temperature because the two systems order antiferromagnetically.

We made ^{7}Li NMR measurements on a powder sample of $LiVSi_2O_6$. They include the mapping of the spectra and the determination of the spin-lattice relaxation rate T_1^{-1} in the temperature range between 5 K and 300 K. At temperatures above 30 K, the temperature dependence of the ^{7}Li NMR response follows $\chi(T)$, indicating that the V^{3+} magnetic moments are in a paramagnetic state. A prominent peak in $T_1^{-1}(T)$ at $T_N = 24$ K is accompanied by an abrupt broadening of the ^{7}Li NMR line upon cooling (see Figure 3.9), indicating the transition to an antiferromagnetically ordered state. The rapid decay of T_1^{-1} with decreasing temperature below T_N is consistent with this scenario.

Combining results of quantum Monte Carlo calculations for interacting S=1 spin chains with a random phase approximation method, we obtain equations for the intrachain coupling J and the interchain coupling J_{perp} as functions of T_N and T_{max}, the latter being the temperature where $\chi(T)$ is maximal. With this procedure we find similar values of the interchain coupling for all the three compounds ($J_{perp}/k_B = 3.3 \pm 0.4$ K), while the intrachain coupling ranges from $J/k_B = 18 \pm 1$ K for $NaVGe_2O_6$ to $J/k_B = 46 \pm 2$ K for $LiVGe_2O_6$ and to $J/k_B = 86 \pm 4$ K for $LiVSi_2O_6$. These results imply that from the considered compounds, $LiVSi_2O_6$ is closest to develop the Haldane phase, the transition occurring for $J_{perp}/J < 0.02$.

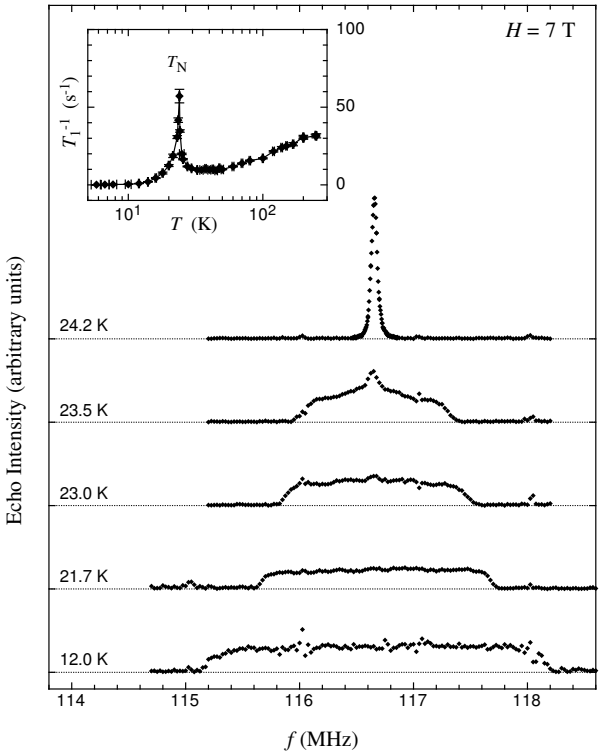

Figure 3.9: ^{7}Li NMR spectra at different temperatures between 12 K and 25K. Inset: ^{7}Li NMR spin-lattice relaxation rate T_1^{-1} as a function of temperature T in logaritmic scale.

The reason for the differences in the values of J is still under investigation. For this analysis, the chains of V^{3+} ions are approximated by a one-dimensional Hubbard model with two low-lying states per site. It is believed that the value of J, related to the hopping matrix elements, is tuned by small differences in the geometrical arrangement of the occupied t_{2g} orbitals at the V sites.

[1] J. L. Gavilano, S. Mushkolaj, H. R. Ott, P. Millet, and F. Mila, Phys. Rev. Lett. **85**, 409 (2000).

[2] B. Pedrini, J. L. Gavilano, D. Rau, H. R. Ott, S. M. Kazakov, J. Karpinski, Phys. Rev. **B70**, 024421 (2004).

3.3.3 Low-temperature Phase Transitions in $Na_{0.5}CoO_2$

B. Pedrini, J. L. Gavilano, J. Hinderer, M. Weller, and H. R. Ott

In collaboration with S. M. Kazakov and J. Karpinski

Compounds of the family Na_xCoO_2, with $0.25 < x < 0.8$ are physical realizations of metallic layered triangular system; the layers of CoO_6 octahedra are intercalated by partially filled Na planes. The interest in these materials was raised by the discovery of large thermolectric power in $Na_{0.7}CoO_2$, as well as that of superconductivity in the hydrated $Na_{0.3}CoO_2 \cdot 1.3H_2O$. Recent investigations have shown that structural parameters, in particular the interlayer distance, and electronic properties strongly depend on the Na concentration. Two metallic phases were identified: for $x < 0.5$, the compounds exhibit Pauli-like magnetism, while for $x > 0.5$ the behaviour is of Curie-Weiss type. The two phases are separated by $Na_{0.5}CoO_2$, which has only very recently been recognised to adopt an insulating ground state, with a Mott transition at $T_{MI} = 53$ K [1].

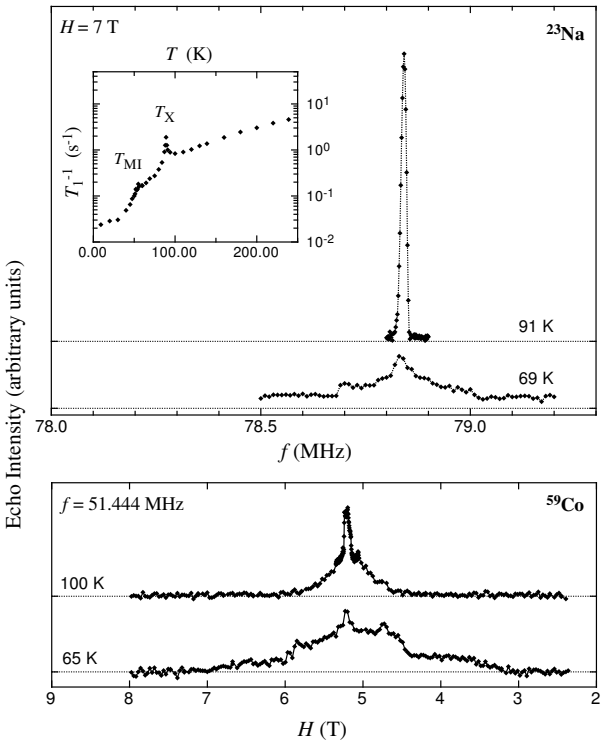

Figure 3.10: Upper panel: ^{23}Na NMR spectra above and below $T_{\rm X}$; the inset represents T_1^{-1} as a function of T. Lower panel: ^{59}Co NMR spectra above and below $T_{\rm X}$.

As a quality test, we measured the resistivity ρ and the magnetic susceptibility χ, as a function of temperature, of a powder sample of $Na_{0.5}CoO_2$, and found good agreement with the published data of ref. [1]. At $T_{\rm MI}$, the Mott transition is reflected by a sudden upturn, with decreasing temperature, of ρ, and by a small peak in $\chi(T)$; in addition, another small anomaly in $\chi(T)$ is detected at $T_{\rm X} = 88$ K. Subsequently, we performed NMR measurements for temperatures between 5K and 300 K. They included the mapping of ^{23}Na and ^{59}Co spectra, as well as the determination of the ^{23}Na spin-lattice and spin-spin relaxation rates T_1^{-1} and T_2^{-1}.

The metal insulator transition at $T_{\rm MI}$ is reflected by small cusps in $T_1^{-1}(T)$ and $T_2^{-1}(T)$, but no anomaly is found in the temperature evolution of the NMR spectra around $T_{\rm MI}$. However, drastic changes in the NMR data are observed around $T_{\rm X}$. Prominent peaks in $T_1^{-1}(T)$ and $T_2^{-1}(T)$ at $T_{\rm X}$ are accompanied by an abrupt broadening of both the ^{23}Na and ^{59}Co NMR line, with decreasing temperature (see Figure 3.3.3). The shape of the ^{59}Co spectra below $T_{\rm X}$ seems consistent with the occurence of magnetic ordering, a scenario compatible with the rapid decrease of T_1^{-1} upon cooling. The internal field $H_{\rm int}$ at the Co-nuclei is approximately 0.8 T, however, and this small value suggests that the NMR-signal arises from non-magnetic Co-sites.

The reported results imply that in $Na_{0.5}CoO_2$, an unusual type of magnetic ordering in the metallic phase precedes the onset of charge ordering and an insulating ground state. This evolution is in contrast to the results of calculation based on the local-density approximation combined with a Hubbard repulsion term [2], which predict a simultaneous charge and magnetic ordering. Further theoretical and experimental research on $Na_{0.5}CoO_2$ thus seems justified. We plan to determine the ^{59}Co spin-lattice relaxation rate for temperatures below 150 K, in order to obtain more information on the two transitions at $T_{\rm MI}$ and $T_{\rm X}$.

[1] Q. Huang et al., J. Phys.: Cond. Matt. **16**, 5803 (2004).

[2] K.-W. Lee, J. Kunes, P. Novak, and W. E. Pickett, Phys. Rev. Lett. **94**, 026403 (2005).

3.3.4 ^{59}Co-NMR studies of $Na_{0.70}CoO_2$

J. L. Gavilano, D. Rau, B. Pedrini, J. Hinderer, H. R.Ott, S. M. Kazakov and J. Karpinski

$Na_{0.7}CoO_2$ is a transition-metal oxide with a layered structure with interesting physical properties, including a tendency to electron localization or an unconventional charge density-wave phenomenon within the Co $3d$ electron system [1]. We have complemented our previous ^{23}Na-NMR studies by measuring the ^{59}Co-NMR response of polycrystalline samples of $Na_{0.7}CoO_2$. Below 300 K the temperature evolution of the ^{59}Co-NMR spectrum reveals a gradual change of the electric field gradients at the Co positions resulting in two inequivalent Co sites in the structure at low temperatures. These sites can be resolved by their different quadrupolar wings below 250 K. This result supports our previous conclusions that changes in the Co $3d$ electron system occur between 250 and 300 K. The Knight shifts K_1, K_2 of the central transitions for these two sites are approximately temperature independent between 40 and 200 K. At temperatures below 40 K the Knight shifts vary with temperature and the difference $|K_1 - K_2|$ increasing with decreasing temperatures. This suggests the development of an unusual magnetic ordering below 40 K.

Below 200 K, the spin-lattice relaxation rate T_1^{-1} varies linearly with T, with a value for $(T_1T)^{-1}$ of the order of magnitude of those found in simple metals. However, above 200 K, $T_1^{-1}(T)$ displays a substantial increase above the linear-in-T behavior observed at low temperatures. This behavior again supports our previous claims of the existence of an instability in the Co $3d$ electron system at temperatures between 250 and 300 K.

Together, the behavior of $T_1(T)$ and $K(T)$ between 40 and 200 K indicates that the ^{59}Co-NMR response of $Na_{0.7}CoO_2$ is dominated by itinerant conduction electrons, as in simple metals. These results confirm that the Co ions occupy the conducting planes. There are magnetic and nonmagnetic Co ions and the latter occupy at least two inequivalent sites. Fermi liquid behavior is observed between 40 and 200 K and some kind of magnetic ordering develops below 40 K.

[1] J. L. Gavilano, D. Rau, B. Pedrini, J. Hinderer, H. R. Ott, S.M. Kazakov and J. Karpinski, Phys. Rev. B **69**, 100404 (2004).

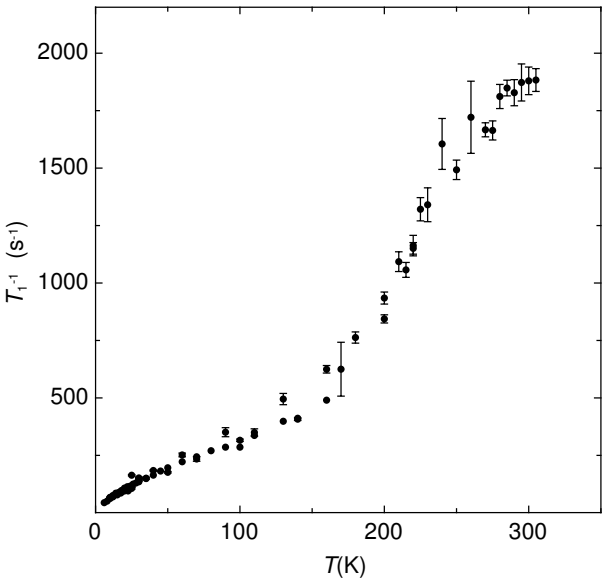

Figure 3.11: Spin-lattice relaxation rate T_1^{-1} as a function of T.

3.3.5 $Na_2V_3O_7$: An unusual low dimensional quantum magnet

J. L. Gavilano, E. Felder, D. Rau, H. R. Ott

In collaboration with P. Millet, F. Mila, T. Cichorek and A. C. Mota

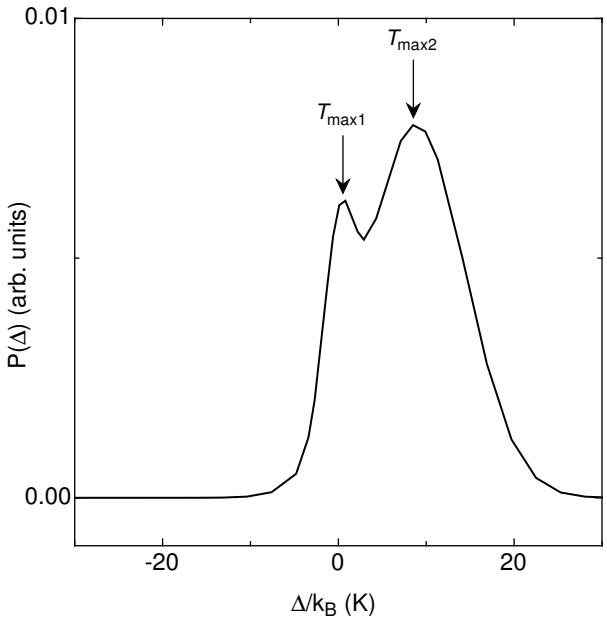

Figure 3.12: Probability distribution $P_1(\Delta) + P_2(\Delta)$ of the spin singlet-triplet energy gap Δ.

We developed a model to explain the extensive experimental data regarding various physical properties of $Na_2V_3O_7$ accumulated during the last few years. $Na_2V_3O_7$ is an insulator with unusual structural features and unusual magnetic properties. Results of our present and previous measurements [1,2] of the NMR response, dc- and ac magnetic susceptibilities and the specific heat at low temperatures suggest that this material is close to a quantum critical point QCP at $\mu_0 H = 0$ T. Our model assumes that at temperatures well above 100 K the system responds paramagnetically with the localized V magnetic moments interacting with each other with a wide range of coupling energies. At temperatures of the order of 100 K, the V moments form pairs with mostly singlet ($\Delta > 0$), but also with some triplet ($\Delta < 0$) ground states.

The singlet-triplet gaps Δ adopt values with a broad distribution which contains at least three terms $P(\Delta) = P_1(\Delta) + P_2(\Delta) + P_3(\Delta)$. Two of the terms P_1 and P_2 are represented by Gaussian functions, as shown in the Fig and involve 1/9 of the V moments. P_3, which characterizes the rest of the V moments (8/9), is given by a very broad distribution of gaps ranging from -15 to 350 K

The degeneracy of the dimers with triplet ground states is lifted by a phase transition at an unusually low temperature of 0.086 K [2]. The application of modest magnetic fields effectively quench this low-temperature state and the system is driven away from the QCP as the applied fields are enhanced to above 1 T. From our results it is suggested that the $V - V$ couplings involve a broad range of interactions, implying that the relevant low-energy effective magnetic model should contain some level of randomness.

[1] J.L. Gavilano, D. Rau, Sh. Mushkolaj, H.R. Ott,P. Millet, F. Mila, Phys. Rev. Lett., **90**, 167202 (2003).

[2] J.L. Gavilano, E. Felder, D. Rau, H.R. Ott,P. Millet, F. Mila, T. Cichorek and A. C. Mota, cond-mat/0501756 (2005).

3.3.6 Optical properties of $Na_{0.7}CoO_2$

G. Caimi, A. Perucchi, H. Berger and L. Degiorgi

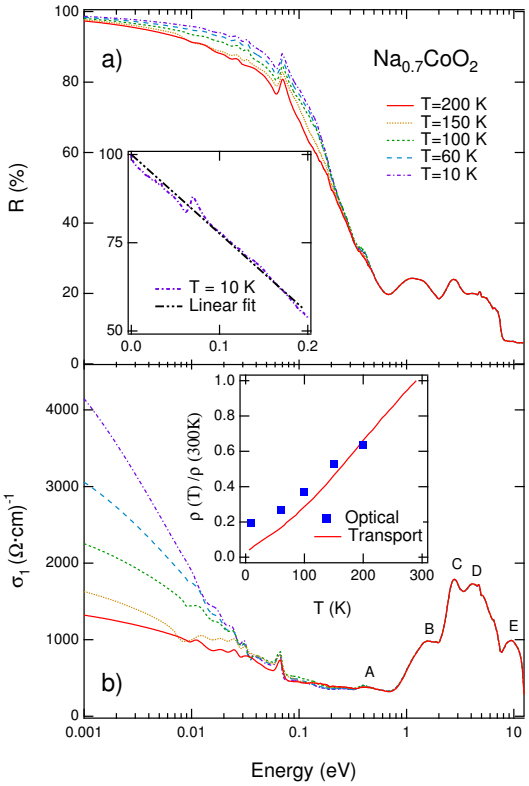

Figure 3.13: a) Reflectivity and b) real part $\sigma_1(\omega)$ of the optical conductivity of $Na_{0.7}CoO_2$ at selected temperatures. The four high frequency absorptions in $\sigma_1(\omega)$ due to the electronic interband transitions are labeled. Inset a): R(ω) at 10 K between 0 and 0.2 eV, emphasizing the linear behavior of R(ω) at low energies. Inset b): Comparison of $\rho_{dc}(T)$ and the estimation of the dc resistivity from the optical experiment (i.e., $\rho_{dc}^{optical}(T) = 1/\sigma_1(\omega \to 0, T)$).

The discovery of superconductivity at 5 K in hydrated sodium cobaltate has attracted considerable attention. How water inclusion triggers superconductivity in Na_xCoO_2 is not fully understood yet. The investigation of non-hydrated sample is therefore of relevance and a considerable research effort has been devoted to Na_xCoO_2 specimens with x ranging between 0.3 and 0.85. As x increases from 0.3, the ground state goes from a paramagnetic metal to a charge-ordered insulator for $x = 0.5$, to a Curie-Weiss metal around 0.7, and finally to a weak-moment magnetically ordered state for $x > 0.75$. This latter phase is supposed to be equivalent to a so called spin-density-wave (SDW) metal. Several recent investigations, based on magnetic, thermal and transport properties as well as muon spin spectroscopy, indicate the formation of a SDW metallic state for $x = 0.75$.

Optical reflectivity experiments (Fig. 3.13a) are well-known tools in order to achieve information about the electrodynamic response of the investigated system, and to shed light on its electronic structure. The capability to cover the energy range from the far-infrared up to the ultraviolet allows us to perform reliable Kramers-Kronig transformation, in order to obtain the absorption spectrum (i.e., the complex optical conductivity). To the complex optical conductivity we apply the generalized Drude model, extracting the frequency dependence of the scattering rate Γ (Fig. 3.14) and effective mass m^* (not shown here) of the itinerant charge carriers.

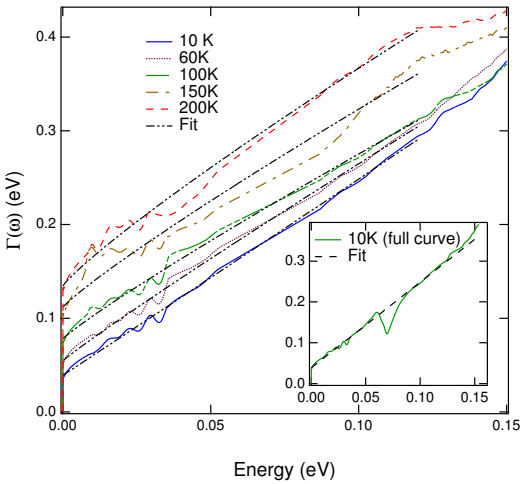

Figure 3.14: Frequency dependence of the scattering rate and its fit according to $\Gamma(\omega) \sim \omega^{\alpha}$ at selected temperatures. Note that the infrared (IR) active phonon has been subtracted in order to better highlight the linear or sub-linear fit. Inset: the original curve of $\Gamma(\omega)$ (i.e., comprehensive of the IR phonon at 0.07 eV) at 10 K is shown with the fit with $\alpha = 1$. The phonon subtraction does not affect the fit of $\Gamma(\omega)$. This is true at all temperatures.

We have provided the complete absorption spectrum of $Na_{0.7}CoO_2$ (Fig. 1b). We have established that $\Gamma(\omega) \sim \omega$ at low temperatures (Fig. 3.14). Ruvalds and Virosztek proposed a while ago a Fermi-surface nesting scenario for

describing the optical properties of superconducting oxides. They showed that Fermi-surface nesting modifies the electron-electron scattering and therefore yields an unusual variation of the optical reflectivity. Within this scenario, also applicable for the charge- and spin-density-wave state where nesting is an essential ingredient, the effective Drude component is characterized by a relaxation rate that is linear in frequency for $\omega > T$ and the reflectivity is also linear in frequency in a broad spectral range. Our data agree with the theoretical predictions. Therefore, $Na_{0.7}CoO_2$ seems to be in the proximity of a spin-density-wave metallic state.

3.4 Instrumentation

J. Hinderer, M. Weller, D. Rau, J. L. Gavilano, H. R. Ott
In collaboration with S. Krämer, I. Sheikin, M. Chiao

We designed and built an experimental setup for NMR measurements under hydrostatic pressure up to 16 kbars at temperatures as low as 0.5 K in magnetic fields up to 8.5 T. A continuous flow ^{3}He cryostat, two BeCu piston cylinder pressure cells and a 70 MHz single conversion spectrometer were home made and are now fully operational.

3.4.1 Continuous flow ^{3}He cryogenic system

The continuously operating ^{3}He system was designed for the big heat loads that are common for NMR measurements at low temperatures. A large cooling power is obtained by a high ^{3}He circulation rate. The advantages of this design are, a relatively high cooling power at temperatures down to 0.4 K, variable magnetic fields and in-situ tunable tank circuits. A large frequency range (several to more than a hundred MHz) is covered by this design in combination with typical NMR coils.

3.4.2 Hydrostatic pressure cells

Two BeCu piston cylinder pressure cells were fabricated. The smaller one, with an inner/outer diameter of 4/14 mm, can stand pressures up to 11 kbars. The larger one, with an inner/outer diameter of 5/40 mm, can be loaded up to 16 kbars and makes use of the full 40 mm experimental space provided by the ^{3}He cryostat.

For the precise control of the loading and unloading procedures of the pressure cells an existing 25 ton press has been equipped with a compensated strain-gauge based force-gauge, a displacement gauge and a PC-based data display unit. The pressure in the loaded cell is measured in situ by the pressure dependent shift of the NQR resonance frequency of a Cu_2O powder sample placed inside the pressure cell.

3.5 Controlling of complex structures

M. Fell, H.M. Singer, O. Wittwer, and J.H. Bilgram

Patterns are formed everywhere in nature. Examples of such phenomena can be found in clouds, snow crystals, magnetic domains, grain structures in cast metals and grain structures in rocks. Models have been developed to describe the formation of patterns in nature. In order to verify and to improve the significance of theoretical models it is necessary to compare results of model calculations and simulations with experimentally observed patterns. Practical applications of these experiments and calculations can be found e.g. in foundry industries.

Dendrites are the best studied structures formed during solidification of undercooled melt. Additionally other complex structures have been found in experiments and numerical studies. We perform 2D/3D-numerical simulations and experiments which allow in situ investigations of three-dimensional growth of xenon crystals into undercooled pure melt. Dendrites, seaweed, doublons, triplons etc. can be produced in experiments and numerical studies depending

on initial conditions. In an interplay of numerical studies and experiments we use simulations to interpret and to plan experiments. Experimental results are used as a basis of model calculations and the development of models of complex shapes. Three-dimensional growth shapes of crystals are reconstructed using sophisticated image processing combined with experimentally determined shape parameters. With a newly developed method of reconstructing the three-dimensional shape of transparent objects it is possible to measure the volume and the surface area of dendrites. By means of phase field simulations a morphology diagram in the parameters undercooling vs. anisotropy of surface tension for 2D and 3D diffusion limited growth of crystals was calculated.

For a dendrite growing in a stationary mode, side branches are initiated by selective amplification of noise. Side branches may also be initiated by an instability at the tip and move in a wave like pattern along the dendrite. They have also been observed to be formed by local instabilities at the fins of the dendrite. If the instability at the tip does not move away from the tip, doublons or higher multiples of tips are formed. Two side branches can develop to two dendrites growing side by side. Due to the interaction of such dendrites periodic oscillations of growth velocity are observed. (Fig. 1) The interaction of two dendrites depends on the distance between them.

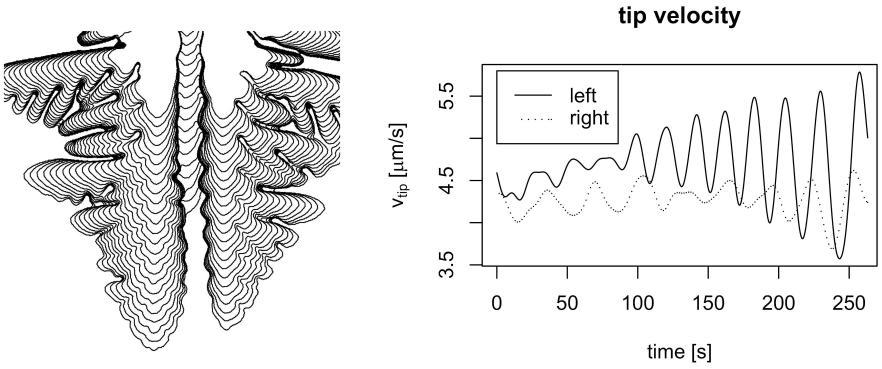

Figure 3.15: Left: Two dendrites growing side by side mutually interacting. Right: Growth velocities of the two interacting dendrites shown in the left figure.

The mechanical and corrosion behaviour of cast products are influenced by the fine structure which is determined by the shape of the crystals as developed during the solidification process. In a new type of experiments we try to control this fine structure by cycling the temperature of the melt during the solidification process.

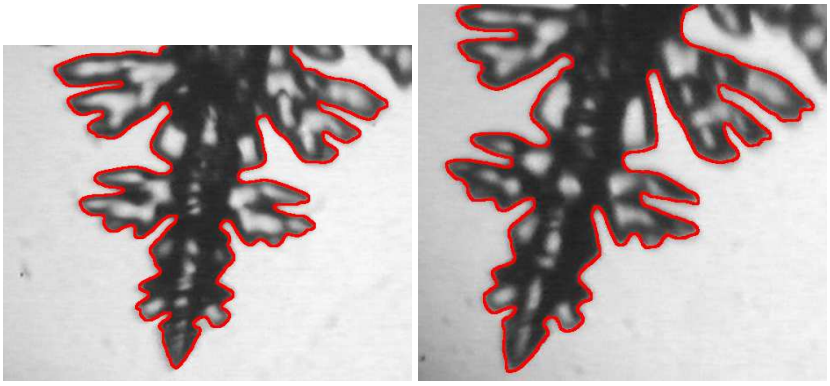

Figure 3.16: A dendrite grown during a sequence of temperature cycles. Xenon crystals have four fold symmetry. left: the crystal is symmetric near the tip region. right: the same crystal 90 rotated, the other two sides are also symmetric.

We cycle the temperature of the melt around the melting temperature. Upon heating the dendrite stops growing or begins to shrink and it restarts to grow after cooling down the melt. The morphology of the newly grown crystal

differs from the morphology of a typical dendrite. Interestingly four absolutely symmetrical lobes start to grow at the main tip. Repeating the melting cycle leads to a controlled formation of side branches and to symmetric crystals.

3.6 Application-oriented thin film research

3.6.1 Epitaxial IV-VI narrow gap semiconductor layers

K. Alchalabi, K. Kellermann, D. Zimin, M. Arnold, A.N. Tiwari and H. Zogg; www.tfp.ethz.ch

Narrow gap lead chalcogenide (IV-VI) layers like PbX, $Pb_{1-x}Sn_xX$ and $Pb_{1-x}Eu_xX$ (X=Te, Se) are investigated for applications and basic research. The layers are grown by solid source molecular beam epitaxy (MBE) onto Si-substrates by employing a CaF_2 buffer layer. The epitaxial layers are heavily lattice- and thermal expansion mismatched. Misfit and threading dislocations therefore are present. The density of threading dislocations ranges from 10^6 cm^{-2} to 10^8 cm^{-2}. Despite of these rather high densities, devices with reasonable quality are fabricated in the layers. They include:

- Heteroepitaxial monolithic two-dimensional Infrared Focal Plane Arrays (2d IR-FPA) on active Si-substrates [for a review, see IEEE Trans. ED50, 209 (2003)].
- Optically pumped mid-IR lasers on Si-substrates consist of PbSe DH (double heterostructures) or QW (quantum wells) embedded in $Pb_{1-x}Eu_xSe$ barrier layers and emit at 3-7 μm wavelength [J. Appl. Phys. 94, 7053(2003)].
- Mid-IR resonant cavity optically pumped light emitters on Si(111) for radiation in a narrow band around 4.2 μm wavelength. [Infrared Phys. Technol. 46, 155 (2004)].
- RCED (resonant cavity enhanced detectors) sensitive on a narrow spectral line only. We realized the first such detectors in the mid IR-range which exhibit a single narrow line and high quantum efficiency: A very thin $Pb_{1-x}Eu_xSe$ layer acts as photodetector and is placed inside an optical cavity whose optical thickness is adjusted with an additional nonabsorbing $Pb_{1-y}Eu_ySe$ layer (y>x). The cavity is terminated on one side with an epitaxial non-absorbing Bragg mirror consisting of a stack of $Pb_{1-z}Eu_zSe/BaF_2$ pairs. High reflectivities are obtained with a few pairs due to the large difference of the optical indices of PbEuSe and BaF_2. The second mirror consists of a metal which in addition forms the photovoltaic junction. In the example shown (Fig. 3.17) we achieved a line width of 70 nm (with peak wavelength 4140 nm) and peak quantum efficiency about 30 % without AR coating.

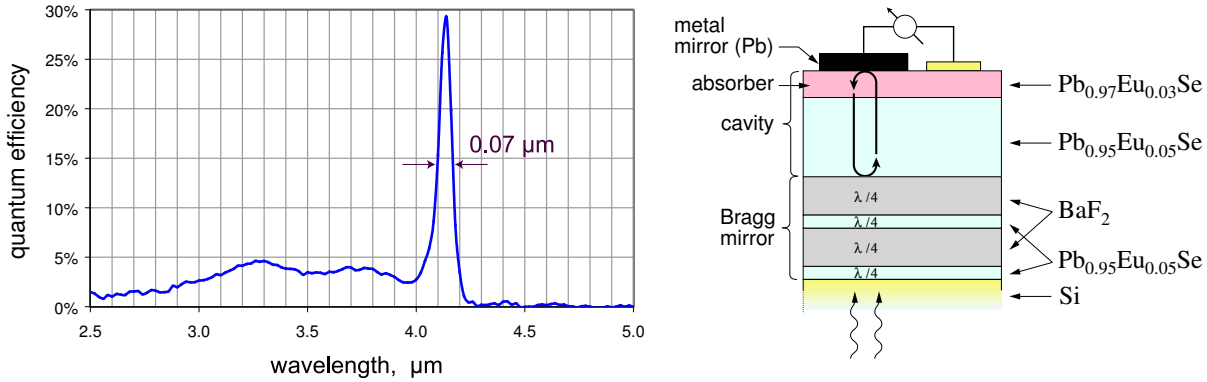

Figure 3.17: Spectral response and schematic structure of a lead-chalcogenide RCED mid-IR detector.

- With a threading dislocation density of 10^7 cm^{-2}, the mean distance between two dislocations is about 3 μm. If arrays of IR-detectors with smaller sizes are fabricated, some of these detectors should be free of any dislocations. A NF-project started to study the influence of the noise currents as a function of the number of dislocations (0,1,2,..) which cross the active parts of the detectors. To this end, an AFM operation in vacuum at low temperature is being built up.

3.6.2 Thin-film solar cells based on Cu(In,Ga)Se_2 compound semiconductors

D. Abou-Ras, D. Brémaud, M. Kaelin, A. Romeo, D. Rudmann, H. Zogg, and A.N. Tiwari; www.tfp.ethz.ch

There is considerable interest in safe, cheap, abundant, renewable, and environment-friendly generation of electricity. Thin-film solar cells based on the polycrystalline compound semiconductor Cu(In,Ga)Se_2 (usually abbreviated as "CIGS") are a promising candidate for this purpose. Flexible CIGS solar cells grown on polymer foils are particularly interesting from an economical perspective, but also because they offer novel applications in space and on Earth. We develop such flexible solar cells and investigate the properties of the involved materials. Preparation and characterization of novel buffer layers deposited by dry methods and development of non-vacuum deposited CIGS absorbers are among further projects.

Flexible solar cells

The main challenges associated with flexible solar cells on polymer substrates (Fig. 3.18, left) are growth of CIGS films at low substrate temperatures, since the polymers cannot withstand temperatures higher than 450-500 °C, and doping with Na in optimum amounts. Our investigations show that Na hinders the interdiffusion of In and Ga during CIGS growth already at higher substrate temperatures, while at lower temperatures also the diffusion of Cu is hindered by Na. Therefore, we have developed growth processes where Na is incorporated after CIGS growth, hence resulting in enhanced crystal quality. The demonstration of the concept using commercially available polyimide foils as substrates led to an independently confirmed conversion efficiency of 14.1 % (Fig. 3.18, right). This presents a new world record for flexible solar cells on polymers.

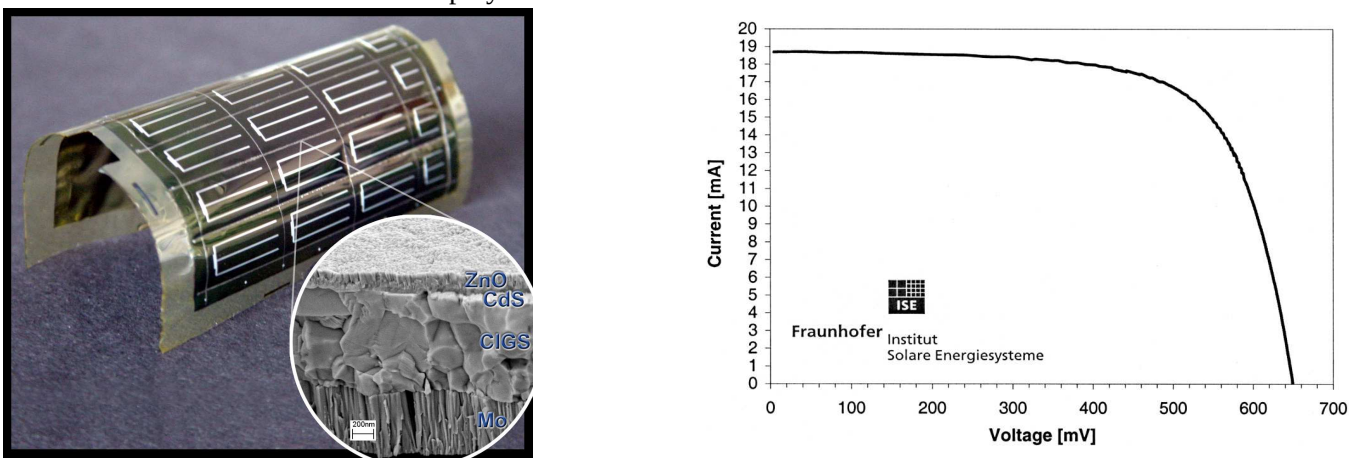

Figure 3.18: *Left:* Flexible CIGS solar cells on a 25 cm^2 polyimide substrate and SEM image of the deposited films. *Right:* Current-Voltage characteristics of a flexible CIGS solar cell with world-record conversion efficiency of 14.1 %.

Structural and chemical characterization of interfaces in CIGS solar cells

(Collaboration with: Institute of Applied Physics, Prof. Dr. G. Kostorz, ETH Zürich)

In_2S_3 buffer layers for the application in high-efficiency thin film solar cells based on CIGS have been studied by means of bright-field, high-resolution (HR-TEM), and energy-filtered transmission electron microscopy, and also by electron diffraction (ED), energy-dispersive X-ray spectroscopy, and scanning electron microscopy. In_2S_3 buffer layers were deposited by atomic-layer deposition, evaporation, or sputtering. The substrate temperatures during In_2S_3 deposition below about 230 °C leads to good efficiencies, but at higher temperatures, cells degrade. The HR-TEM image shows an abrupt interface between the In_2S_3 layer deposited at 210 °C and CIGS, whereas at 240 °C, an intermediate phase formed (Fig. 3.19). By means of ED, this phase was identified as $CuIn_5S_8$; its microstructure contains a large number of vacancies and planar defects. They may act as recombination centres at the p-n heterojunction of the solar cell and thus be responsible for the degrading photovoltaic performance.

An intentionally grown, intermediate $MoSe_2$ layer between an indium tin oxide (ITO) back contact and the CIGS absorber improves the efficiency of CIGS solar cells with transparent back contact. The orientation of the layered

structure of $MoSe_2$ influences electrical and mechanical contact properties between back contact and CIGS absorber. The reaction kinetics of $MoSe_2$ formation and the crystallographic properties of the $MoSe_2$ layer have been investigated by selenization of Mo layers in Se vapor at different temperatures and for different periods of time.

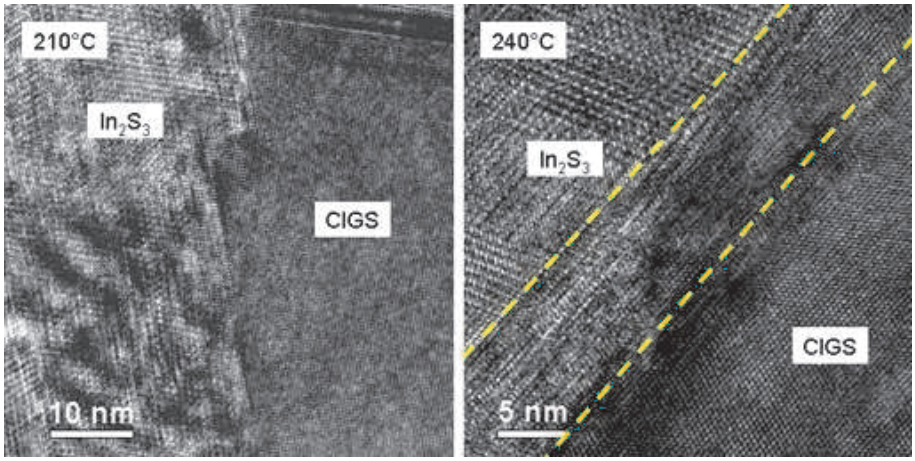

Figure 3.19: High-resolution transmission electron micrograph from the interface of CIGS with In_2S_3 layers grown at 210 °C and 240 °C. While there is a good lattice match between In_2S_3 and CIGS for the 210 °C sample, an intermediate phase formed between CIGS and In_2S_3 in the 240 °C sample.

Chapter 4

Magnetism, Electron Spectroscopy

(http://www.microstructure.ethz.ch)

Head
Prof. Dr. D.Pescia (Nanoscale magnetism), Prof. Dr. M. Erbudak (Surface Physics)

Academic Staff

Dr. A. Vaterlaus (40%)	Dr. U. Ramperger	Dr. M. Hochstrasser
R. Lüscher	M. Buess	O.Portmann
Y. Weisskopf	T. Michlmair	M.Dorn
J-N. Longchamp (from 1.10.04)		
S. Metzger		

Technical Staff

T. Bähler (75%)	U. Maier (20%)

Academic Guests
Dr. Thomas Flückiger, 1.01.04 - 31.03.04
Prof. Dr. Muhittin Mungan, Bogazici Universität, 08.08.04 - 22.08.04
Dr. R. Lüscher, 1.10.04 - 31.12.04
Dr. Zorka Papadopolos, Universität Thübingen, 15.10.04 - 26.10.04
Prof. Dr. Silvia Picozzi, L' Aquila University, 29.10.04 - 3.12.04
Prof. Dr. Sondan Durukanoglu, Istanbul Technische Universität, 19.12.04 - 25.12.04
T.P.J. Knowles, 1.04.04 - 30.06.04

4.1 Nanoscale magnetism

4.1.1 Fourier transform imaging of spin vortex eigenmodes

M. Buess, R. Höllinger, T. Haug, K. Perzlmaier, U. Krey, D. Pescia, M.R. Scheinfein, D.Weiss, C.H. Back, Phys. Rev. Lett. **93**, 077207 (2004)

We have studied the spin dynamics in 15 nm thick ferromagnetic permalloy disks ranging in diameter from 0.5 to 6 μm and patterned by e-beam lithography onto a Si substrate. A 500 nm thick Cu-microcoil was prepared around the element using e-beam lithography and electro-plating. It surrounds the sample with an inner diameter of 8 μm and an outer diameter of 12 μm. The magnetic ground state of the elements exhibits an in-plane, flux closure, vortex-like spin configuration. A current pulse of about 100 ps rise time launched into the microcoil provides a perpendicularly oriented magnetic tipping field pulse (with strength $\approx$ 50 Oe) exciting a spin precessional motion away from the ground state configuration. The figure shows a stroboscopic sequence of polar Kerr microscopy images obtained

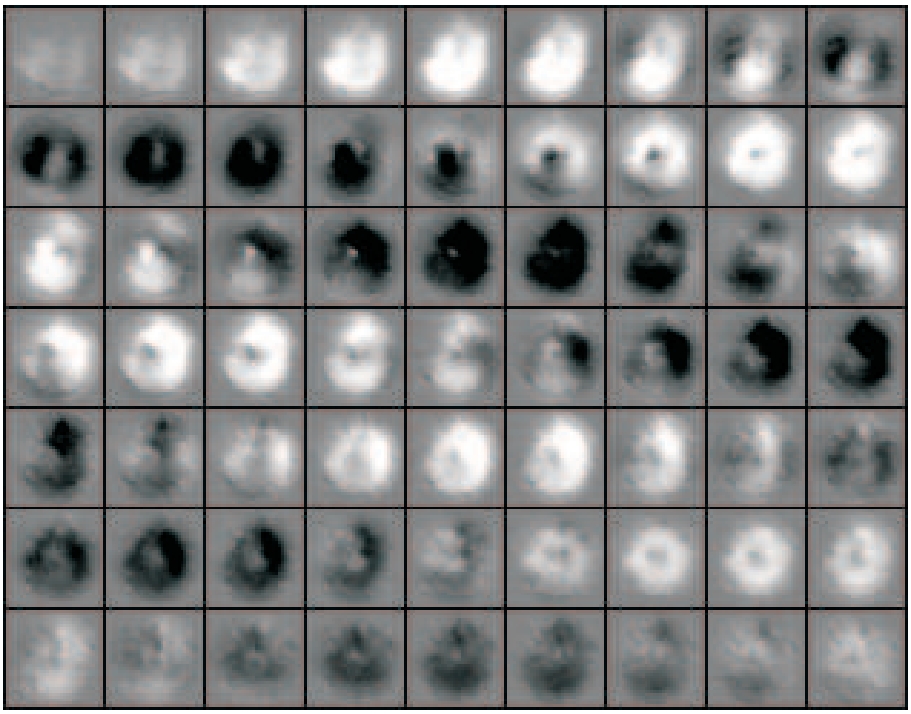

immediately after application of the field pulse. The time delay between each image is 30 ps. The image contrast is produced by the z-component of the magnetization vector undergoing a spatially non-uniform motion. Despite the complexity of the sequence, one recognizes an overall periodicity of the motion with maxima (bright) and minima (dark) of M_z recurring after a characteristic time of the order of 350 ps. This motion is the result of Larmor precession. The non-uniform contrast shows that the tipping pulse excites **several** modes with slighlty different frequencies. The modal structure of the motion is not immediately apparent from the overall time sequence but can be obtained by applying a **phase sensitive** Fourier-transform imaging processing to the overall time-sequence, invented in this paper. The amplitude and the phase of the various eigenmodes contributing to the spin motion are displayed in the following figures. We distinguish two types of eigenmodes: those with a circular nodes (figure on the left) and those with diametric nodes (figure on the right). The image with the circular nodes shows the experimental spectral weight and phase on the right half of the circle, to be compared with the micromagnetic calculation in the left half of the image. The modes can be classified according to the number of nodes: the fundamental and most intensive mode has a node only in the center of the disk and at its border (A). The phase is uniform over the disk. The next mode has a node at approximately half distance between the core and the boundary (B). Going across the node the phase changes by π. Finally, we observe a third mode with two nodes within the disk (C) and with π phase jump across each node.

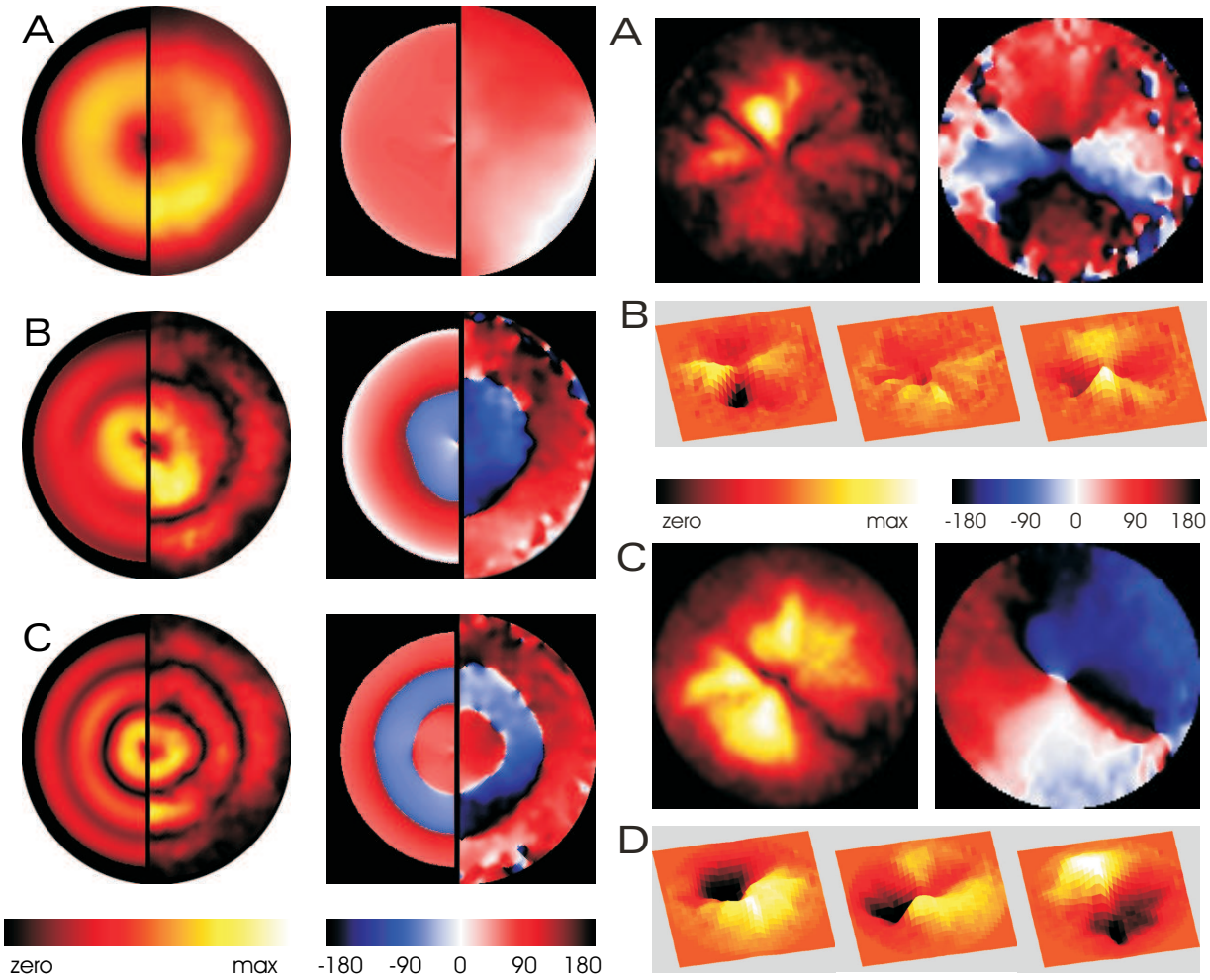

The figure of the right shows Fourier-amplitude (left) and Fourier-phase (right) of the lowest lying modes with diametric nodes (A and C). The mode in A has two mutually orthogonal nodes. In going across each node the phase changes by π. Images of this mode in the time domain can be reconstructed by **back-Fourier transforming** the amplitude and the phase maps of Fig.A. Some snapshots of the time sequence are shown in B. In contrast to the original time sequence, the time sequence in B images only the specific mode under consideration. The mode with one diametric node in C (left: amplitude, right: phase) is reconstructed in D in the time domain. For more details of the Fourier imaging method see the original paper.

4.2 Surface Physics

The method of crystal growth known as epitaxy is used in fabrication of solid-state devices, which are impossible to achieve by any other technique. A continuous growth can only be achieved if the ratio between the evapotarion rate and the surface temperature remains below a certain limit. Additionally, there is a stringent condition imposed on the temperature of the substrate for different morphologies that are identified during growth of Al on the pentagonal surface of the quasicrystal $Al_{70}Pd_{20}Mn_{10}$, Al-Pd-Mn. At the high-temperature limit, on the other hand, a crystalline overlayer is instantly absorbed by the quasicrystalline bulk.

4.2.1 Absorption kinetics of Al in icosahedral quasicrystal Al-Pd-Mn

R. Lüscher, T. Flückiger, Y. Weisskopf, M. Erbudak

We have studied the thermodynamical stability of crystalline Al layers on the pentagonal surface of Al-Pd-Mn quasicrystal by depositing thin Al films. The decrease of the film thickness, and consequently the amount of Al absorbed by the bulk, is monitored as a function of time at different substrate temperatures *T* using Auger electron spectroscopy. The amount of Al that diffuses from the surface into the bulk can be represented as an analytic function depending on the square root of time in order to extract the diffusion coefficient *D* related to the absorption process for a given temperature. For a thermally activated diffusion process, a plot of *D* vs *1/T* is called the Arrhenius plot, the slope of which represents the activation energy *Q(T)* for diffusion and the ordinate intersection gives the pre-exponential factor D_{o}. The values of *Q(T)* and D_{o} are characteristic of the type of diffusion. The activation energy around 100 kJ/mol $\approx$ 1 eV together with the relatively large pre-exponential factor imply that the absorption of Al is governed by a fast vacancy-mediated diffusion mechanism. These results are in agreement with the observation that the Debye temperature of this surface is around 300 K and can be raised by 100 upon Al absorption. This suggests that the pentagonal surface of Al-Pd-Mn is open structured, yet the vacancies can readily be filled with Al. By using these values characteristic of diffusion, we can find the substrate temperature for a stable thin Al surface film. By allowing only 1/10 atomic layers diffusing into the pentagonal surface within a typical experimental time of 1 h, we find that the temperature should be no higher than 299 K for a 3-nm thick Al film.

4.2.2 Al nanostructures on the pentagonal surface of Al-Pd-Mn

R. Lüscher, Y. Weisskopf, A.R. Kortan, M. Erbudak

We have monitored the growth and structure of vapor-deposited Al textures on the pentagonal surface of Al-Pd-Mn as a function of the substrate temperature between 200 and 300 K so that diffusion of Al into the bulk is impeded to a great extend. Vacuum deposition up to 0.5 nm of Al causes a decrease of the low-energy electron diffraction (LEED) spot intensities. Quasicrystalline and crystalline patterns coexist up to 1.5 nm after which no further changes could be detected in the LEED pattern. The observation for submonolayers can be understood in terms of epitaxial and continuous growth of Al on the pentagonal surface of Al-Pd-Mn. At this initial stage of growth, the resulting morphology is probably governed by kinetic effects. A crucial factor influencing the (kinetic) growth process is the energy barrier of an Al atom that is trapped at surface vacancies. This will impede the surface diffusion and create a seed for the growth of Al. Regardless of the affinity of Al to an Al-Pd-Mn surface, in all heteroepitaxial systems some strain is always involved. This strain is first concentrated at those sites where nucleation occurs and changes with film thickness. When the Al film gradually adopts its bulk lattice properties, the strain relaxes. Thus, the strain influences the nucleation kinetics in a layer-dependent way and a competition between the epitaxy-imposed ordering versus the stable bulk phases of the film is encountered.

Figure 4.1 shows a LEED pattern from the clean surface at a primary-electron energy of 61 eV. The pattern demostrates the overall structural quality of the substrate surface. As the film grows thicker we observe the evolution of a new surface structure. At a substrate temperature of 300 K, we observe the pattern depicted in Fig. 1b. With increasing electron energy, the spots converge to directions, tilted away from the surface normal. This observation implies that the film consists of crystalline textures exposing surfaces, which are inclined with respect to fivefold-symmetry surface. Detailed analyses show that the surface structure consists of 5 Al crystalline domains exposing their (110) surfaces and aligned in such a way that two $\langle 111 \rangle$ and one $\langle 100 \rangle$ visible axes coincide with threefold- and twofold symmetry directions of the quasicrystal, respectively. In this orientation, the $(0, 1, \tau)$ direction of the domains are aligned parallel to the surface normal of the substrate, where τ is the golden mean.

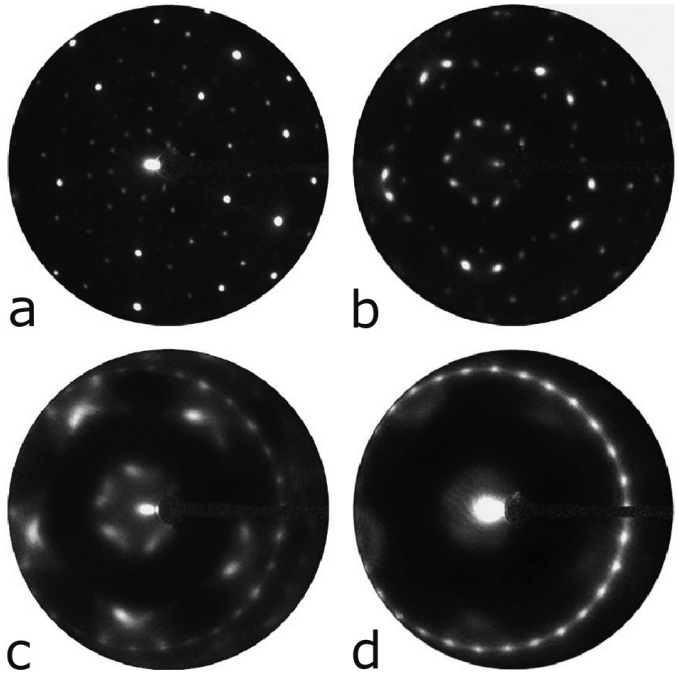

Figure 4.1: LEED patterns observed (a) from the clean and 1.1-nm Al-covered pentagonal surface kept at (b) 300, (c) 242, and (d) 200 K during deposition.

If the substrate temperature is lowered below about 250 K, a distinctly different growth mode is observed. As shown in Fig. 1d ($T = 200$ K), a ring of 30 diffraction spots appears that converges towards the surface normal as the primary energy is increased. In this case, we have the formation of five Al domains in the face-centered cubic structure exposing their (111) surfaces parallel to the substrate surface. Fig. 1c is obtained after depositing Al at 242 K. In addition to 30 spots observed for low-temperature evaporation, also features are discernible typical of the high-temperature growth. We observe that, at the high-temperature regime, three-dimensional Al islands develop in contrast to layer-by-layer growth. The reason for this growth mode is essentially due to the low surface energy of the quasicrystalline substrate compared to the corresponding values for Al and the interface.

Hence, during growth of Al on Al-Pd-Mn, two different alignments of the nanocrystals below and above 250 K is observed. These alignments decide upon the macroscopic structure in which the crystallites evolve. Generally, both kinetics and thermodynamics influence the interface formation in the initial stage of growth. In particular, diffusion along and into the substrate surface as well as intermixing and subsequent alloying have to be considered in the first stage of the interface formation.

4.2.3 Growth of Al on the threefold-symmetry surface of Al-Pd-Mn

R. Lüscher, T. Flückiger, M. Erbudak

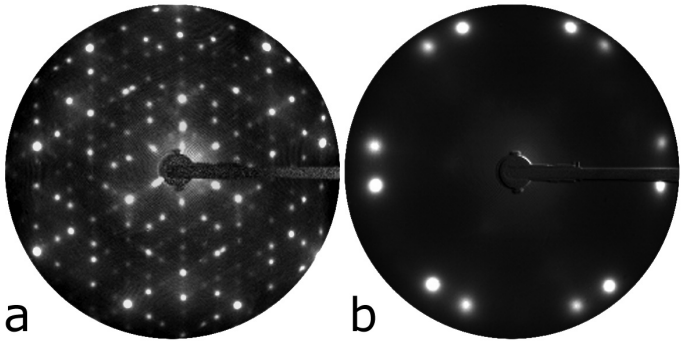

Figure 4.2: (a) LEED pattern obtained from the threefold-symmetry surface of Al-Pd-Mn. (b) After depositing a 6.6-nm thick Al layer.

Figure 4.2(a) shows a LEED pattern obtained from the threefold-symmetry surface of Al-Pd-Mn at 61 eV. The pattern displays the overall symmetry as expected from a flat macroscopic surface. Closer inspection, however, shows several other contributions to the pattern. As the electron energy is increased, diffraction spots are discerned which move towards 3 separate directions, lying at a polar angle of $\theta = 37.4°$ and distributed equally in azimuth. Another set

of 3 groups of spots converge for higher electron energies towards directions lying at $\theta = 41.8°$. This set is rotated in azimuth by $\phi = 60°$ with respect to the first set. These particular polar angles are identified as the fivefold- and threefold-symmetry directions of the icosahedral substrate, respectively. Individual specular reflections are also identified at these locations, confirming the faceted structure of the threefold-symmetry surface of Al-Pd-Mn.

Al evaporation onto this threefold-symmetry surface shows the expected behavior. No change of symmetry in the pattern is observed up to 0.5-nm Al except for a decrease in the overall spot intensity. For thicker layers, the properties of the pattern change drastically and almost abruptly. We find that the macroscopic textures of Al crystallites grow with their (111) axes aligned parallel to the surface normal, as well as minute contribution from crystallites parallel to the three threefold-symmetry directions lying at $\theta = 41.8°$. Figure 2b presents the LEED pattern from the sample with a 6.6-nm thick Al film. We do not observe any growth of Al along the three fivefold-symmetry directions lying at $\theta = 37.4°$. In contrast, we find that twinned Al face-centered cubic nanocrystals grow with their [111] axes parallel to one of the threefold-symmetry axes of the icosahedral substrate. These findings are in agreement with our observations on Al growth on the macroscopic fivefold-symmetry surface of Al-Pd-Mn. Interestingly, all the observed diffraction spots of the pattern in Fig. 4.2(b) have a corresponding counterpart in the pattern from the bare threefold-symmetric surface. This suggests the presence of a crystalline superstructure in 2 orientations on the quasicrystalline surface.

Chapter 5

Publications

D. Abou-Ras, H. Heinrich, G. Kostorz, M. Powalla, S. Spiering, A.N. Tiwari
Structural and chemical investigations of Cu(In,Ga)Se2/ALD-In2S3 interfaces
Proceedings of the 19th European Photovoltaic Solar Energy Conference, Paris, 2 (2004) 1772-1775

M. Angst, D. DiCastro, D.G. Eshchenko, R. Khasanov, S. Kohout, I.M. Savic, A. Shengelaya, S.L. Budḱo, P.C. Canfield, J. Jun, J. Karpinski, S.M. Kazakov, R.A. Ribeiro, H. Keller
Anisotropy and internal field distribution of MgB2 in the mixed state at low temperatures
Phys. Rev. B **70**, 224513 (2004)

M. Angst, D. DiCastro, R. Puzniak, A. Wisniewski, J. Jun, S.M. Kazakov, J. Karpinski, S. Kohout, H. Keller
Anisotropic properties of MgB2 by torque magnetometry
Physica C: Superconductivity, Volumes **408-410**, 88 (2004)

M. Angst, R. Puzniak
Two band superconductivity in MgB2: basic anisotropic properties and phase diagram
Chapter 1 in Focus on Superconductivity, B.P. Martins (ed.), p. 1-49, Nova Science Publishers, New York (2004)

M. Angst, R. Puzniak, A. Wisniewski, J. Roos, H. Keller, and J. Karpinski
Comment on Superconducting anisotropy and evidence for intrinsic pinning in single crystalline MgB2
Phys. Rev. B **70**, 226501 (2004)

E. Annese, J-P. Rueff, G. Vank, M. Grioni, L. Braicovich, L. Degiorgi, R. Gusmeroli, and C. Dallera
Valence of YbS under pressure: A resonant inelastic x-ray emission study
Phys. Rev. **B70**, 075117 (2004)

D.L. Bätzner, A. Romeo, M. Terheggen, M. Döbeli, H. Zogg, A.N. Tiwari
Stability aspects in CdTe/CdS solar cells
Thin Solid Films 451-452 (2004) 536-543

C.H. Back, D.Pescia
Speed limit ahead
Nature **428**, 808 (2004)

D. Baeriswyl and L. Degiorgi
Introduction“ (Chapter 1) in Strong Interactions in Low Dimensions
Physics and Chemistry of Materials with Low-Dimensional Structures, Vol. 25, Kluwer Academic, p. 1, Dordrecht 2004

J.H. Bilgram and H.M. Singer
Complex Structures: A symbiosis of Experiments and Numerical Studies
D. Herlach (Ed.) Solidification / Crystallization, Willey-VCH, Weinheim, pp. 1-8 (2004)

M. Brühwiler, S. M. Kazakov, N. D. Zhigadlo, J. Karpinski, and B. Batlogg
Superconductivity in the geometrically frustrated pyrochlore RbOs$_2$O$_6$
Phys. Rev. B **70**, 20503 (2004)

M. Buess, T.P.J. Knowles, U.Ramsperger, D.Pescia and C.H. Back
Phase-Resolved Pulsed Precessional Motion at a Schottky Barrier
Phys. Rev. B **69**, 174422 (2004)

M. Buess, T. P. J. Knowles, U. Ramsperger, D. Pescia, and C. H. Back
Phase-resolved pulsed precessional motion at a Schottky barrier
Virtual Journal of Ultrafast Science **3**, Issue 3, June 2004

M. Buess, R. Höllinger, T. Haug, K. Perzlmaier, U. Krey, D. Pescia, M.R. Scheinfein, D.Weiss, C.H. Back
Fourier Transform Imaging of Spin Vortex Eigenmodes
Phys. Rev. Lett. **93**, 077207 (2004)

G. Caimi, L. Degiorgi, H. Berger, N. Barisic, L. Forro' and F. Bussy
Optical evidence for the proximity to a spin-density-wave metallic state in Na0.7CoO2
Eur. Phys. J. **B40**, 231 (2004)

G. Caimi, L. Degiorgi, N. N. Kovaleva, P. Lemmens, and F. C. Chou
Infrared optical properties of the spin-1/2 quantum magnet TiOCl
Phys. Rev. **B69**, 125108 (2004)

G. Caimi, L. Degiorgi, P. Lemmens and F.C. Chou
Analysis of the phonon spectrum in the titanium oxyhalide TiOBr
J. Phys.: Condens. Matter **16,** 5583 (2004)

G. Caimi, S. Broderick, H. R. Ott, L. Degiorgi, A. D. Bianchi, and Z. Fisk
Magneto-optical Kerr effect in Eu1–xCaxB6
Phys. Rev. **B69**, 012406 (2004)

M. Chiao, S.S. Saxena, J.L. Gavilano, D. Rau, and H.R. Ott
Tuning of magnetic order in CePd2I
J. Magn. Magn. Mat. **272-276**, 77 (2004)

D. Chrastina, G. Isella, B. Rössner, M. Bollani, E. Müller, T. Hackbarth, and H. von Känel
High quality SiGe electronic material grown by low energy plasma enhanced chemical vapour deposition
Thin Solid Films **459**, 37 (2004)

L. Degiorgi
Electrodynamic response in ‚one-dimensional' chains" (Chapter 6) in 'StrongInteractions in Low Dimensions
Edited by D. Baeriswyl and L. Degiorgi, in Physics and Chemistry of Materials with Low-Dimensional Structures, Vol. 25, Kluwer Academic, p. 165, Dordrecht 2004

C.D. Dewhurst, R. Cubitt, M.R. Eskildsen, J. Jun, S.M. Kazakov, J. Karpinski
Vortex lattice reorientation and anisotropy in MgB2 - effects of two-band superconductivity
Physica C **404** (1-4), 135 (2004)

D. DiCastro, M. Angst, D.G. Eshchenko, R. Khasanov, J. Roos, M. Savic, A. Shengelaya, S.L. Bud'ko, P.C. Canfield, K. Conder, J. Karpinski, S. M. Kazakov, R. A. Ribeiro, and H. Keller
Absence of a boron isotope effect in the magnetic penetration depth of MgB2
Phys. Rev. B **70**, 014519 (2004)

A. Dorn, E. Bieri T. Ihn, K. Ensslin, D. D. Driscoll, and A.C. Gossard
AFM-defined antidot lattices with top- and back-gate tunability
Physica E **22,** 749 (2004)

A. Dorn, M. Peter, S. Kicin, T. Ihn, K. Ensslin, D. D. Driscoll, and A. C. Gossard
Charging effects of ErAs islands embedded in AlGaAs heterostructures
Physica E **21**, 426 (2004)

A. Dorn, T. Ihn, K. Ensslin, W. Wegscheider, and M. Bichler
Electronic transport through a quantum dot network
Phys. Rev. B. **70**, 205306 (2004)

T.B. Doyle, A.Wisniewski, M.Zehetmayer, H.W.Weber, J.Karpinski
Equilibrium behaviour and vortex pinning in MgB2 single crystals
Physica C: Superconductivity, Volumes **408-410**, 526 (2004)

D. Dvorsek, V.V. Kabanov, J. Demsar, J. Karpinski, S.M. Kazakov, D. Mihailovic
Femtosecond pump-probe polarization dependent investigation of relaxation dynamics in YBa2Cu4O8
J. Superconductivity **17** (1), 89 (2004)

S. Engemann, Harald Reichert, Helmut Dosch, Jörg Bilgram, Veijo Honkimäki, Anatoly Snigirev
Interfacial melting of ice in contact with SiO2
Phys. Rev. Lett. **92**, 205701 (2004)

K. Ensslin
Edge state equilibration in a two-subband system
Superl. & Microstr. **33**, 425 (2003)

K. Ensslin
Riesengrosse Anlagen für kleinste Strukturen
io new managment **6**, 66 (2004)

M. Erbudak, T. Flückiger, A. R. Kortan, and R. Lüscher
Crystal-quasicrystal interfaces on Al-Pd-Mn
Prog. Surf. Sci. **75**, 161 (2004)

M. Erbudak
Dogal Simetriler ve Kuasikristallerin Atom Yapilari
Cagdas Fizik **23**, 2 (2004)

J.D. Fletcher, A.Carrington, S.M.Kazakov, J.Karpinski
Damping o the de Haas-van Alphen oscillations in the superconducting state of MgB2
Phys. Rev. B **70**, 144501 (2004)

A. Fuhrer, M. Sigrist, L. Meier, T. Ihn, K. Ensslin, W. Wegscheider and M. Bichler
Quantum Rings as Phase Coherent Detectors
Physica E **25**, 303 (2004)

A. Fuhrer, T. Ihn, K. Ensslin, W. Wegscheider, and M. Bichler
Kondo Effect in a Many-Electron Quantum Ring
Phys. Rev. Lett. 93, 176803 (2004)

J.L. Gavilano, D. Rau, B. Pedrini, J. Hinderer, H.R. Ott, S.M. Kazakov, J. Karpinski
Unconventional Charge Ordering in Na0.70CoO2 below 300 K
Phys. Rev. B 69, 100404 (R) (2004)

J.L. Gavilano, D. Rau, B. Pedrini, J. Hinderer, H.R. Ott, S.M. Kazakov and J. Karpinski
Unconventional charge ordering in Na0.70CoO2 below 300 K
Physical Review B **69**, 100404(R) (2004)

J.L. Gavilano, D. Rau, C. Beeli, M. Weller, H.R. Ott, A.P. Tsai
Magnetic propertiers of amorphous and quasicrystalline Al75 Cu15V10
J. Magn. Magn. Mat. **272-276**, 1304 (2004)

C. Goldmann, C. Krellner, K. P. Pernstich, S. Haas, D. J. Gundlach, and B. Batlogg
Investigation of charge transport in organic single crystals using a ”flip-crystal” field-effect technique
Proceeding of the 34th European Solid-State Device Research conference, Leuven, Belgium, September 21st - 23rd (2004)

C. Goldmann, S. Haas, C. Krellner, K.P. Pernstich, D.J. Gundlach, and B. Batlogg
Hole mobility in organic single crystals measured by a ”flip-crystal” field-effect technique
Journal of Applied Physics **96**, 2080-2086 (2004)

R.S. Gonelli, D. Daghero, A. Calzolari, G.A. Ummarino, V. Dellarocca, V.A. Stepanov, S.M. Kazakov, J. Karpinski, C. Portesi, E. Monticone, V. Ferrando, C. Ferdeghini
Point-Contact Spectroscopy in MgB2: from Fundamental Physics to Thin-Film Characterization
Supercond. Sci. Technol. **17**, 93 (2004)

R.S. Gonnelli, D. Daghero, A. Calzolari, G.A. Ummarino, V. Dellarocca, V.A. Stepanov, J. Jun, S.M. Kazakov, and J. Karpinski
Magnetic-field dependence of the gaps in a two-band superconductor: A point-contact study of MgB2 single crystals
Phys. Rev. B **69**, 100504(R) (2004)

R.S. Gonnelli, D.Daghero, G.A.Ummarino, V.Dellarocca, A.Calzolari, V.A.Stepanov, J.Jun, S.M.Kazakov, J.Karpinski
Directional point-contact spectroscopy of MgB2 single crystals in magnetic field: two-band superconductivity and critical fields
Physica C: Superconductivity, Volumes **408-410**, 796 (2004)

B. Grbic, C. Ellenberger, T. Ihn, K. Ensslin, D. Reuter, and A. D. Wieck
Magnetotransport in C-doped AlGaAs heterostructures
Appl. Phys. Lett. **85**, 2277 (2004)

V.F. Gremenok, A.V. Mudryi, A.V. Ivaniukovich, V.B. Zalesski, F.V. Kurdesau, M. Kaelin, A.N. Tiwari
Optical characterization of CuInSe2 films from nanoparticle precursors
Proceedings of the 19th European Photovoltaic Solar Energy Conference, Paris, 2 (2004) 1855-1858

M.J. Hale, J.Z. Sexton, D.L. Winn, A.C. Kummel, M. Erbudak, and Passlack
The influence of bond flexibility and molecular size on the chemically selective bonding of In_2O and Ga_2O on GaAs(001)-c(2x8)(2x4)
J. Chem Phys. **120**, 5745 (2004)

T. Heinzel, S. Lüscher, M. Furlan, and K. Ensslin
Measuring the Energy Level Repulsion in Quantum Dots
Superl. & Microstr. **33**, 291 (2003)

T. Ihn
Scanning Probes for Semiconductor Nanostructures
Contribution to the Ecyclopedia of Nanoscience and Nanotechnology, ed. H.S. Nalwa, ISBN 1-58883-001-2, American Scientific Publishers (2004)

T. Ihn
Electronic Quantum Transport in Mesoscopic Semiconductor Structures
Springer Tracts in Modern Physics, Vol. 192, ISBN 0-387-40096-6, Springer Verlag, New York (2004)

M.D. Iosip, S. Destri, M. Pasini, W. Porzio, K. P. Pernstich, B. Batlogg
New Dithieno[3,2-b:2',3'-d]thiophene oligomers as promising materials for organic field-effect transistor applications
Synth. Met. **146**, 251-257 (2004)

G. Isella, D. Chrastina, B. Rössner, T. Hackbarth, H.-J. Herzog, U. König, and H. von Känel
Low-energy plasma-enhanced chemical vapor deposition for strained Si and Ge heterostructures and devices
Solid-State Electronics **48**, 1317 (2004)

I. Jerjen, E.C. Kirk, Ph. Lerch, A. Mchedlischivili, M. Furlan, D. Twerenbold, A. Zahnder, H.R. Ott
Responsivity of Ta-based STJ's to visible light as a function af Al trapping layer thickness
Nuclear Instrum. and Methods in Phys. Research A520, **519** (2004)

M. Kaelin, D. Rudmann, A.N. Tiwari
Low cost processing of CIGS thin film solar cells
Solar Energy 77 (2004) 749-756

M. Kaelin, H. Zogg, A.N. Tiwari, O. Wilhelm, S.E. Pratsinis, T. Meyer, A. Meyer
Electrosprayed and selenized Cu/In metal particle films
Thin Solid Films 457 (2004) 391-396

H. von Känel, D. Chrastina, B. Rössner, G. Isella, J.P. Hague, and M. Bollani
High mobility SiGe heterostructures fabricated by low-energy plasma-enhanced chemical vapor deposition
Microelectronic Engineering **76**, 279 (2004)

V. Kargl, A. Mirmelstein, P. Böni, D. Sheptyakov, A. Amato, S. Kazakov, J. Karpinski and A. Erb
Neutron diffraction, specific heat and SR study of the spin-chain compounds Ca2+xY2-xCu5O10
Physica B: Condensed Matter, Volume **350** (1-3), Supplement 1, E257-E259 (2004)

J. Karpinski, S.M.Kazakov, J.Jun, N.D.Zhigadlo, M.Angst, R.Puzniak, A.Wisniewski
MgB2 and Mg1-xAlxB2 single crystals: high-pressure growth and physical properties
Physica C: Superconductivity, Volumes **408-410**, 81 (2004)

S.M. Kazakov, J. Karpinski, J. Jun, P. Geiser, N.D. Zhigadlo, R. Puzniak, A.V. Mironov
Single crystal growth and properties of MgB2 and Mg(B1-xCx)2,
Physica C: Superconductivity, Volumes **408-410**, 123 (2004)

S.M. Kazakov, N.D.Zhigadlo, M.Brühwiler, B.Batlogg, J.Karpinski
Synthesis of superconducting pyrochlore RbOs2O6
Supercond. Science Technol. **17**, 1169-1172 (2004)

K. Kellermann, Dmitri Zimin, Karim Alchalabi, Philippe Gasser, Hans Zogg
Optically pumped lead-chalcogenide infrared emitters on Si-substrates,
Physica E 20, 536-539, 2004 (Proc. ngs11 conference, Buffalo, June 2003)

K. Kellermann, Karim Alchalabi, Dmitri Zimin, Hans Zogg
Optically pumped mid-infrared lasers on Si-substrates
Spectrochimica Acta A60, 2004, 3341-3344 (Proc. TDLS-2003, Tunable Diode Laser Spectroscopy conference, Zermatt, CH, 14-18 July 2003)

F. Kessler and D. Rudmann
Technological Aspects of Flexible CIGS Solar Cells and Modules
Solar Energy 77 (2004) 685-695

R. Khasanov, D.G.Eshchenko, J.Karpinski, S.M.Kazakov, N.D.Zhigadlo, R.Brütsch, D.Gavillet, H.Keller
Pressure effects on the transition temperature and the magnetic field penetration depth in the pylochlore superconductor RbOs2O6
Phys. Rev. Lett. **93**, 157004 (2004)

R. Khasanov, T.Schneider, J.Karpinski, H.Keller
Finite size and pressure effects in YBa2Cu4O8 probed by the magnetic field penetration depth measurements
Phys. Rev. B **70**, 1 (2004)

S. Kicin, A. Pioda, T. Ihn, K. Ensslin, D. C. Driscoll, and A. C. Gossard
Backscattering in the Quantum Hall Regime
Phys. Rev. B **70**, 205302 (2004)

S. Kicin, A. Pioda, T. Ihn, K. Ensslin, D. D. Driscoll, and A. C. Gossard
Scanning gate measurement in the quantum Hall regime at 300 mK
Physica E **21**, 708 (2004)

F. Kurdesau, M. Kaelin, V. B. Zalesski, V. I. Kovalewsky, V. F. Gremenok, E. P. Zaretskaya and A. N. Tiwari
In situ resistivity measurements during selenization process
Thin Solid Films 451-452 (2004) 245-249

F. Kurdesau, M. Kaelin, V.B. Zalesski, V.I. Kovalewsky
In situ resistivity measurements of Cu-In thin films during their selenization
Journal of Alloys and Compounds 378 (2004) 298-301

R. Lüscher, T. Flückiger, M. Erbudak, and A. R. Kortan
Debye Temperature at the Fivefold- and Threefold-Symmetry Surface of the Al-Pd-Mn Quasicrystal
Quasicrystals 2003, ed. E. Belin-Ferre, M. Feuerbacher, Y.O. Ishii, and D.J. Sordelet, Mat. Res. Soc. Sym. Proc. **805**, 299 (2004)

R. Lüscher, T. Flückiger, and M. Erbudak
Growth of Al on the faceted threefold-symmetry surface of the Al-Pd-Mn quasicrystal
Ferroelectrics **305**, 245 (2004)

R. Lüscher, M. Erbudak, T. Flückiger, Y. Weisskopf
Absorption kinetics of thin Al films on quasicrystalline Al-Pd-Mn
Appl. Surface Science **233**, 129 (2004)

R. Lüscher, M. Erbudak, Y. Weisskopf
Al nanostructures on quasicrystalline Al-Pd-Mn
Surface Science **569**, 163 (2004)

I. Landau and H.R. Ott
Temperature dependencies of the upper critical field and the Ginzburg-Landau parameter of single-crystalline NbSe2
J. Magn. Magn. Mat. **272-276**, 1095 (2004)

I.L. Landau, H.R. Ott
On the interpretation of the equilibrium magnetization in the mixed state of high-Tc superconductors
Physica C 411 (2004) 83-88

P. Lemmens, K. Y. Choi, G. Caimi, L. Degiorgi, N.N. Kovaleva, A. Seidel, and F.C.Chou
Giant phonon softening in the pseudogap phase of the quantum spin system
TiOCPhys. Rev. **B70**, 134429 (2004)

R. Leturcq, D. Graf, T. Ihn, K. Ensslin, D. Driscoll, and A.C. Gossard
Multi-terminal transport through quantum dots
Europhys. Lett. **67**, 439 (2004)

S. Lindemann, T. Ihn, T. Heinzel, K. Ensslin, K. Maranowski, and A.C. Gossard
Zeeman splitting in quantum dots
Quantum computing and quantum bits in mesoscopic systems, Kluwer Academic 2004, p. 185, New York, Eds. A.J. Leggett, B. Ruggiero, P. Silvestrini

X. Mathew, J. P. Enriquez, A. Romeo, A.N. Tiwari
CdTe/CdS solar cells on flexible substrates
Solar Energy 77 (2004) 831–838

L. Meier, A. Fuhrer, T. Ihn, K. Ensslin, W. Wegscheider, and M. Bichler
Single-Electron Effects in a Coupled Dot–Ring System
Phys. Rev. B **69**, 241302 (2004)

S. Mitrovic, L. Perfetti, C. Søndergaard, G. Margaritondo, M. Grioni, N. Barii, L. Forró, and L. Degiorgi
Electronic structure of a quasi-one-dimensional insulator: The molybdenum red bronze K0.33Mo3
Phys. Rev. **B69**, 035102 (2004)

D. Oberhoff, K. P. Pernstich, D. J. Gundlach and B. Batlogg
Modeling and Parameter Extraction of Pentacene TFTs
49th Annual International Society for Optical Engineering's Conference, Proceedings of SPIE, vol. **5522**, pp. 69-80 (2004)

J.E. Olsen, E.C. Kirk, Ph. Lerch, M.E. Huber, K. Arzner, W. Hajdas, A. Zehnder, H.R. Ott
Study of a Mo-Au TES deposited directly on a freestanding membrane
Nuclear Instrum. and Methods in Phys. Research A 520, **296** (2004)

H.R. Ott
Aspects of Magnetism and Superconductivity in Metals
Proc. Int. School of Physics „Enrico Fermi", Course CLVII, The Electron Liquid Paradigm in Condensed Matter Physics", Eds. G.F. Giuliani and G. Vignale (Societa Italiana di Fisica, Bologna 2004) p. 385

B. Pedrini, J. L. Gavilano, D. Rau, H. R. Ott, S. M. Kazakov, J. Karpinski, S. Wessel
NMR and dc susceptibility studies of NaVGe2O6
Phys. Rev. B **70**, 024421 (2004)

B. Pedrini, J.L. Gavilano, D. Rau, H.R. Ott, S.M. Kazakov, J. Karpinski and S. Wessel
NMR and dc susceptibility studies of NaVGe2O6
Physical Review B **70**, 024421 (2004)

G.K. Perkins, Y. Bugoslaysky, A.D. Caplin, J. Moore, T.J. Tate, R. Gwilliam, J. Jun, S.M. Kazakov, J. Karpinski, L.F. Cohen
Effects of proton irradiation and ageing on the superconducting properties of single crystalline and polycrystalline MgB2
Supercond. Science Techn. **17**, 232-235 (2004)

K.P. Pernstich, A. N. Rashid, S. Haas, G. Schitter, D. Oberhoff, C. Goldmann, D. J. Gundlach and B. Batlogg
Threshold Voltage Shift in Organic Field Effect Transistors by Dipole-Monolayers on the Gate Insulator
J. Appl. Phys, **96**, 6431-6438 (2004)

K.P. Pernstich, C. Goldmann, C. Krellner, D. Oberhoff, D. J. Gundlach, B. Batlogg
Shifted Transfer Characteristics of Organic Thin Film and Single Crystal FETs
Synt. Metal **146**, 325-328 (2004)

A. Perucchi, C. Søndergaard, S. Mitrovic, M. Grioni, N. Barisic, H. Berger, L. Forró and L. Degiorgi
Spectroscopic and dc-transport investigations of the electronic properties of TaSe3
Eur. Phys. J. **B39**, 433 (2004)

A. Perucchi, G. Caimi, H. R. Ott, L. Degiorgi, A. D. Bianchi, and Z. Fisk
Optical evidence for a spin-filter effect in the charge transport of Eu0.6Ca0.4B6
Phys. Rev. Lett. **92**, 067401 (2004)

A. Perucchi, L.Degiorgi and R.E. Thorne
Optical investigation of the charge-density-wave phase transitions in NbSe3
Phys. Rev. **B69**, 195114 (2004)

A. Perucchi, L. Degiorgi, H. Berger and P. Millet
Infrared spectroscopy of tetrahedral quantum spin systems Cu2Te2O5X2 (X = Br and Cl)
Eur. Phys. J. **B38**, 65 (2004)

A. Pioda, Slavo Kicin, Thomas Ihn, Martin Sigrist, Andreas Fuhrer, Klaus Ensslin, Andreas Weichselbaum, Sergio E. Ulloa, Matthias Reinwald and Werner Wegscheider
Spatially resolved manipulation of single electrons in quantum dots using a scanned probe
Phys. Rev. Lett. 93, 216801 (2004)

T. Plackowski, C. Sulkowski, J. Karpinski, J. Jun, and S.M. Kazakov
Magneto-thermopower of single-crystal MgB2: Evidence for strong electron-phonon coupling anisotropy
Phys. Rev. B **69**, 104528 (2004)

B. Rössner, D. Chrastina, G. Isella, and H. von Känel
Scattering mechanisms in high-mobility strained-Ge channels
Appl. Phys. Lett. **84**, 3058 (2004)

D. Rau, J.L. Gavilano, Sh. Mushkolaj, C. Beeli, H.R. Ott
Inhomogeneous Mn-magnetism in Al-Pd-Mn quasicrystals
J. Magn. Magn. Mat. **272-276**, 1330 (2004)

A. Romeo, G. Khrypunov, F. Kurdesau, D.L. Bätzner, H. Zogg and A.N. Tiwari
High Efficiency Flexible CdTe Solar Cells on Polymer Substrates
Technical Digest of the 14th International Photovoltaic Science and Engineering Conference, Bangkok, Thailand (2004) 715-716

A. Romeo, M. Terheggen, D. Abou-Ras, D.L. Bätzner, F.-J. Haug, M. Kälin, D. Rudmann, A.N. Tiwari
Development of thin-film Cu(In,Ga)Se2 and CdTe solar cells
Progress in Photovoltaics: Research and Applications 12 (2004) 93-111

A. Romeo, R. Gysel, S. Buzzi, D. Abou-Ras, D. L. Bätzner, D. Rudmann, H. Zogg, A. N. Tiwari
Properties of CIGS Solar Cells Developed with Evaporated II-VI Buffer Layers
Technical Digest of the 14th International Photovoltaic Science and Engineering Conference, Bangkok, Thailand (2004) 705-706

C. Rost, D. J. Gundlach, S. Karg, and W. Riess
Ambipolar Organic Field-effect Transistor Based on an Organic Hetero-structure
Applied Physics Letters, vol. **95**, n. 10, pp. 5782-5787, (2004)

D. Rudmann, A.F. da Cunha, G. Bilger, M. Kaelin, F. Kurdesau, H. Zogg and A.N. Tiwari
Efficiency enhancement of Cu(In,Ga)Se2 solar cells due to postdepositionNa incorporation
Applied Physics Letters 84 (2004) 1129

D. Rudmann, D. Brémaud, H. Zogg, A.N. Tiwari
Na incorporation for low-temperature Cu(In,Ga)Se2 growth
Proceedings of the 19th European Photovoltaic Solar Energy Conference, Paris, 2 (2004) 1710-1713

S. Süllow, I. Maksimov, A. Otop, F. J. Litterst, A. Perucchi, L. Degiorgi, and J. A.Mydosh
Metallic ground state and glassy transport in single crystalline Urh2Ge2: enhancement of disorder effects in a strongly correlated electron system
Phys. Rev. Lett. **93**, 266602 (2004)

R. Schleser, E. Ruh, T. Ihn, K. Ensslin, D. C. Driscoll and A. C. Gossard
Time-Resolved Detection of Individual Electrons in a Quantum Dot
Appl. Phys. Lett. **85**, 2005 (2004)

H.L. Seng, M.B.H. Breese, M. Kummer, and H. von Känel
Characterization of thick graded Si$_{1-x}$Ge$_x$/Si layers grown by low energy plasma enhanced chemical vapour deposition
Nucl. Instr. Meth. B **215**, 235 (2004)

M. Sigrist, A. Fuhrer, T. Ihn, K. Ensslin, D. D. Driscoll, and A. C. Gossard
Multiple layer local oxidation for fabricating semiconductor nanostructures
Appl. Phys. Lett. **85**, 3558 (2004)

M. Sigrist, A. Fuhrer, T. Ihn, K. Ensslin, S. E. Ulloa, W. Wegscheider, and M. Bichler
Magnetic field dependent transmission phase of a double dot system in a quantum ring
Phys. Rev. Lett. **93**, 66802 (2004)

M. Sigrist, A. Fuhrer, T.Ihn, K.Ensslin, W.Wegscheider, and M.Bichler
Transmission Phase Through Two Quantum Dots Embedded in a Four-Terminal Quantum Ring
Physica E **22**, 530 (2004)

H.M. Singer and J.H. Bilgram
Extracting contours of crystals
J. Crystal Growth, **261**, 122 (2004)

H.M. Singer and J.H. Bilgram
Generalized length scales for three-dimensional dendritic growth
Phys. Rev. E **69**, 032601 (2004)

H.M. Singer and J.H. Bilgram
Quantitative description of morphological transitions in diffusion limited growth of xenon crystals
Phy. Rev. Lett. E**70**, 031601 (2004)

H.M. Singer and J.H. Bilgram
Three-dimensional reconstruction of xenon dendrites
Europhys. Lett. **68**, 240 (2004)

H.M. Singer and J.H. Bilgram
Three-dimensional reconstruction of experimentally grown xenon dendrites
D. Herlach (Ed.) Solidification / Crystallization, Willey-VCH, Weinheim, pp. 166-174 (2004)

A.V. Sologubenko and H.R. Ott
Energy transport in one-dimensional spin systems
in: Strong Interactions in Low Dimensions, eds. D. Baeriswyl and L. Degiorgi, (Kluwer, Dordrecht 2004) p. 383

A.V. Sologubenko, R. Dell'Amore, H.R. Ott, and P. Millet
Anisotropic field dependence of the magnetic transition in Cu2Te2O5Br2
Eur. Phys. J.B **42**, 549-553 (2004)

A.V. Sologubenko, S.M. Kazakov, H.R. Ott, T. Asano, and Y. Ajiro
Diffusive energy transport in the S=1 Haldane spin chain compound AgVP2S6
J. Magn. Magn. Mat. **272-276**, 689 (2004)

J. Takeya, T. Nishikawa, T. Takenobu, S. Kobayashi, Y. Iwasa, C. Goldmann, C. Krellner, and B. Batlogg
Effects of polarized organosilane self-assembled monolayers on organic single-crystal field-effect transistors
Applied Physics Letters **85**, 5078 (2004)

M. Terheggen, H. Heinrich, G. Kostorz, D. Baetzner, A. Romeo, A.N. Tiwari
Analysis of Bulk and Interface Phenomena in CdTe/CdS Thin-Film Solar Cells
Interface Science 12 (2004) 259-266

A.N. Tiwari, G. Khrypunov, F. Kurdzesau, D.L. Bätzner, A. Romeo, H. Zogg
CdTe solar cell in a novel configuration
Progress in Photovoltaics: Research and Applications 12 (2004) 33-38

T. Uchihashi, U. Ramsperger
Fabrication and Properties evaluation of surface one-dimensional nanostructures
NIMS Now International, **2**, No.12, 4 (2004)

A. Vaterlaus, O. Portmann, C. Stamm, D. Pescia
Domain configuration in perpendicularly magnetized atomically thin iron particles
J. Magn. Magn. Mat. **272-276**, 1137 (2004)

G.A. Wigger, C. Beeli, E. Felder, H.R. Ott, A.D. Bianchi, and Z. Fisk
Percolation and the Colossal Magnetoresistance of Eu-Based Hexaboride
Physical Review Letters **93**, 147203-1 (2004)

G.A. Wigger, E. Felder, S. Weyeneth, H.R. Ott, and Z. Fisk
Kondo behaviour of U in CaB6
Europhys. Lett. **68**, 685 (2004)

G.A. Wigger, R. Monnier, and H.R. Ott
Electronic transport in EuB6
Physical Review B **69**, 125118 (2004)

Y. Xu, M.Khafizov, L.Satrapinsky, P.Kus, A.Plecenic, J.Karpinski, J.Jun, S.M.Kazakov, R.Sobolewski
Picosecond dynamics of the superconducting state in MgB2
Physica C: Superconductivity, Volumes **408-410**, 90 (2004)

M. Zehetmayer, M. Eisterer, J. Jun, S.M. Kazakov, J. Karpinski, B. Birajdar, O. Eibl, and H.W. Weber
Fishtail effect in neutron-irradiated superconducting MgB2 single crystals
Phys. Rev. B **69**, 054510 (2004)

M. Zehetmayer, M. Eisterer, J.Jun, S. M. Kazakov, J. Karpinski, A.Wisniewski, H. W. Weber
Anisotropy in superconducting MgB2: A comparison of SQUID and torque measurements
Physica C: Superconductivity, Volumes **408-410**, 111 (2004)

M. Zehetmayer, M. Eisterer, J. Jun, S.M. Kazakov, J. Karpinski, A. Wisniewski, H.W. Weber
Field dependence of the reversible mixed-state properties of superconducting MgB2 single crystals and the influence of artificial defects
Phys. Rev. B **70**, 214516 (2004)

M. Zehetmayer, M. Eisterer, S. M. Kazakov, J. Karpinski, A.Wisniewski, R.Puzniak, A.Daignere, H. W. Weber
Effects of neutron and electron irradiation on superconducting HgBa2CuO4+x single crystals
Physica C: Superconductivity, Volumes **408-410**, 30-31 (2004)

H. Zogg, Klaus Kellermann, Karim Alchalabi, Dmitri Zimin
Optically pumped lead-chalcogenide mid-infrared emitters on Si-substrates
Infrared Phys. Technol. 46 (2004) 155-159

Chapter 6

Talks

(* = invited)

Abou-Ras D.
Structural and chemical investigations of Cu(In,Ga)Se_2/ALD-In_2S_3interfaces
19th European Photovoltaic Solar Energy Conference, Paris, 7-11June 2004

Abou-Ras D.
Structural and chemical investigations of CBD- and PVD-CdS bufferlayers and interfaces in Cu(In,Ga)Se_2-based thin film solarcells
E-MRS Spring Meeting, Strasbourg (F), 24-28 May 2004

Abou-Ras D.
Formation and characterisation of $MoSe_2$ in Cu(In,Ga)Se_2-basedsolar cells
E-MRS Spring Meeting, Strasbourg (F), 24-28 May 2004

Arnold M.
Lead salt mid-IR photodetectors with narrow linewidth
MBE2004, 2004 International Conference on Molecular Beam Epitaxy,Edinburgh, Scotland, 22-27 Aug. 2004

Arnold M.
Bleichalkogenid IR-Detektoren mit schmaler Bandbreite
34. IR-Kolloquium, Freiburg i.Br., 20-21 April 2004

* Batlogg B.
Correlated electrons on a triangular lattice
Colloquium, Walther Meissner Institut, TU München, 22.01.2004

* Batlogg B.
Na_xCoO_2: correlated electrons on a triangular lattice
Workshop on Novel Materials and Superconductors, Planneralm,Austria, 23.02.2004

* Batlogg B.
Charge mobility in Organic Semiconductors
Winterschool on Organic Electronics, Donnersbach, Austria, 09.03.2004

* Batlogg B.
Erfolgreiches Forschen
Eröffnung der Forschungszentren, Fachhochschule Vorarlberg,Dornbirn, Austria, 17.03.2004

* Batlogg B.
Organic molecular crystals
Colloquium, Austrian Society for Physical Chemistry, Universityof Innsbruck, Austria, 28.06.2004

Baumgartner A.
Local Selective Backscattering in an Electron Gas in the Classical andthe Quantum Hall Regime Using the Scanning Gate Technique
27th International Conference on the Physics of Semiconductors,Flagstaff, Arizona, USA, 29.07.2004

* Bilgram J.H.
Noble gases as model systems to study the solidification behaviourof metals
DPG, Regensburg, March 8-12, 2004

* Bilgram J.H.
Noble gases as model systems to study the solidification behaviourof metals
Colloquium, Institute de Physique, Neuchâtel, March 22, 2004

Bilgram J.H.
Noble gases as model systems to study solidification behaviourof metlas
ICCG 14, Grenoble, August 13, 2004

Bilgram J.H.
Three-dimensional reconstruction of experimentally grown xenondnedrites and characterization of their morphological transitions
SGK/SSCr Meeting 2004, Neuchâtel, October 6, 2004

Borgström M.
Photon antibunching in GaAsP quantum dots in GaP nanowires
Science and technology of inorganic nanowires, Bad Honnef, Germany,15.02.2004

Brühwiler M.
Magnetic Field dependent Quasiparticle Mass in Strongly CorrelatedNa$_{0.7}$CoO$_2$
APS March Meeting, Montreal Canada, 23.03.2004

Buess M.
Spin Dynamik in Permalloy Kreisscheiben mit Vortex Struktur
Frühjahrstagung des Arbeitskreises Festkörperphysik der DPG 8.März.-12.März 2004, Regensburg, Deutschland

Buess M.
Spin Dynamics in NiFe Disks with Vortex Structure
APS March Meeting, 22nd March - 26th March 2004, Montreal

Buess M.
Spin Dynamics in NiFe Disks with Vortex Structure (Poster)
KNAW Masterclass on ”Ultrafast spin dynamics”, 18-19 June 2004, Royal Netherlands Academy of Arts and Sciences, Amsterdam

Caimi G.
Magneto optical response of $Eu_{1-x}Ca_xB_6$
Manep-Meeting, Neuchâtel, March 3-4, 2004

Degiorgi L.
Optical evidence for a spin-filter effect in the charge transportof $Eu_{0.6}C_{0.4}B_6$
March Meeting of the American Physical Society, March 22-26 2004, Montreal, Canada

Degiorgi L.
Optical investigation of the charge-density-wave phase transitionsin $NbSe_3$
March Meeting of the American Physical Society, March 22-26 2004, Montreal, Canada

Degiorgi L.
Infrared optical properties of the spin-1/2 quantum magnet TiOCl
March Meeting of the American Physical Society, March 22-26 2004, Montreal, Canada

* Degiorgi L.
Optical properties of correlated systems
Physics Colloquium at University of Augsburg, May 14 2004,Augsburg, Germany

Degiorgi L.
Optical evidence for a spin-filter effect in the charge transportof $Eu_{0.6}Ca_{0.4}B_6$
International Conference on Strongly Correlated Electron Systems(SCES04), July 26-30 2004, Karlsruhe, Germany

* Degiorgi L.
Magneto-optical investigation on novel superconductors: $MgB_2$and $Na_{0.7}CoO_2$
International Conference on Nanoscale heterogeneity and quantumphenomena in complex matter (Stripes04), September 26-October2 2004, Rome, Italy

* Degiorgi L.
Light and Matter
Physics Colloquium at University of Lipsia, January 4 2005,Lipsia, Germany

Dorn A.
Electronic transport through a quantum dot network
13th International Winterschool on New Developments in Solid State Physics, Mauterndorf, Austria, 17.02.2004

* Ensslin K.
Quantum physics in quantum dots
Physics colloquium, University of Kaiserlautern, Germany, 12.01.2004

* Ensslin K.
Manipulating spin and charge in quantum dots
Physics colloquium, University of Cologne, Germany, 13.01.2004

* Ensslin K.
Quantum physics in quantum dots
Physics colloquium, University of Duisburg, Germany, 02.02.2004

* Ensslin K.
Quantum physics in quantum dots
Physics Seminar, National Research Council, Ottawa, Canada, 07.04.2004

* Ensslin K.
Quantum physics in quantum dots
Solid State Physics Colloquium, University of Ohio, Athens, USA,08.04.2004

* Ensslin K.
Coherent electron transport in coupled dot-ring geometries
CNSI seminar, University of California, Santa Barbara, USA, 05.08.2004

* Ensslin K.
AFM nanolithography
Seminar, Asylum research, Santa Barbara, USA, 06.08.2004

* Ensslin K.
Electronic read-out of quantum dots
Seminar, TU Delft, The Netherlands, 17.09.2004

* Ensslin K.
Facts and strategies at ETH Zurich
Seminar, Paul Drude Institute, Berlin, Germany, 10.12.2004

* Ensslin K.
Phase coherence in ring structures
XXXIXth Rencontes des Moriond, Quantum information and decoherencein nanosystems, La Thuile, Aosta Valley, Italy, 27.01.2004

* Ensslin K.
Tutorial introduction to quantum dots
13th International Winterschool on New Developments in SolidState Physics, Mauterndorf, Austria, 15.02.2004

* Ensslin K.
Manipulation of spin and charge in quantum dots
Latsis Symposium on Quantum Communication, Lausanne, Switzerland,02.03.2004

* Ensslin K.
Nano-bio-quantum
Symposium on the occasion of Prof. Kotthaus 60th birthday, Munich,29.05.2004

* Ensslin K.
AFM lithography
Summer school on Fabrication, Manipulation and Spectroscopy ofNanostructures, Porquerolles Island, France, 28.06.2004

* Ensslin K.
Quantum physics in quantum dots
Summer school on Mesoscopic Physics, Les Houches, France,29.06.2004

* Ensslin K.
Manipulating spin and charge in quantum dots
XXVIII International conference of Theoretical Physics, Electroncorrelations in nano and macrosystems, Ustron, Poland, 05.09.2004

* Ensslin K.
Semiconductor nanostructures and quantum information processing
Nanofair, St. Gallen, Switzerland, 15.09.2004

* Ensslin K.
Scanning probe lithography for semiconductor nanostructures
IV Spanish Congress on Scanning Probe Microscopy, Vic, Spain,23.09.2004

* Ensslin K.
Local spectroscopy of quantum materials
International Symposium on Quantum Hall Systems and QuantumMaterials, Hamburg, Germany, 23.09.2004

* Ensslin K.
Semiconductor nanostructures and quantum information processing
Workshop Nanoscience-linking disciplines, Venice, Italy, 30.09.2004

* Erbudak M.
Natural Packing of Objects
Barut memorial Lecture, Bogazici University, Istanbul, 17. Mai 2004

Erbudak M.
Experimental and computational study of vacuum deposited Al grown on the decagonal surface of the Al-Co-Ni quasicrystal
IVC16/ICSS12/NANO8, Venedig, 29. Juni 2004

* Erbudak M.
Recent advances in statistical and solid-state physics
General Meeting of TPS, Bodrum, 14 September 2004

* Erbudak M.
Recent advances in nano-sciences
Seminar in physics, Istanbul Technical University, 30. September 2004

* Gavilano J.
Unconventional Charge Ordering in $Na_{0.7}C_oO_2$ below 300 K?
The International Conference on Strongly Correlated ElectronSystems, Karlsruhe July 26-30, 2004

Gavilano J.
Unusual d-electron dynamics in $Na_{0.7}C_oO_2$
Swiss Physical Society Meeting MANEP, Neuchâtel, March 3-4,2004

Gavilano J.
59Co-NMR studies of $Na_{0.7}CoO_2$
The 20th General Conference of the Condensed Matter Divisionof the European Physical Society, Prague July 19-23

Gavilano J.
Low-temperature specific heat of $Na_2V_3O_7$
Manep-Meeting, Neuchâtel, March 3-4, 2004

Gavilano J.
NMR studies of $Na_{0.7}CoO_2$
Manep-Meeting, Neuchâtel, March 4, 2004

Gavilano J.
59Co-NMR studies of $Na_{0.7}CoO_2$
Poster, The 20^{th} General conference of the Condensed MatterDivision, Prague, Czech Republic, 19.-23.6.2004

Geiser P.
Growth of $Al_xGa_{1-x}N$ bulk single crystals
E-MRS Spring Meeting, Strasbourg, France, 24.05.2004

Geiser P.
Growth of $Al_xGa_{1-x}N$ bulk single crystals
INW04, Pittsburg, USA, 19. 07.2004

Geiser P.
$Al_xGa_{1-x}N$ bulk single crystals
SPS and MaNEP Meeting, Neuchâtel, Switzerland, 03.03.2004

Geiser P.
$Al_xGa_{1-x}N$ bulk single crystals
ICSSC-7PCCG, Zakopane, Poland, 17.05.2004

Geiser P.
$Al_xGa_{1-x}N$ bulk single crystals
E-MRS Fall Meeting, Warschau, Poland, 06.09.2004

Gildemeister A.
Local Spectroscopy of Semiconductor Nanostructures
Nanospectra Summerschool, Porquerolles, France, 22.06.2004

Goldmann C.
Hole mobility of organic single crystal FETs: Rubrene, pentacene,and tetracene
APS March Meeting, Montreal Canada, 24.03.2004

Goldmann C.
Hole Mobility in Organic Single Crystal Field-Effect Transistors
TMS Electronic Materials Conference, and 2004 IEEE Device ResearchConference, University of Notre Dame, Notre Dame, IN, USA, 23.06.2004

Goldmann C.
Charge Transport Studies in Organic Single Crystals: a ”Flip-Crystal” Field-Effect Technique
34th European Solid-State Device Research conference, Leuven, Belgium, 23.09.2004

Grbic B.
Electronic properties of C-doped (100) AlGaAs heterostructures
27th International Conference on the Physics of Semiconductors,Flagstaff, Arizona, USA, 27.07.2004

Grbic B.
Electronic properties of p-type C-doped AlGaAs heterostructures
XVI Serbian National Symposium on Condensed Matter Physics, Sokobanja,Serbia and Montenegro, 23.09.2004

Gundlach D.J.
Gate Dielectric Surface Modification for Controlling the Subthreshold Performance of OTFTs
46th Electronic Materials Conference Digest, Notre Dame University,Notre Dame, Indiana, 24.06.2004

Gundlach D.J.
Modeling and parameter extraction of pentacene TFTs
SPIE, Denver/Colorado, USA, 04.08.2004

Haas S.
Iodine Doping of Pentacene Single Crystals and Thin Films
APS March Meeting, Montreal Canada, 26.03.2004

Hinderer J.
Inhomogeneous Mn-magnetism in Al-Pd-Mn quasycrystals
Manep-Meeting, Neuchâtel, March 3-4, 2004

Hinderer J.
NMR studies of $PrCu_2$
European Physical Society Meeting, Prague, July 21-25, 2004

Hinderer J.
NMR studies of $PrCu_2$
Poster, The 20^{th} General conference of the Condensed MatterDivision, Prague, Czech Repuclic, 19.-23.6.2004

* Ihn T.
Spin effects in a quantum ring
3rd International conference on quantum dots, Banff, Canada, 20.05.2004.

* Ihn T.
Phase coherence and interactions
Nanospectra Summer School on Fabrication, Manipulation, and Spectroscopy of Nanostructures, Porquerolles Island, France, 07.06.2004.

* Ihn T.
Spin effects in quantum rings
Advanced Research Workshop on the Fundamentals of Electronic Nanosystems, St. Petersburg, Russia, 18.06.2004

* Ihn T.
Single electrons and spins in quantum dots and quantum rings
Interdisciplinary lectures: Quantum Phenomena in 0D, Universität Ulm, Germany, 11.11.2004

Kaelin M.
Low Cost CIGS solar cells by Paste coating and selenization
E-MRS Spring Meeting, Strasbourg (F), 24-28 May 2004

* Karpinski J.
Anisotropic properties and substitutions in MgB_2 single crystals
NATO Advanced Research Workshop, University of Miami Workshop on Unconventional Superconductivity, Miami, USA, 12.01.2004

* Karpinski J.
Influence of substitutions in MgB_2 crystals on structural and superconducting properties
invited lecture on Superconductivity Seminar in Atomic Institute of the Austrian Universities, Vienna, Austria, 10.05.2005

* Karpinski J.
Crystal growth, anisotropic properties and substitutions in MgB_2 single crystals
International Conference on Solid State Crystals (ICSSC), Ko?cielisko, Zakopane, Poland, 17.05.2004

* Karpinski J.
Influence of substitutions, defects and inhomogeneities on properties and structure of borides and oxides superconductors
From Solid State To BioPhysics II : Role of Inhomogeneities in Solid, Soft and Bio-Matter, Cavtat, Dubrovnik, Croatia, 28.06.

* Karpinski J.
High pressure crystal growth and superconducting properties of pure and substituted MgB_2
E-MRS 2004 Fall Meeting and NATO "Advanced Research Workshop", Warsaw, Poland, 08.09.2004

* Karpinski J.
Substitutions in MgB_2 single crystals
4^{th} International Conference Stripes 2004, Nanoscale Heterogeneity in Condensed Matter, Quantum Phenomena in Complex Electronic Matter, Roma, Italy, 26.09.2004

Kazakov S.M.
Synthesis and superconducting properties of $RbOs_2O_6$ pyrochlore
Int. Workshop MSU-HTSC VII, High Temperature Superconductors and Novel Inorganic Materials Engineering, Moscow, Russia, 22.06.2004.

Kazakov S.M.
Superconductivity in the pyrochlore related oxide $RbOs_2O_6$: Synthesis and structural studies
Physik Institut, Uni Zürich, 26.05.2004

Kazakov S.M.
Superconductivity in the pyrochlore related oxide $RbOs_2O_6$
Paul Scherrer Institut (PSI), CH-Villigen, 09.06.2004

Knowles T.
Metallic wires on the nanometer scale: fabrication and electronic transport
APS March Meeting, 22nd March - 26th March 2004, Montreal

Knowles T.
Phase resolved imaging of micron-scale spin excitations in ultrathin ferromagnetic films (Poster)
Nanoconference, St. Gallen, Switzerland, 14-16 Steptember 2004

Kobayashi K.
Coherence of electrons through quantum hybrid systems
CNRS-CRTBT, Grenoble, France, 11.05.2004

Kobayashi K.
Mesoscopic Fano effect
TU Vienna, Wien, Austria, 15.07.2004

Kobayashi K.
Fano Effect in Nanostructures
Max-Planck-Institut für Festkörperforschung, Germany, 22.09.2004

Kobayashi K.
High Frequency Properties of Quantum Dots
Workshop of Quantum Systems for Information Technology, Castasegna, Switzerland, 17.10.2004

Kobayashi K.
Fano Effect in Nanostructures
Universitat Munchen, München, Germany, 02.10.2004

Kobayashi K.
Fano Effect in Mesoscopic Transport
University of Genève, Genève, Switzerland, 10.12.2004

Krellner C.
Transport and Defect Studies on Rubrene Single Crystals
2004 Winter School on Organic Electronic Materials and Devices, Planneralm, Austria, 09.03.2004

Lüscher R.
Nanocrystalline Al growth on quasicrystalline Al-Pd-Mn
APS March Meeting, CND-Montreal, 23. April 2004

Lüscher R.
Thin Al films on quasicrystalline Al-Pd-Mn: The impact of structural affinities on the crystal-quasicrystal interface
EPS CMD 20, Prag, 20. Juli 2004

* Lüscher R.
Crystal-Quasicrystal Interfaces
Festkörperseminar, ETHZ, 11. November 2004

* Landau I.
On the interpretation of the equilibrium magnetization in themixed state of high-T_c superconductors
Technische Universität Berlin, March 26, 2004

* Landau I.
Scaling of the equilibrium magnetization in the mixed state ofType-II Superconductors
NATO AR Workshop on ”Vortex dynamics in superconductors andother complex systems” Yalta, Crimea, Ukraine, September 13-17, 2004

* Landau I.
Scaling analysis of the equilibrium magnetization in the mixedstate of Type-II superconductors
Kapitza Institute for Physical Problems, Moscow, Russia, September22, 2004

Leturcq R.
Multi-terminal transport through a quantum dot
39e Rencontres de Moriond on Quantum Information and Decoherencein Nanosystems, La Thuile, Italy, 26.01.2004

* Leturcq R.
Resistance noise scaling in a dilute 2D hole system in GaAs
International Workshop on Ring Exchange and Correlated Fermions,Cargese, France, 15.04.2004

Leturcq R.
Tunneling through a multi-terminal semiconductor quantum dot
Swiss-Japan Nanoscience Workshop, Nara, Japan, 25.06.2004

Leturcq R.
Multi-terminal transport through semi-conductor quantum dots
27th International Conference on the Physics of Semiconductors,Flagstaff, USA, 28.07.2004

Leturcq R.
Transport through multi-terminal quantum dots
Mid-term Nanospectra Meeting, Lille, France, 01.01.2004

* Leturcq R.
Transport through multi-terminal quantum dots
Laboratoire des Champs Magnétiques Intenses, Grenoble, France,24.03.2004

* Leturcq R.
Transport through multi-terminal semiconductor quantum dots: from spatial spectroscopy to non-equilibrium Kondo effect
Service de Physique de l'Etat Condensé, CEA Saclay, France, 05.11.2005

* Leturcq R.
Transport through multi-terminal semiconductor quantum dots: from spatial spectroscopy to non-equilibrium Kondo effect
Laboratoire de Photonique et Nanostructures, Marcoussis, France, 08.11.2004

Leturcq R.
Multi-terminal transport through semi-conductor quantum dots
13th International Winterschool on New Developments in Solid State Physics, Mauterndorf, Austria, 16.02.2004

Meier L.
Detection of local magnetic fields by time-resolved Faraday rotation
2nd NTT-BRL School, Fuji, Japan, 11.10.2004

Metzger S.
The structure of Al_2O_3(100) surface
IVC16/ICSS12/NANO8, Venedig, 28. Juni, 2004

Michlmayr T.
Comparison of tungsten and cobalt STM-tips for magnetic investigation and manipulation on the nano scale
APS March Meeting, 22nd March - 26th March 2004, Montreal

* Monnier R.
A new look at an old material: lanthanum hexaboride
Festkörperseminar, IFW Dresden, November 24, 2004

Oberhoff D.
OTFTs: Modeling and Parameter Extraction
2004 Winter School on Organic Electronic Materials and Devices, Planneralm, Austria, 09.03.2004

* Ott H.R.
Magneto transport in Eu-based hexaborides
Maui, USA, NEDO Workshop, March 20, 2004

* Ott H.R.
Thermal transport in C-doped MgB_2
Maui, USA, NEDO Workshop, March 30, 2004

Ott H.R.
Open problems in electronic properties of condensed matter: Strongelectron correlations
Student Day, General Conference Condensed Matter Division ofEPS, Prague, Czech Republic, 19.-23.7.2004

Ott H.R.
Superfluidity and Superconductivity: Experimental Aspects
3. Summer School on Condensed Matter Research, Zuoz, Switzerland,7.-14.8.2004

Ott H.R.
Magnetotransport in Eu-based Hexaborides
Int. Workshop on Ordering Phenomena in Transition Metal Oxides,Wildbad Kreuth, Germany 26.-29.9.2004

Pedrini B.
Haldane State versus Magnetic Order in $NaVGe_2O_6$
Manep Conference Neuchâtel, March 2004

Pedrini B.
Haldane State versus magnetic Order in Alkali Metal Pyroxenes
EPS Conference, Prague, July 2004

Pernstich K. P.
Impact of Dipole-Monolayers on the performance of organic FETs
EUROFET meeting Strasbourg, France, 05.10.2004

Pernstich K. P
Interface Modification in Organic thin Film and Single Crystal FETs
E-MRS Spring Meeting, E-XI.2, Strasbourg, France, 26.05.2004

Pernstich K. P.
Threshold Voltage Shift in OTFTs by Surface Modification of the Gate Insulator
Winter school on Organic Electronics OEWS, Planneralm, Austria, 09.03.2004

Perucchi A.
The Excitation Spectrum of Transition Metal TrichalcogenidesXSe3 (X=Ta and Nb)
2004 Swiss Physical Society - (MANEP Meeting), Neuchatel (CH)March 3-4, 2004

* Perucchi A.
The superconductor MgB2 and the charge density wave NbSe3 system:an optical perspective of their broken symmetry ground states
LEES 04 - Low Energy Electrodynamics in Solids, Kloster Banz(Germany) - July 18-23, 2004

* Perucchi A.
The superconductor MgB2 and the charge density wave NbSe3 system:an optical perspective of their broken symmetry ground states
IMAS - Infrared Microscopy and Spectroscopy with AdvancedLight Sources, Trieste (Italy) - October 28-30, 2004

* Pescia D.
Imaging Magnetism with temporal and spatial resolution
Seminar, Dept. of Physics, University of California at San Diego, 5. March 2004

* Pescia D.
Non-linear aspects of ultrathin film magnetism
”The third international Workshop on surface, interface and thin film physics”, May 27-30, 2004, Shanghai

* Pescia D.
Non-linear aspects of ultrathin film magnetism
Turkish Physical Society 22nd Physics Conference, 14-17 September 2004, Bodrum, TR

* Pescia D.
Non-linear aspects of ultrathin film magnetism
51st Symposium of the American Vacuum Society, Anaheim, CA, November 14-19, 2004

* Pescia D.
Tunnelmikroskopie
Seminar, Kantonsschule am Burggraben, St. Gallen, 30. Juni 2004

* Pescia D.
Symmetrien in der Natur: die Rolle der Physik
Seminar, Kantonsschule im Lee, Winterthur, 23. September 2004

* Pescia D.
Das Physik Studium an der ETH Z”urich
Kolloqium für Lehrpersonen, ETH Zürich, 6.November 2004

Pioda A.
Scanning gate experiments on a quantum dot with tunable electron number
13th International Winterschool on New Developments in Solid State Physics, Mauterndorf, Austria, 17.02.2004

Pioda A.
Scanning Gate Microscopy on a Semiconductor Quantum Dot Electrometer
27th International Conference on the Physics of Semiconductors,Flagstaff, Arizona, USA, 28.07.2004

Portmann O.
An inverse transition of magnetic domain patterns in ultrathin Fe films on Cu(100)
APS March Meeting, 22nd March - 26th March 2004, Montreal

R. Ott H.
Electrons in Metals at Low Temperatures
Int. Workshop on Quantum Phenomena at Low TemperaturesLammi Biological Station, Finland, 7.-11.1.2004

Rössner B.
Scattering mechanisms in very high mobility p-Ge/SiGe heterostructures
APS March Meeting, Montreal Canada, 25.03.2004

Rössner B.
Quantum hall effect studies in high mobility p-Ge/SiGe quantum wells
APS March Meeting, Montreal Canada, 25.03.2004

Rau D.
Anomalous low-temperature in the Al-Pd-Mn alloy system
Meeting of the EPS CMD, Prague, July 22, 2004

Rau D.
d-Electron Magnetism in Quasicrystals
Meeting of the Swiss Physics Society, Neuchâtel, March 4, 2004

Rau D.
Anomalous low-temperature in the Al-Pd-Mn alloy system
Meeting of the Swiss Physics Society, Neuchâtel, March 4, 2004

Rau D.
Anomalous low-temperature magnetism in the Al-Pd-Mn alloy system
Poster, The 20^{th} General conference of the Condensed MatterDivision, Prague, Czech Republic, 19.-23.7.2004

* Refik Kortan A.
Epitaxy on quasicrystal surfaces
Physics seminar, National Taiwan University, Taipei, Taiwan, 6. Mai 2004

Romeo A.
Properties of CIGS solar cells developed with evaporated II-VIbuffer layers
14^{th} International Photovoltaic Science and Engineering Conference,Bangkok, Thailand, January 26–30, 2004

Rudmann D.
Na incorporation for low-temperature Cu(In,Ga)Se_2 growth
19th European Photovoltaic Solar Energy Conference, Paris, 7-11June 2004

Rudmann D.
Sodium incorporation strategies for CIGS growth at differenttemperatures
E-MRS Spring Meeting, Strasbourg (F), 24-28 May 2004

Schuck G.
Internet basierende Lehre in der Kristallographie - Ein Erfahrungsbericht
DGK 2004 Conference, Jena, Germany, 16.03.2004

Schuck G.
Al substitution in MgB_2 single crystals: influence on structural properties and phase separation
ECM 22 Conference, Budapest, Hungary, 30.08.2004

Schleser R.
Time-Resolved Detection of Individual Electrons in Quantum Dots
Annual SPS Meeting 2004, Neuchâtel, Switzerland, 03.03.2004

Schleser R.
Time-Resolved Detection of Individual Electrons in Quantum Dots
Quantum Systems for Information Technology Meeting, Flums, Switzerland, 06.03.2004

Schleser R.
Time Resolved Single Electron Detection in a Quantum Dot
27th International Conference on the Physics of Semiconductors, Flagstaff, Arizona, USA, 26.07.2004

Sigrist M.
Double Quantum Dot with Integrated Charge Readout Fabricated by Layered AFM-Lithography
27th International Conference on the Physics of Semiconductors, Flagstaff, Arizona, USA, 26.07.2004

Simovic B.
High pressure study of layered copper oxide superconductors and doped fullerenes
European high pressure research group meeting, Lausanne, Switzerland, 04.09.2004

Singer H.M.
Experiments and simulations for a quantitative description ofgrowth morphologies of experimentally grown xenon crystals andcomparison to 3D phase-field models
Solidification and Simulation II, DFG Priority Research Program,Karlsruhe January 27, 2004

* Singer H.M.
Modelling of phase transitions and interface dynamics acrossthe length scales
Workshop ”Modelling of phase transitions and interface dynamicsacross the length scales”, DFG Priority Research Program, Karlsruhe January 28, 2004

* Singer H.M.
Experimente und Simulationen zur quantitativen Beschreibung derWachstumsmorphologien von Xenon-Kristallen in drei Dimensionen
Seminar Institut für Raumsimulation, DLR, Köln 4. Februar2004

Singer H.M.
Three-dimensional reconstruction of experimental xenon dendrites
SPG, Neuchâtel, March 4, 2004

Singer H.M.
Three-dimensional reconstructions of experimentally grown xenondendrites and doublons
DPG, Regensburg, March 8-12, 2004

Singer H.M.
Comparison of three-dimensional simulations of dendrites withexperimentally grown 3D xenon crystals
DPG, Regensburg, March 8-12, 2004

Singer H.M.
Analysis of scale-invariant properties in experimentally grownmorphologies of diffusion limited growth of 3D xenon crystals
Conference on Statistical Physics of Non-Equilibrium and DisorderedSystems, Nancy, May 26-28, 2004

Singer H.M.
Solid-liquid surface free energy anisotropy of xenon using moleculardynamics simulations
ICCG 14, Grenoble, August 9, 2004

Singer H.M.
Tree-dimensional reconstruction of experimentally grown xenoncrystals and characterization of their morphological transitions
ICCG 14, Grenoble, August 9, 2004

Singer H.M.
Comparison of three-dimensional simulations of dendrites withexperimentally grown 3D grown xenon crystals
ICCG 14, Grenoble, August 10, 2004

Singer H.M.
3D single crystals morphologies of diffusion limited growth inexperiments and phase field simulations
Conference on Solidification and Gravity, Miskolc-Lillafüred,Ungarn, September 6, 2004

Singer H.M.
Three-dimensional reconstruction of experimentally grown xenondendrites and quantitative analysis of their morphological transitions
Junior Scientist Award Talk, Materials Week München, September21, 2004

Singer H.M.
3D reconstruction of experimentally grown xenon crystals andcharacterization of their morphological transitions
Junior Scientist Award, Materials Week München, September 21,2004

* Singer H.M.
Three-dimensional reconstruction of experimentally grown xenondendrites and quantitative analysis of their morphological transitions
Seminar, Ecole Polytechnique, Paris

Sologubenko A.V.
Influence of carbon substitution on the heat transport in singlecrystalline MgB_2
The 20th General Conference of the Condensed Matter Divisionof the European Physical Society, Prague, The Czech Republic,July 19-23, 2004

Strohm A.
ZnO/In_xS_y/Cu(In,Ga)Se_2 solar cells fabricated by coherentheterojunction formation
E-MRS Spring Meeting, Strasbourg (F), 24-28 May 2004

Suter K.
Tuning Fork AFM with conductive cantilever
Spring meeting of the Swiss Physical Society, Neuchatel, Switzerland, 04.03.2004

Tiwari A.N.
High efficiency flexible CdTe solar cells for space applications
19th European Photovoltaic Solar Energy Conference, Paris, 7-11June 2004

* Vaterlaus A.
Das Physikstudium an der ETH Zürich
Vortrag an der Kantonschule Luzern, 2.11.2004

Weisskopf Y.
Self-assembly of aluminum nanocrystals on the decagonal surface of Al-Co-Ni quasicrystal a low-energy electron diffraction study
22nd European Crystallographic Meeting, H-Budapest, 27. August 2004

Weisskopf Y.
Growth of Al nanocrystals on the decagonal surface of the Al-Co-Ni quasicrystal
8th European Conf. Crystallography and Dynamics, Segovia, 20. Juli 2004

Wigger G.
Percolation and CMR in the Hexaborides
The 20th General Conference of the Condensed Matter DivisionEuropean Physical Society, Prague, June 19-23, 2004

Wigger G.
Kondo Behaviour of U in CaB_6
The International Conference on Strongly Correlated ElectronSystems SCES'04, Karlsruhe, June 26-30, 2004

Wigger G.
Percolation and CMR in the Hexaborides
Manep-Meeting, Neuchâtel, March 3-4, 2004

* Wigger G.
Magnetism in the Hexaborides
Universität Zürich, March 1, 2004

Wittwer O.
Analysis of solidification dynamics by wavelet transformationtechniques
DPG, Regensburg, March 8-12, 2004

Zhigadlo N. D.
High pressure growth and properties of $Mg_{1-x}Al_xB_2$ single crystals
International Conference on Solid State Crystals (ICSSC), Ko?cielisko, Zakopane, Poland, 18.05.2004

Zhigadlo N.D.
High pressure crystal growth, substitutions and properties in MgB_2 single crystals
Int. Workshop MSU-HTSC VII, High Temperature Superconductors and Novel Inorganic Materials Engineering, Moscow, Russia, 21.06.2004

* Zogg H.
Lead chalcogenide IRemitters and detectors on Sisubstrates
MSCMP2004, 2^{nd} International Conference on Materials Scienceand Condensed Matter Physics, Chisinau, Rep. of Moldova, 21-26Sept. 2004

Zogg H.
Bleichalkogenid Heterostrukturen auf Si-Substraten: Wachstum,Eigenschaften und Anwendungen
Seminarvortrag Universität Köln, 2. Phys. Institut (Prof.Schieder), 3. Aug. 2004

* Zogg H.
Optically excited leadchalcogenide mid IR emitters and resonantcavity detectors on Sisubstrates
MIOMD-VI, 6^{th} Int Conf. on Mid-Infrared Optoelectronic Materialsand Devices, 27 June- 1 July 2004, St. Petersburg, Russia

Zogg H.
Optisch gepumpte Bleichalkogenid IR-Laser auf Si- und BaF_2-Substraten
34. IR-Kolloquium, Freiburg i.Br., 20-21 April, 2004